Thesis Report

Assessment on the potential use of vessel motion limit criteria for subsea cable installation

Thesis Report

Assessment on the potential use of vessel motion limit criteria for subsea cable installation

by

Anneli Lammers

to obtain the degree of Master of Science in Offshore Engineering at at the Delft University of Technology and Master of Science in Technology (Wind Energy) at the Norwegian University of Science and Technology, to be defended publicly on Wednesday September 23, 2020 at 2:30 PM.

Student number:	4395921 (TU Delft)	517536 (NTNU)
Supervision:	Prof. dr. ir. S. Sævik	NTNU
	Prof. dr. ir. A.V. Metrikine	TU Delft
	Ir. P. van der Male	TU Delft
	Ir. G. Vazquez Perez	Van Oord
	Ir. B.D. van den Berg	Van Oord

An electronic version of this thesis is available at `http://repository.tudelft.nl/`.

TU Delft NTNU Van Oord Marine ingenuity EWEM

Preface

This thesis marks the last stage of my time with the European Wind Energy Master (EWEM) program. The thesis is executed in partial fulfillment of the Offshore Engineering master degree at TU Delft and the Engineering - Wind Energy master degree at NTNU. This project is carried out in cooperation with Van Oord, a leading marine contractor in the offshore wind energy industry.

I would like to thank my daily supervisor Pim van der Male from TU Delft for his understanding guidance though out the project and for encouraging me to question my results. Furthermore, I would like to thank Professor Svein Sævik from NTNU for his bi-weekly guidance and expertise view on the challenges associated with subsea cable installation. I would like to express my gratitude to Gabriel Vazquez Perez and Bas van den Berg from Van Oord for their professional guidance, inspiring discussions regarding my thesis topic and introducing me to the challenges of offshore cable operations. Last, I would like to thank Professor Metrikine for acting as chair of my thesis committee.

Beyond the help regarding this thesis, I would like to thank my fellow students of the EWEM program, with whom I got the privilege to travel around Denmark and Norway during our master, for making our journey more than worth wile. In particular, I would like to thank Marieke Pouwels for our many successful projects and study days during both our Bachelor and Master degree, and not to mention the fun we had during out time in university. On top, I would like to thank all my friends in Delft for the wonderful years. Last, I would like to thank my roommates for supporting me during my thesis work in these unexpected circumstances regarding the COVID-19 outbreak.

Finally, I would like to thank both of my parents for teaching me to retain a good balance between educational performance and joy. On top, I would like to thank my mom for her unconditional support during my studies and life, and my dad for his interest in my field of study and loving support as my personal study counselor.

Anneli Lammers
Delft, September 2020

Abstract

Van Oord is active in the subsea cable installation industry and executes most of their cable lay projects with their cable laying vessel: The Nexus. In this thesis the focus lies on the normal lay phase of the cable installation, which comprises the phase when the vessel is pulling out the cable and putting it down on the seabed following the desired cable route. In order to ensure cable integrity during cable installation, a normal cable lay analysis is executed in the dynamic analysis software Orcaflex. The aim of the cable installation analysis is to define the installation limits in terms of the sea state. However, the vessel motions of the Nexus can be measured instantaneously and accurately on board of the vessel. Therefore, an assessment into the use of vessel motions for the expression of the handling limits during cable installation is performed. The assessment is executed for a normal lay configuration with an export cable and a 50 meter water depth. The focus lies on the maximum curvature and maximum tension response of the cable.

The cable dynamics result from both the vessel motions and the direct cable loads. First, the effect of these phenomena is assessed independently with the use of Orcaflex simulations. The influence of the vessel motions on the cable dynamics is found to be low for short wave periods, as the vessel hardly reacts to these kinds of waves. As a result, vessel motion limit criteria are less suitable for expressing cable installation limits at less severe sea conditions. However, the handling limits of the cable are not likely to be exceeded during these kinds of sea states, therefore this does not directly prevent the use of vessel motion limit criteria. Next, the most suitable vessel motion, measured at the chute of the vessel, for application of vessel motion limit criteria is determined based on the time lagged cross correlations between the cable response and the vessel motions. By using this method, the vessel motion which is most linearly related to the cable response is selected. In the case study, the heave acceleration and axial acceleration of the vessel are identified as most suitable candidates for application of vessel motion limit criteria. Finally, the performance of the selected vessel motion as limit parameter is compared to the use of the wave elevation, equivalent to sea state limit criteria. The performance of both is assessed by a linear regression analysis of the peaks in the limit parameter time history and the associated peaks in the cable response. This analysis led to the conclusion that in the case study higher certainty can be given to vessel motion limit criteria compared to sea state limit criteria, which eventually can lead to an increase of the workability.

Furthermore, a sensitivity analysis is performed to identify if the selected vessel motion for the application of vessel motion limit criteria is sensitive to changes in the normal lay configuration. The selected vessel motion and accompanied magnitude of the correlation were prone to changes in the normal lay configuration. Therefore, the applicability of vessel motion limit criteria for the base case in this thesis cannot straightforwardly be generalised for other normal lay configurations.

Due to the nonlinear nature of the cable lay system, all cable installation analysis are executed using time domain simulations in Orcaflex, which are associated with large computational time. In light of reducing the computational time for normal lay analysis, the potential use of a transfer function for estimation of the maximum cable response is evaluated. The transfer function is set up based on the first order frequency response of the cable system to regular waves. Before application of the transfer function approach, the nonlinear behaviour of the system is studied on the basis of the spectral response of the cable towards regular wave simulations in Orcaflex. Especially the contribution of the higher order frequency components and the effect of the nonlinear drag term in the

Morison equation are addressed.

In order to check the performance of the cable response transfer function, the maximum cable response estimation of the transfer function for a three hour time duration is compared to the statistical three hour maximum resulting from non-linear Orcaflex simulations. The transfer function is found to underestimate both the curvature and the tension response of the cable, leading to the conclusion that this transfer function approach is not suitable for the prediction of the maximum cable response. The underestimation is caused by the high dynamic complexity of the normal lay system.

Contents

List of Tables

List of Figures

List of Symbols

Symbol	Description	Unit
a	Acceleration	[m/s^2]
a_s	Contract area	[m^2]
A	Area	[m^2]
A_j	Amplitude	[m]
A_e	External area	[m^2]
B	Buoyancy	[N]
C	Damping	[N$\cdot$ s^2/m]
C_D	Drag coefficient	[-]
C_M	Inertia coefficient	[-]
d	Water depth	[m]
D	Diameter	[m]
Dcrit	Critical displacement	[m]
f	Frequency	[s^{-1}]
f_0	Input frequency	[s^{-1}]
f_{min}	Minimum frequency	[s^{-1}]
$f_{nyquist}$	Nyquist frequency	[s^{-1}]
f_p	Peak frequency	[s^{-1}]
F	Force	[N]
F_D	Drag force	[N]
H	Wave height	[m]
H_a	Significant wave height	[m]
k	Wave number	m^{-1}
k_s	Shear stiffness	[N/m^2]
K	Stiffness	[N/m]
K_L	Linearisation coefficient	[-]

Symbol	Description	Unit
l	Length	[m]
L	Lackback distance	[m]
m_0	0^{th} order spectral wave moment	[m^2]
M	Mass	kg
p	Pressure	[n/m^2]
p_e	External pressure	[n/m^2]
r	displacement	[m]
R	Reaction force	[N]
R_{min}	Minimum bending radius	[m]
s	Arc length	[m]
s^*	Total arc length	[m]
S_ζ	Spectral wave density	[m^2/Hz]
t	Time	[s]
T	Tension	[N]
T_0	Bottom tension	[N]
T_{eff}	effective tension	[N]
T_p	Peak period	[s]
T_{wave}	Wave period	[s]
u	Water particle velocity	[m/s]
$\dot{u}$	Water particle acceleration	[m/s^2]
UDF	Damping force value	[N]
v	velocity	[m/s]
v_{rel}	relative velocity	[m/s]
W	Weight	[N]
w_c	Cable weight	[N/m]
w_s	Submerged weight	[N/m]
γ	Peak enhancement factor	[-]
ϵ	Difference in relative velocity	[m/s]
ζ	Wave elevation	[m]
κ	Curvature	[rad/m]
λ	Wave length	[m]
μ	Friction coefficient	[-]
$\rho_{i,j}$	cross correlation	[-]
ρ_w	Density of sea water	[kg/m^3]
ϕ	Phase	[rad]
φ	Departure angle	[deg]
ω	Angular frequency	[s^{-1}]

1

Introduction

In recent years offshore wind energy has become a viable green energy production option. In order to reduce CO_2 emissions, the aim of the Dutch government is to have 4450 MWe installed capacity in the North Sea by 2023 [SER, 2013]. This is equivalent to approximately 3 of the largest gas fired power plants in The Netherlands[1]. Therefore the offshore wind energy industry plays an important role in the plans of the Dutch government to reduce CO_2 emissions. As a result, many new offshore wind farms are planned for development in the North Sea.

Electricity must be transported from the production site to the consumers. In case of offshore wind farms this means that construction of new electrical infrastructure is required. Figure 1.1 shows the trend of the increasing distance to shore of offshore wind turbines. Larger distances to shore also means longer cables to transport the electricity. This emphasises the need for reduced installation cost of subsea export electricity cables. One way to achieve this is by improving the cable installation analysis with the goal to reduce cable installation costs.

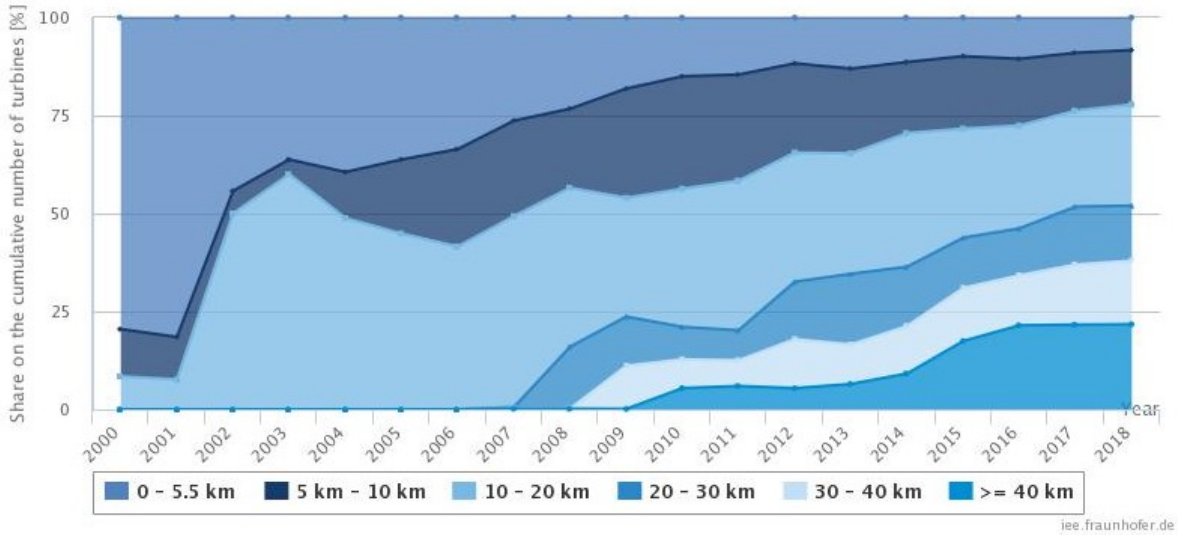

Figure 1.1: The distance to shore for yearly installed wind turbines [IWES, 2018].

[1] `https://powerplants.vattenfall.com/#/countries=Netherlands/view=map/sort=name` [Cited on: 10-01-2020]

1.1. Background

In cable lay analysis, the dynamic response of the cable to vessel motions and direct cable loads is assessed. Direct cable loads are the hydrodynamics loads acting on the submerged section of the cable directly. The aim of the cable installation analysis is to ensure cable integrity during the installation process. The loads on the cable during installation should not exceed the specified handling limits of the cable.

Dynamic cable lay analysis comprises the insurance of the cable integrity during the normal lay phase of the cable installation. In this phase of the installation the Cable Laying Vessel (CLV) is slowly moving forward, while laying the cable on the seafloor. The cable lay system is a non-linear system, therefore the dynamic cable lay analysis is performed using time domain simulations. The simulations are carried out for a discretised set of sea states, which contains all possible combinations of H_s and T_p for the considered H_s and T_p range. The results are combined into workability tables. These tables indicate whether all cable handling limits are ensured during installation for each sea state in the discretised set of sea states. During the actual cable installation the crew interprets the on-site conditions in relation to the workability tables.

1.2. Problem description

The discretisation of the wave height in the sea states for which simulations are performed, causes a workability loss. This is caused by the discontinuity in the operational conditions, meaning cable lay operations are executed for any sea state inside the accepted range of sea states. The true limit might be slightly higher than the highest accepted value contained in the discretised set.

Furthermore, the loads on the cable are not the direct result of the sea state, but result from a combination of vessel motions and direct cable loads. This emphasizes the possibility to express limiting conditions in vessel motions, instead of sea state. Vessel motions can be accurately and continuously measured on the cable laying vessel, making them suitable for on board decision making.

The current approach to dynamic cable lay analysis is associated with a large number of simulations. The nonlinear nature of the system makes it hard to predict which conditions will cause the most severe cable loads, requiring simulations for all site conditions. This same nonlinear character arises the need for time domain simulations, which are computationally expensive. Therefore decreasing computational time involved with dynamic cable lay analysis is of interest.

Combining these aspects, results in the idea of establishing a transfer function between the vessel motion and cable load. Before this approach can be applied in practice, its suitability and applicability are to be accessed.

1.3. Literature review

Loos [2017] investigated the relation between vessel motions and the response of subsea power cables that may be limiting cable installation. He concluded that compression in the touchdown zone is the main limiting mechanism. He found a strong relation between the chute velocities in the direction of the cable axis and tension loss in the touchdown zone. The effect of direct wave loads on the cable was not considered in the relation stated above. They proved to add significant scatter to the near-perfect relation found based on vessel motions only. Additionally, the effect of wave shielding by the ship was not considered by Loos. The effects of wave shielding on the cable loads are currently unclear.

Koloshkin and Saevik [2016] investigated the effect of vessel motions, in particular cyclic heave mo-

tions, on kink formation in the cable during installation. This motion can lead to kink formation along the catenary depending on the magnitude of the heave motions and the initial torsion utilization. Additionally it was found that compression at the touchdown point can result from the cyclic heave motions.

In recent years definition of cable compression limits became more common. This means that whereas before no compression at all was allowed in the cable, now a certain amount of compression is accepted during cable installation. So all though cable compression still has to be checked, this caused a shift in the limiting conditions for cable integrity. Here emerges the need to study vessel limit criteria with respect to cable handling limits other than compression. Therefore this thesis focuses on the maximum curvature and the maximum tension in the cable during installation.

1.4. Thesis objective and approach

The problem description and literature review are translated into the objective of this thesis. The research questions are based on the thesis objective. Furthermore the approach to answer the research questions is defined.

1.4.1. Problem definition

Combining the results of the problem definition and literature review, leads to an assessment on the potential use of vessel limit criteria for normal lay operations. With respect to the calculation time for normal lay analysis, a transfer function approach is chosen. It is a given fact that frequency domain functions are significantly faster than time domain simulations. Therefore this study focuses on the potential use of a transfer function to estimate the cable responses during the normal lay phase. All assessments are executed for the maximum curvature and maximum tension response in the cable as already stated in section 1.3.

The thesis objective is defined as:

"Assess the potential use of vessel motion limit criteria for normal cable lay operations with the aim to increase workability and decrease computational time for normal lay analysis"

In order to achieve the objective the following research questions are defined:

1. *What is the independent effect of direct cable loads and vessel motions on the cable dynamics?*
2. *Which type of vessel motion is most suitable for application of vessel motion limit criteria?*
3. *Is the use of vessel motion limit criteria preferred over sea state limit criteria?*
4. *What is the contribution of higher order effects in the cable response with respect to the first order contribution?*
5. *Can a transfer function be used to predict the cable response based on vessel motions with sufficient accuracy?*

1.4.2. Approach

First, a general introduction into subsea cable installation is given in Chapter 2. The assessment in this thesis is performed on the basis of the normal lay model and base case defined in Chapter 3.

From this point, the project can be divided into three stages. A schematic overview of these stages is given in Figure 1.2. The methods used in each stage, and their accompanied purpose, are listed in this figure. Each stage aims at working towards an answer to one of the research questions. The research question belonging to each description is bold indicated, based on their numbering in subsection 1.4.1.

The first stage is the vessel motion limit criteria assessment. The aim is to identify the strengths and weaknesses of the use of vessel motion limit criteria. The first part of this stage is found in Chapter 4. The application of reduced time domain simulation method is presented in Chapter 5.

In the second stage, the Discrete Fourier Transform (DFT) analysis, the frequency response of the system to regular waves is studied. This stage focuses on providing insight in the behaviour of the system. The results are documented in Chapter 6.

In the last stage, the transfer function definition & performance, the application of a first order transfer function, to predict the maximum curvature and maximum tension response towards a certain sea state, is assessed. The procedure and the results of the assessment are given in Chapter 7.

To conclude, the sensitivity of the DFT response of the cable towards changes in the cable properties is evaluated. Furthermore, the sensitivity of the vessel motion selection, for the application of vessel motion limit criteria towards changes in the normal cable lay model configuration, is assessed. These results can be found in Chapter 8.

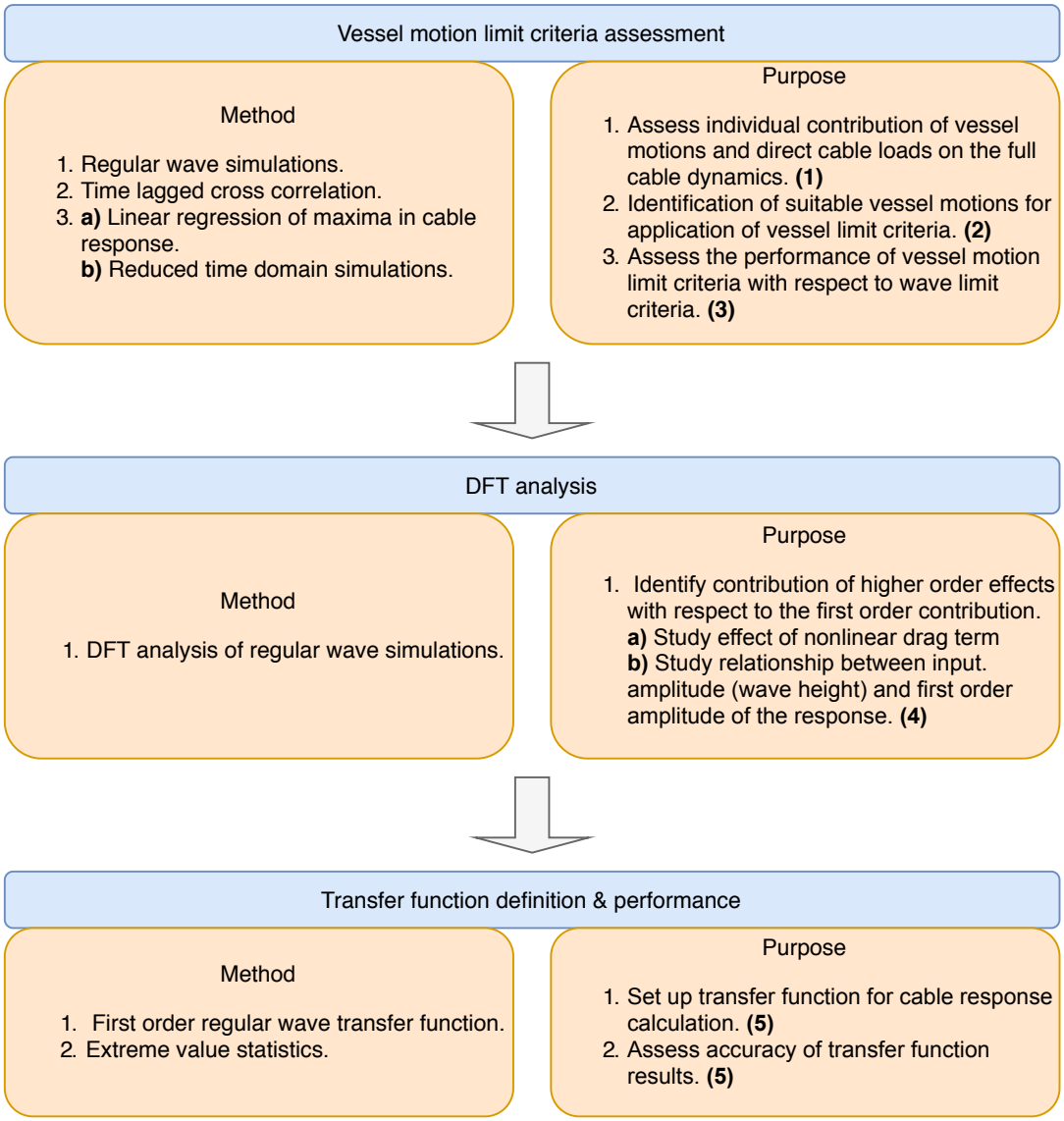

Figure 1.2: Schematic overview of the approach.

2

Subsea cable installation

This chapter gives a general introduction into subsea cable installation. First the cable installation in general is discussed. Then the cable installation vessel of Van Oord, the Nexus, is presented. Next, an overview of the properties of subsea power cables and their handling limits is given. Last, the cable lay mechanics during normal lay operations are discussed.

2.1. Cable installation procedure

The cable installation procedure starts with the loading of the cable onto the Cable Installation Vessel (CLV). Then the CLV sails to the project site. Once at the project site, each cable is installed following the steps presented in Figure 2.1. In general the procedure starts at the Offshore Substation (OSS) towards the end of the string. The first end pull-in comprises the installation of the first end of the cable, during which the cable is pulled into the turbine tower or OSS. In the second phase of the cable installation, the CLV sails towards the next turbine in the string via the prescribed cable routing. This is known as the normal lay phase. Upon arrival at the turbine the second end pull-in is performed, finalising the cable installation process. This thesis focuses on the normal lay phase of the cable installation.

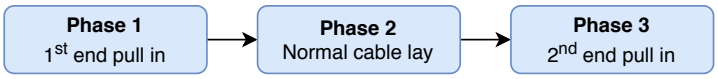

Figure 2.1: Schematic overview of cable installation process.

2.1.1. Cable installation method

The most common method to for subsea cable installation is the S-lay cable installation method. This method is discussed in more detail below.

In S-lay installation the cable is offloaded from the vessel horizontally. The cable is supported into the water by a chute. This results in a S-shape configuration of the cable. After the transition from the horizontal position into the departure angle, the behaviour of the cable can be described by the catenary equation, which will be described in subsection 2.5.2. A graphical representation of the installation method is given in Figure 2.2. The chute is attached at the rear of the CLV and has a radius larger than the Minimum Bending Radius (MBR) of the cable. In general, installation in shallow water is governed by both the effect of the bending stiffness of the cable and the stiffness

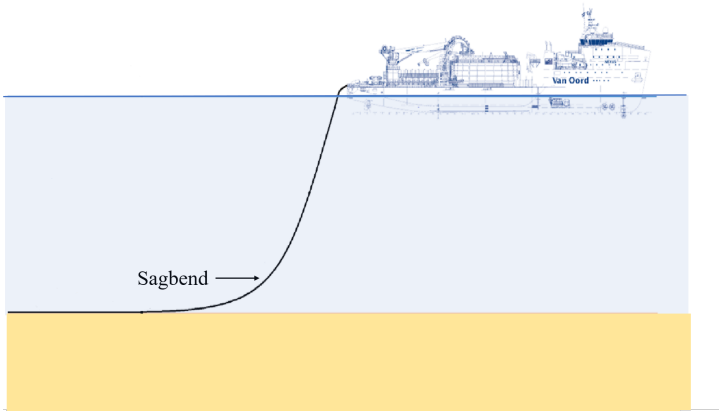

Figure 2.2: S-lay installation with chute.

originating from the applied tension, while installation in deeper water is more governed by the effect of the axial force stiffness only.

2.2. Cable installation vessel Nexus

Van Oord executes most of the cable lay projects with their CLV: the Nexus. Schematic overviews of the Nexus with starboard (SB) and top view are presented in Figure 2.3 and Figure 2.4, respectively. The storage system on the nexus consists of the carousel and loading arm. This type of cable storage prevents the introduction of torsion into the cable due to the turning of the carousel when loading cable. The cable is transported towards the chute by the cable transportation system. This system consists of the Portside (PS) tensioner, the SB tensioner and the cable highway. The routing of the cable is depicted in Figure 2.4. The cable is transported to the PS tensioner below deck, then moves via the quadrant towards the SB tensioner, which is located just before the chute. This systems allows for active departure angle control, where the cable on the highway acts as 'buffer'. The SB tensioner can temporarily pay out extra cable to reduce the departure angle of the cable. In this case the quadrant slightly moves to the aft of the vessel, and the carousel will slowly adjust its speed to restore the cable highway to the original position. This system is required due to the slow rate at which the pay out speed of the carousel can be changed. The cable departure system on the Nexus comprises the chute and the Departure Angle Measurement System (DAMS). The departure system is designed to carry out cable laying using the s-lay installation method. The nexus is equipped with two chutes, the PS chute and the SB chute. During normal operation the Nexus uses the SB chute. The cable thus departs off-center from the CLV. In general, the Nexus can perform normal lay operations in sea states with a significant wave height up to 2.5m. Important vessel data of the Nexus is provided in Table 2.1

Table 2.1: Data sheet of the Nexus.

Length overall	122.68 [m]
Breadth overall	27.45 [m]
Draft (design)	5.82 [m]
Carousel Capacity	5000 [t]

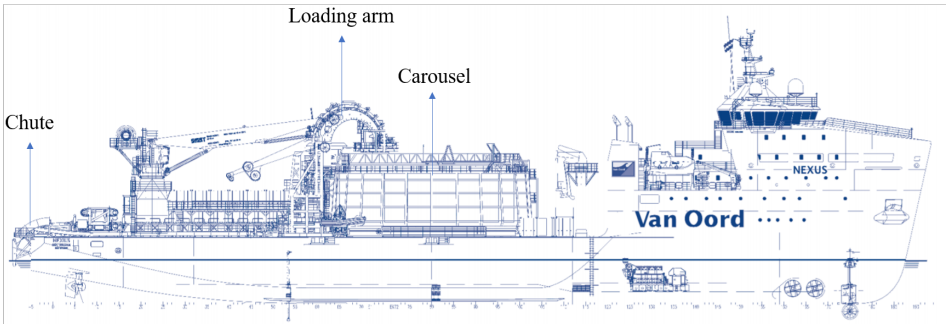

Figure 2.3: Schematic overview of the Nexus: Starboard view.

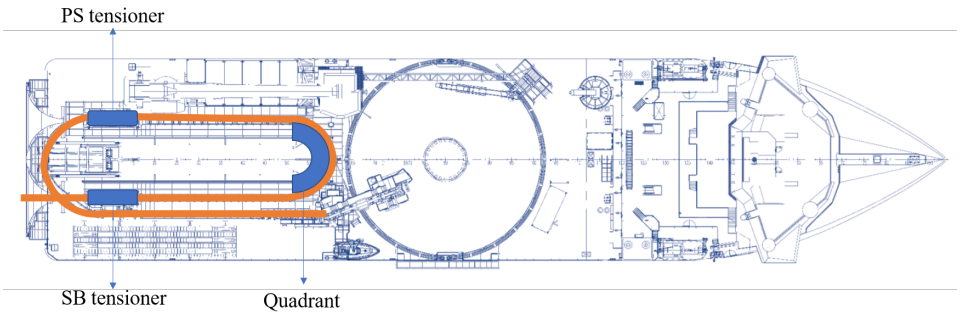

Figure 2.4: Schematic overview of the Nexus: top side.

2.3. Subsea power cables

Subsea power cables come in a range of different types. Based on the specific application of the cable, the internal structure and properties of the cable vary. Inter array cables provide the electricity transfer within the windfarm itself, while export cables transport the electricity to shore. Apart from the transportation of electricity, subsea cables also transport information and enable the control of the turbines from shore. Dependent on the distance to shore, the export cable can either be a Active Current (AC) or Direct Current (DC) cable. The internal structure and properties of subsea power cables and the differences between the types of subsea power cables are discussed below.

2.3.1. Internal structure

A schematic overview of the internal structure of subsea power cables is given in Figure 2.5. The different components are listed and described below.

1. **Conductor core(s)** - Wires made of aluminium or copper which carry the electrical current. The latter comprising the majority of the submarine power cables [Worzyk, 2009].
2. **Conductor screen** - A layer made of a semi-conducting material is present around the conductor core(s). It's purpose is to minimise the electric field strength outside of the conductor core(s) [Thies et al., 2012].
3. **Insulation** - This layer is made from a material with high electrical resistance and provides electrical insulation to the conductor core(s) [Thies et al., 2012].
4. **Sheath** - A metal layer around each core to provide protection against fault currents. This layer also serves as an additional water resistant layer [Thies et al., 2012].

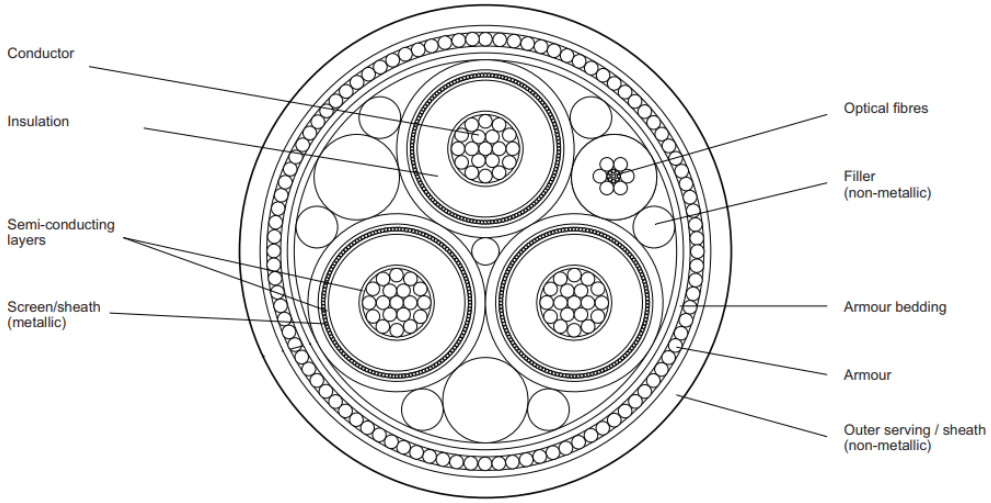

Figure 2.5: Schematic overview of the internal structure of a subsea cable [DNVGL-RP-0360, 2016].

5. **Optical fiber cable** An optical fiber cable can be present to transport data, for example for monitoring purposes.

6. **Wire armour** - One or two layers of steel cables to provide resistance against tension and torque. Mostly two layers with opposite rotation angle (lay angle) around the inner cable are used to create a torsion balance [Sævik, 2017].

7. **Protecting Sleath** - This is the outer layer of the cable. It is a water resistant layer and provides mechanical protection and protection against abrasion [Sævik, 2017] [Thies et al., 2012].

2.3.2. Properties

For modelling purposes, it is important to have a good understanding of the properties of the power cable. Due to the interaction between different layers of the cable, non-linear load-displacement responses are found [Vaz et al., 1998]. It is important to keep this in mind when modelling subsea power cables. Therefore, the different properties with respect to axial loads and bending loads are discussed below.

Axial stiffness

The axial stiffness of a subsea power cable is a result of both the axial stiffness of the armour wires and axial stiffness of the core. In general, the axial loads on the cable are taken up by the armour package [Vaz et al., 1998]. The contribution of the core to the axial stiffness is dependent on the configuration of the core itself. For cables with a single core the contribution is significant and should be taken into account. In cables with multiple cores, like AC cables, the conductor area is so small that the contribution can be neglected [Kurt, 1984].

When performing dynamic analysis on cables with a copper conductor it should be kept in mind that copper has a non-linear axial stiffness. On the contrary, aluminium conductors do behave linear within the operating limits. In addition, Knapp [1979] derived a stiffness matrix for straight cable elements based on the non-linear geometric equations, which include the non-linear internal behaviour of the cable. This implies the linearisation of the stiffness equations, which is useful as the observed load-deformation response of cable is nearly-linear. Finally, Kurt [1984] states: "Both measured cable behaviour and the non-linear governing equations behave in a linear manner over the

small strains (e_c < 1 percent) typical of most operating conditions.". Indicating that cable modelling using linear axial stiffness can provide reliable results.

Bending stiffness

Subsea cables have a low bending stiffness. This gives flexibility to the cable and allows it to bend in the required radii during installation and in the final position. The bending stiffness is dependent on the number, thickness and material of the layers inside the cable. Generally, the bending stiffness of the tensile armour can be ignored for high curvatures, as these layers will have slipped for this situation [API RP 17B, 2002].

The bending stiffness of a subsea cable is subject to hysteresis. Hysteresis is caused by the slipping of the different layers within the cable. This effect can be described using Figure 2.6. Initially, the cable is in the undeformed position. When gradually applying a curvature the bending stiffness is resulting from the bending stiffness of the individual layers. In this stage, the tensile forces in the wire elements do not overcome the friction forces between the different layers, resulting in the linear behaviour seen in line AB. Then starting from point B, the different wire elements start to slip, reducing the effective bending stiffness of the cable (line section BC in Figure 2.6). Reducing the curvature of the cable leads to the same situation as before, the wire elements are hold in place by the internal friction and a linear bending stiffness is experienced (line segment CD). Further reduction of the curvature results in slipping between the wire elements and a non-linear bending stiffness. It should be noted that a zero bending moment will now result in a non-zero curvature. This process results in the hysteresis loop presented in Figure 2.6 [Tan et al., 2009]. The total bending stiffness is thus a combination of the linear bending stiffness of each layer and the bi-linear coulomb friction curve.

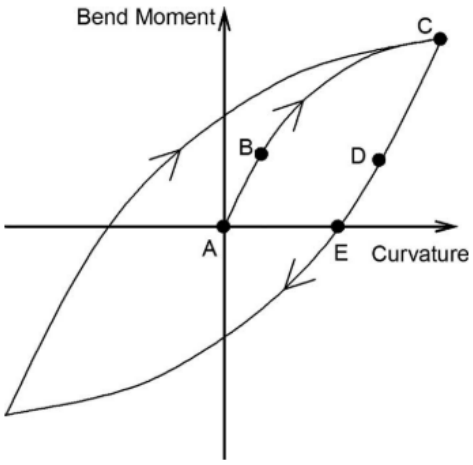

Figure 2.6: Schematic overview of the bending hysteresis cycle of a subsea cable [Tan et al., 2009].

2.4. Subsea cable handling limits

During subsea cable installation, different types of loads are experienced by the cable. Therefore, a range of handling limits are in place to ensure cable integrity. Here an overview of these handling limits is given.

2.4.1. Maximum tension

First, the absolute maximum tension on the cable is determined by the maximum allowed strain in the material of the conductor of the cable [McConnon et al., 2017]. For a copper conductor a strain of approximately 0.15% is allowed. Next to the strain experienced by the conductor, the helix structure of the armour of the subsea cable causes tension in the cable to be accompanied by an internal pressure in the cable. The maximum tension handling limits also safeguards that this compression does not damage the internal components of the cable.

2.4.2. Minimum bending radius

The MBR (R_{min}) specifies the minimum radius in which a cable can be bend without loss of integrity. The maximum curvature can be related to R_{min} by Equation 2.1, where κ_{max} represents the maximum curvature of the cable. Bending in the cable leads to axial stresses in the different layers of the cable. When this bending becomes excessive, it can lead to faults like, signal loss in optical cables, loss of insulation integrity or water ingress [Loos, 2017]. The MBR is specified by the cable manufacturer and defined at a specific tensile load and for a specific time during the installation [DNVGL-RP-0360, 2016].

$$R_{min} = \frac{1}{\kappa_{max}} \tag{2.1}$$

2.4.3. Maximum side wall pressure

The maximum side wall pressure handling limit combines the maximum tension in the cable to the MBR. An example of the side wall pressure handling limit is given in Figure 2.7. The allowable tension in the cable reduces as the cable is subject to bending. The bend has the effect of multiplying the tension due to frictional forces. The risk of residual strains after the installation procedure persist if frictional coefficients are high [McConnon et al., 2017].

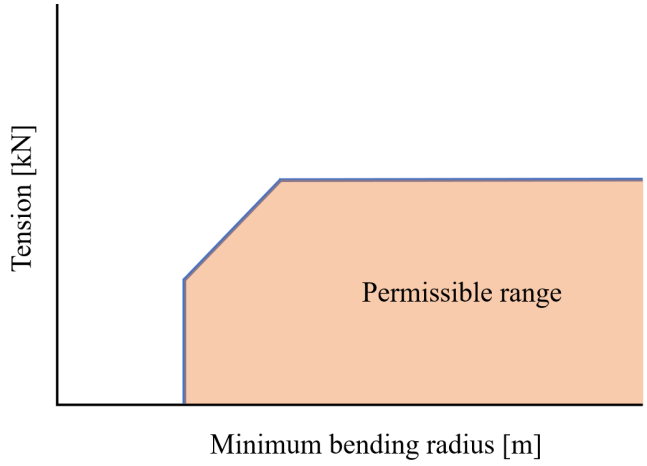

Figure 2.7: Graph of the maximum side wall pressure of a subsea cable.

2.4.4. Cable compression

The handling limit for cable compression refers to pure axial compression of the subsea cable. An axial compression loading on a subsea cable can lead to buckling, bird-caging or loop forming dur-

ing the installation process [Marta et al., 2015]. Until recently, there was no industry accepted standard to assess the compression limits of cables. As a result, subsea cable manufactures mostly specified that no axial compression was allowed in the cable [Reda et al., 2016]. In recent years pressure on cable manufactures has resulted in efforts to define cable compression limits. Therefore specifications for the compression limits are now becoming available.

2.5. Cable lay mechanics

In this section the general cable dynamics in normal lay operations are discussed. First the definitions used during normal lay analysis are presented in subsection 2.5.1. Then the static cable lay problem is discussed in subsection 2.5.2. In subsection 2.5.3 the environmental loads on the cable are presented and in subsection 2.5.4 the operational loads are discussed. The general behaviour of the cable with respect to the curvature and tension response is presented in subsection 2.5.5.

2.5.1. Definitions

A graphical representation of the cable lay configuration is given in Figure 2.8. The general definitions used in cable laying are indicated in the figure.

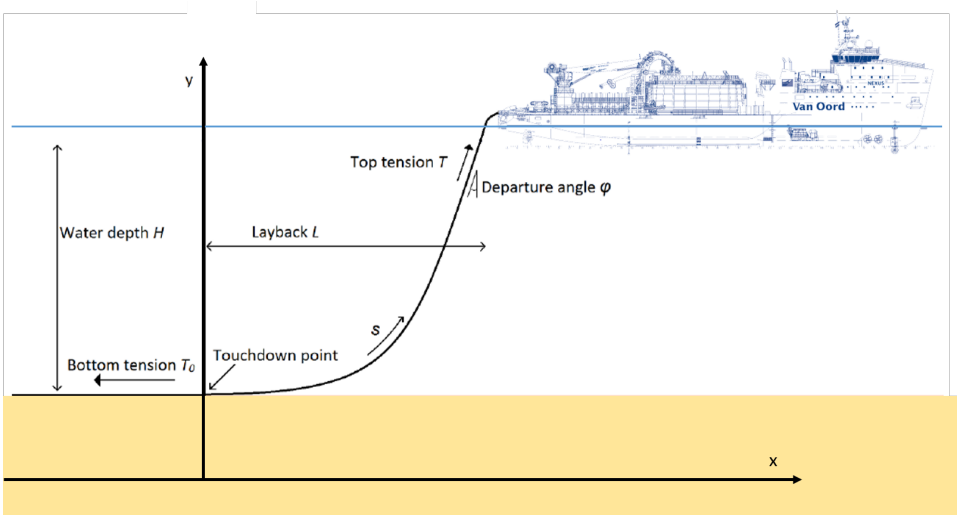

Figure 2.8: Definitions of cable installation configuration[1] [Oord, 2015].

The top tension in the cable, T_{top}, is defined as the tension at the connection between the vessel and the cable. The angle between the vertical and the cable at the location where the cable leaves the vessel is the departure angle, denoted by the symbol φ. The Touch Down Point (TDP) is the location where the cable first touches the seabed. The horizontal distance between the cable connection and the TDP is the layback distance L. The tension in the cable section along the seabed is defined as the bottom tension and marked with the symbol T_0.

2.5.2. Static cable lay problem

In this subsection the static configuration of the cable lay problem is discussed. First the static loads are presented, followed by the catenary equation, an approximation to the static configuration.

[1] http://dot.tudelft.nl/career/

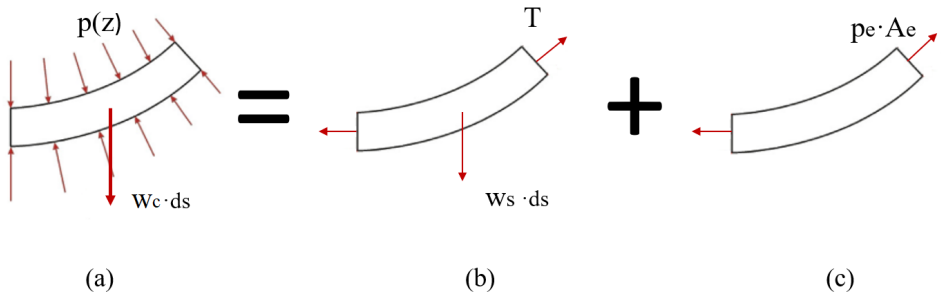

Figure 2.9: The system with external pressure and intrinsic-weight of the cable (a) is equivalent to the system described by the submerged weight, the tension term (b) and the hydrostatic pressure term at the end of the cable (c).

Static loads

The static loads acting on the cable are the hydrostatic pressure forces, the volume forces and current forces. The effect of the hydrostatic pressure forces and volume forces is presented here, the current forcing is discussed in more detail in subsection 2.5.3.

The cable weight and hydrostatic pressure acting on the cable are illustrated in Figure 2.9a. This system can be represented by the submerged weight of the cable, a tension term and the hydrostatic pressure term at the top and bottom of the cable. The hydrostatic pressure term $p_e A_e$ results from a difference in hydrostatic pressure on the upper and lower side of the cable. The effective tension is found by the tension term and hydrostatic pressure term at the ends of the cable, as found in Equation 2.2. The cable weight can be represented as the weight per unit length of the cable. The gravitational forces resulting from the cable weight are defined by Equation 2.3, where w_c is the weight of the cable per unit length and ds is the arc length of the cable element.

$$T_{\text{eff}} = T + p_e A_e \tag{2.2}$$

$$W = w_c ds \tag{2.3}$$

The buoyancy forces acting on the cable are related to the weight of the displaced water volume. This principle is known as Archimedes law. According to Archimedes law, the resulting buoyancy force acting on a cable element is given by Equation 2.4. Here g is the gravitational constant, ρ_w the density of sea water and A_e the area of the cross section of the cable. The weight of the cable in water, also know as the submerged weight w_s, is then defined by Equation 2.5.

$$B = g\rho_w A_e ds \tag{2.4}$$

$$w_s = w_c - g\rho_w A_e \tag{2.5}$$

The system with hydrostatic pressure, tension and cable weight is equivalent to the same system described by the submerged weight together with the effective tension term. The submerged weight and effective tension term are depicted in Figure 2.9.

Catenary equation

The catenary equation describes the configuration of the cable due to the application of the static loads. The derivation of the catenary equation is based on force equilibrium in both the horizontal and vertical direction. The catenary equation given an approximation of the shape of the cable based on the bottom tension T_0 and the submerged weight of the cable w_s. The equation is based on the following assumptions:

1. The bending stiffness of the cable is neglected.
2. The elongation of the cable is neglected.
3. The cable is assumed to be made out of a homogeneous material.

The bending stiffness can be neglected while retaining reasonable results as the bending stiffness of subsea cables is small [Vaz et al., 1998]. Within the workability limits the elongation of the cable is limited to $< 1\%$, which justifies the assumption for neglecting the cable elongation [Kurt, 1984]. Therefore, the catenary equation is a good approximation of the cable laying system as depicted in Figure 2.8. The general definitions found in Figure 2.8 can be approximated using the relations below.

The catenary shape of the cable is described by Equation 2.6 and is obtained based on the horizontal en vertical force equilibrium.

$$\text{Catenary shape: } y = \frac{T_0}{w_s} \cosh \frac{x}{\frac{T_0}{w_s}} \tag{2.6}$$

The total arc length of the cable is found by Equation 2.7.

$$\text{Total arclength: } s^* = \sqrt{d^2 + \frac{2T_0 d}{w_s}} \tag{2.7}$$

The departure angle can be derived based on a simple angle calculation between the bottom tension in the cable and the total weight hanging in the vertical direction, following Equation 2.8.

$$\text{Departure angle: } \varphi = \tan^{-1}\left(\frac{T_0}{w_s s^*}\right) \tag{2.8}$$

The top tension itself is defined by summation of the bottom tension and the total weight of the catenary part of the cable, as seen in Equation 2.9.

$$\text{Top tension: } T = T_0 + w_s d \tag{2.9}$$

Finally, the layback of the cable can be determined by Equation 2.10.

$$\text{Layback distance: } L = \frac{T_0}{w_s} \ln\left[1 + \frac{w_s d}{T_0} + \sqrt{\left(1 + \frac{w_s d}{T_0}\right)^2 - 1}\right] \tag{2.10}$$

2.5.3. Environmental loads

The environmental loads on the cable result from water particle movements. The movement of water particles results from current and waves. Both types of loading are addressed separately below.

Waves

Waves introduce dynamic loads on a cable during installation. For modeling purposes it is important to have a clear understanding of wave mechanics. Waves can, among many other ways, be represented by regular waves or irregular waves. For regular waves, the wave crest and trough have equal amplitude and are represented by a single period wave train. In modelling, regular waves are represented by circular or oval water particle movements. An often used theory for regular waves is Airy's linear wave theory. Based on Airy's linear wave theory, the wave-induced velocities and accelerations can be found by Equation 2.11. Here ζ represents the wave elevation, ω the wave frequency, k the wave number and ϕ the phase angle of the wave. C_i is dependent on the water depth and wavelength. If the particle velocities and accelerations are not affected by the presence of the seabed, the deep water approximation can be made. The different representations of C are given in Equation 2.12. Here d represents the water depth and λ the wavelength of the considered wave. The coordinate along the vertical z starts at zero at the mean water level and runs to -d at the seabed.

$$\begin{aligned} u(x,t) &= \zeta\omega C(z)\cos(\omega t - kx + \phi) \\ \dot{u}(x,t) &= -\zeta\omega^2 C(z)\sin(\omega t - kx + \phi) \end{aligned} \tag{2.11}$$

$$C(z) = \begin{cases} e^{kz}, & \text{if } d > \frac{1}{2}\lambda \\ \frac{\cosh k(z+d)}{\sinh kd}, & \text{otherwise} \end{cases} \tag{2.12}$$

Airy's linear wave assumes the pressure at the mean water level to be zero. Therefore, it is not able to properly describe the wave-induced velocities in the wave crest. Different methods are used to predict the wave velocities and accelerations in the wave crest. Figure 2.10 depicts three different methods used to estimate the velocities and accelerations in the wave crest.

Method A depicts Wheeler stretching. Here the wave potential calculated at the surface is assumed to be correct at the instantaneous water surface. As a result, the wave potential is stretched and compressed according to the length of the instantaneous water column. In method B the wave potential is assumed to be correct up to the mean water level. The solution is then uniformly expanded into the wave crest. In the last method, method C, the gradient of the profile at the mean water level is linearly extrapolated up to the instantaneous water surface. This is known as extrapolation stretching.

The validity range of Airy's linear wave theory is presented in Figure 2.11. The validity range is expressed as function of the Ursell number, defined as $\frac{H\lambda^2}{d^3}$, and the wave steepness, given by $\frac{H}{\lambda}$. The Ursell number indicates the degree of non-linearity in long surface gravity waves. The wave steepness is an indicator of the shape of the wave, expressed as the wave height relative to the wave length. For deep water depths the applicability of linear wave theory is dependent on the steepness of the wave, while for shallow water the Ursell number is limiting. Hedges [1995] found that linear wave theory may be applied for some wave characteristics even outside the range presented in Figure 2.11. The use of linear wave theory outside its validity range mainly results in an under prediction of the wave crest elevation and celerity, the speed of propagation of the wave. Therefore

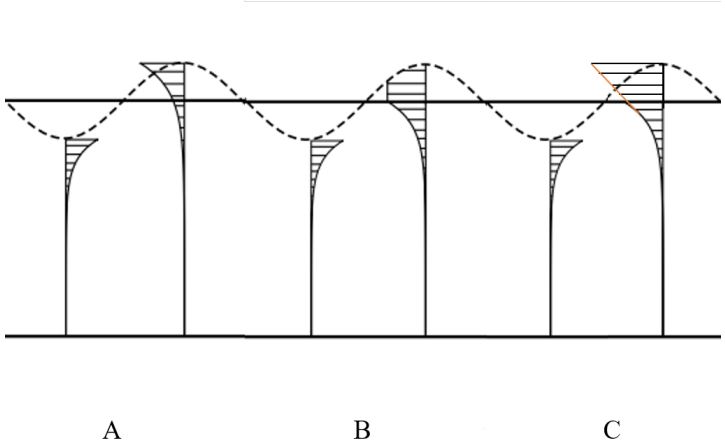

Figure 2.10: Methods to predict wave kinematics in the wave crest SINTEF Ocean [2019].

Dominic Reeve and Fleming [2004] states: "For engineering design purposes, the main implication of using linear theory outside its range of validity is that wave celerity and wavelength are not strictly correct, leading to some inaccuracies in refraction and shoaling analysis." Both of these phenomena are not of main interest in this research. All regular wave theories become inaccurate for breaking or near breaking waves. The breaking limit of waves can be approximated by Equation 2.13 [Orcina, cited August 2020].

$$H_B = \frac{0.88}{k}\tanh(0.98kd) \tag{2.13}$$

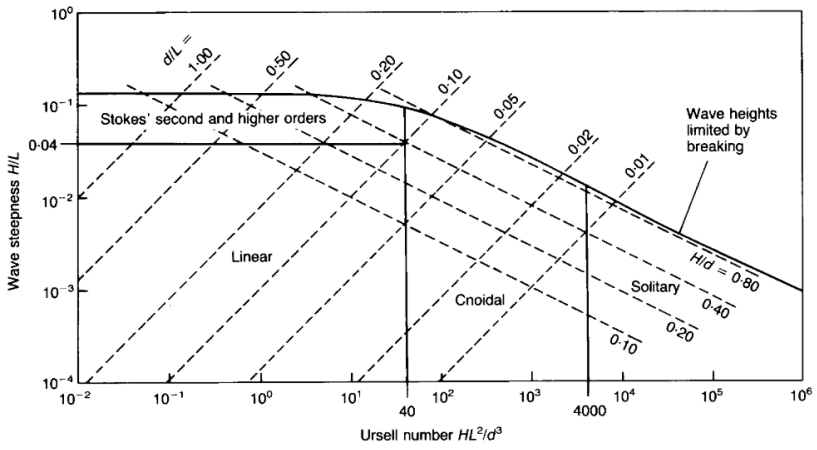

Figure 2.11: Approximate regions of validity of analytical wave theories Hedges [1995].

For the description of real seastates irregular waves are used. Irregular waves consists of a summation of regular waves. A sea state is described by a wave spectrum. A wave spectrum is the power spectral density function of the vertical displacement of the sea. The spectrum relates the frequency domain representation to the time domain representation of the sea state. It assumes the sea state can be described as a random stationary process over a certain period of time, usually three hours. Two standard wave spectra are the JONSWAP and the Pierson-Moscowitz spectrum. The Pierson-Moscowitz spectrum is developed for a fully-developed sea state, while the JONSWAP

spectrum is proposed for fetch limited seas [Faltinsen, 1990]. The JONSWAP spectrum is defined by Equation 2.14. The peak shape factor γ describes the shape of the peak of the spectrum. For γ=1 the JONSWAP spectrum reduces to the Pierson-Moscowitz spectrum.

$$S_\zeta(f) = \alpha g^2 (2\pi)^{-4} f^{-5} \exp\left[-\frac{5}{4}\left(\frac{f}{f_{\text{peak}}}\right)^{-4}\right] \gamma^{\exp\left[-\frac{1}{2}\left(\frac{f/f_{\text{peak}}-1}{\sigma}\right)^2\right]} \tag{2.14}$$

The wave induced velocity and acceleration based on an arbitrary wave spectrum are defined by Equation 2.15. The random phase angle ϕ_j is sampled from a uniform distribution between [- π, π]. The amplitude A_j is defined in Equation 2.16, where S_ζ is the spectral density as a function of the frequency as defined in Equation 2.14 [DNVGL-RP-C205, 2010].

$$\begin{aligned} u(x,t) &= \sum_{j=1}^{N} A_j \omega_j \frac{\cosh k_j(z+d)}{\sinh k_j d} \cos(\omega_j t - k_j x + \phi_j) \\ \dot{u}(x,t) &= \sum_{j=1}^{N} -A_j \omega_j^2 \frac{\cosh k_j(z+d)}{\sinh k_j d} \sin(\omega_j t - k_j x + \phi_j) \end{aligned} \tag{2.15}$$

$$A_j = \sqrt{2 S_\zeta(\omega) \Delta\omega} \tag{2.16}$$

Wave statistics

For normal cable lay simulations the the statistical behaviour of sea states is of importance. A single sea state can have infinitely many time domain representations, depending on the set of random phase angles used to generate the time domain representation. The statistics of waves are described based on the assumption that the wave elevation is a stationary, Gaussian process. Based on this assumption, the distribution of the maximum crest height per wave can be described by a Raleigh distribution, from now on denoted as Q_{crest}. The only parameter on which this Rayleigh distribution is dependent is the 0^{th} order spectral moment, m_0, of the wave spectrum. The 0^{th} order spectral moment is defined by Equation 2.17

$$m_0 = \int_0^\infty S_\zeta(f)\, df \tag{2.17}$$

Now the probability distribution of a single wave crest is known, the most probable maximum during a time domain representation of the sea state can be estimated. The probability distribution of the maximum wave in a time domain representation of the sea state is defined as $(1 - Q_{crest})^N$, where N is the number of waves contained in the time history. The Most Probable Maximum (MPM) wave elevation during a sea state is equivalent to the mode of the probability distribution and can be found by Equation 2.18.

$$\text{mod}(\underline{\eta}_{\text{max,crest}}) \approx \sqrt{2 \ln N} \sqrt{m_0} \tag{2.18}$$

Figure 2.12 shows the value of $\sqrt{2 \ln N}$ as function of N, the number of waves contained in the sea state representation. The graph shows the value of $\sqrt{2 \ln N}$ starts to flatten for higher N, meaning the maximum probable values becomes insensitive for additional waves added to the time domain representation. The required simulation time for a normal lay analysis is three hours, as defined in DNVGL-RP-N103 [2017]. For waves with a mean zero crossing period of eight seconds, the MPM

wave elevation during a three hour simulation is given in Table 2.2, together with the effect of simulation elongation on the MPM wave elevation. In this table the increase of the MPM wave elevation with respect to the three hour simulation value is indicated by the column labeled 'Error'.

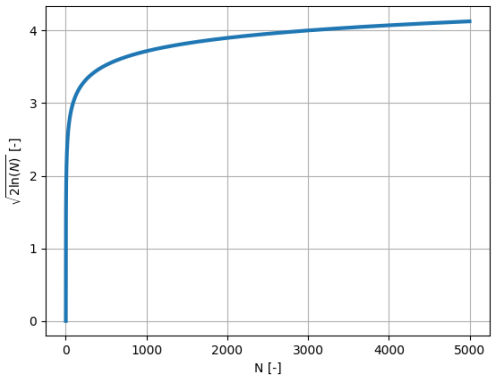

Figure 2.12: The dependency of $\sqrt{2\ln N}$ on the number of waves N.

Table 2.2: The effect of simulation time for a sea state with mean zero crossing period of 8 seconds.

N	Simulation time	$\sqrt{2\ln N}$	Error
1350	3 h	3.80	-
2025	4.5h (+50%)	3.90	2.63%
2700	6h (+100%)	3.98	4.73%

Current

Current originates from the circulation systems in the ocean. Examples are the tidal circulation or circulation due to a difference in sea water density. The result is a steady current profile with constant velocity over a limited time span. The resulting current force originates from the drag forces on the cable caused by the current velocity. Variations in current are generally slow, therefore current can be considered a static load within the reference frame of cable installation. The resulting force can be determined by the drag term of the Morison equation, which is discussed in Figure 2.5.3

Morison equation

Hydrodynamic loads result from movements of a structure through water. These movements can be induced by the movement of the structure itself or by waves and current water particle kinematics, as described in subsection 2.5.3 and Figure 2.5.3. The resulting hydrodynamic loads can be approximated by Morison's equation, given in Equation 2.19 [Faltinsen, 1990]. The first term in this equation is related to viscous effects and describes the drag forces on the body. The second and third term represent the inertia forces. The inertia forces can be subdivided into the hydrodynamic mass force and the undisturbed wave pressure force (Froude-Krylov force). Important to note is that the undisturbed wave pressure force is independent of the movement of the body itself. Morison's equation is valid for slender structures, were the structure itself does not change the characteristics of the forcing wave. Therefore it is commonly used to describe the hydrodynamic loads on subsea power cables [Sævik, 2017].

$$dF_n = \frac{1}{2}\rho_w C_{D,n} D|(u_n - \dot{r})|(u_n - \dot{r})dz + \rho_w(C_M - 1)A(\dot{u}_n - \ddot{r})dz + \rho_w A\dot{u}_n dz \tag{2.19}$$

In Equation 2.19 dF represents the force on a cable element of length dz. The diameter of the cable is given by D and A represents the dislocated fluid per unit length. The mass and drag coefficients, C_D and C_M, are dependent on many different effects and parameters including, the Reynolds number, form of the body and sea-floor effects. This explains why there is no straight forward way to determine the mass and drag coefficient for a specific situation. As a result the mass and drag coefficient should be determined empirically. u_i and $\dot{u}_i$ represent the water particle velocity and water particle acceleration normal to the midpoint of the element, respectively. The lift forces resulting

from vortex shedding around the cylinder are not considered by the Morison equation. The third element in Equation 2.19 is not dependent on the acceleration of the body, which signifies that this represents the wave pressure force.

2.5.4. Operational loads

Vessel motions can be described by a Response Amplitude Operator (RAO). The RAO relates the incoming wave to the corresponding vessel motions. The RAO is defined for each degree of freedom of the vessel and for a discretis ed set of wave headings. The RAO is a complex amplitude operator, which means both the magnitude and phase of the corresponding vessel motion are transferred. The relation between the wave height, RAO and heave motion of the vessel is given in Equation 2.20. This shows that the RAO is a function of the frequency of the incoming wave. Based on this relationship, it is clear that the relation between the vessel motion and wave height is linear. Therefore the use of RAO's exiles non-linearities between the incoming waves and the vessel motions.

$$z_{vessel} = RAO(\omega) z_{\text{wave}} \tag{2.20}$$

The RAO's of a vessel are dependent on waterdepth. This is mostly due to the effect of the seabed on wave radiation, which effects the motion of the vessel. The roll damping of a vessel is mostly governed by viscous damping along the hull [Ultramarine, 2011]. An example of a heave RAO is given in Figure 2.13. Based on this graph, it can be concluded that for very long period waves, corresponding to long wavelengths, this vessel will move up and down with the wave, thus the RAO amplitude is one. For shorter waves, the vessel is less effected in heave motion and moves in heave direction with a specific fraction of the incoming wave height.

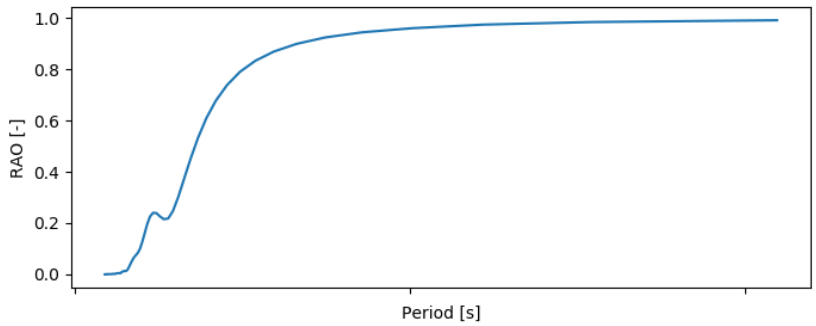

Figure 2.13: Example of heave RAO of CLV vessel.

2.5.5. General cable behaviour

In this section the general behaviour of the cable is explained by the use of simplified methods. The aim is to get an impression of the effect the vessel heave motion has on the tension and curvature found in the cable. For the tension in the cable it is generally easy to create a simplified model, which is given in Figure 2.5.5. For the curvature the response to movements of the vessel this is somewhat harder, therefore this effect is studied in the static configuration.

Curvature

The changes in the curvature in the cable are studied using the catenary equation described in subsection 2.5.2. An important note it that the shape of the catenary is an approximation to the static configuration, thus dynamic effects are not accounted for in this approach. However, it can be used to get a basic understanding of the change in curvature due to a excitation of the CLV in heave direction.

Figure 2.14 gives the static configuration of the cable, and the change in this static configuration due to a 1m and 2m heave excitation of the vessel. The corresponding curvature along the full arc length of the cable is given in Figure 2.15. Based on these plots, it is concluded that the curvature in the sagbend area increases due to heave excitation of the CLV, while the curvature near the connection of the cable to the CLV decreases.

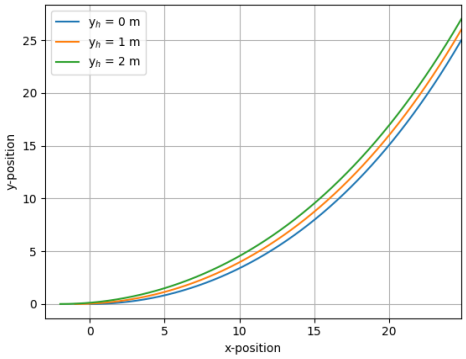

Figure 2.14: Change in catenary configuration due to heave excitation, for H = 25m and ws = 418N.

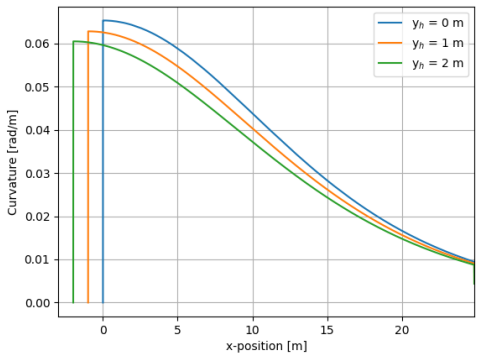

Figure 2.15: Change in curvature along the arc length of the cable due to heave excitation.

Tension

The simplified model for the tension response is given in Figure 2.16. The tension response in this model is described by means of a 1-DOF dynamic model, which means only heave motions of the vessel are considered. Here K represents the stiffness of the system, which is a combination of the stiffness of the cable itself and the geometrical stiffness of the system with respect to vertical motions. Likewise, C represents the damping in the system to vertical movement, which is a combination of multiple mechanisms, like drag damping and internal damping in the cable. Based on an equilibrium in the vertical direction, the tension in the cable can be found by Equation 2.21. It is concluded that any positive vertical vessel motion is associated with an increase in the top tension of the cable.

$$T = M_{\text{cable}}\ddot{x}_h + C\dot{x}_h + Kx_h + M_{\text{cable}}g \tag{2.21}$$

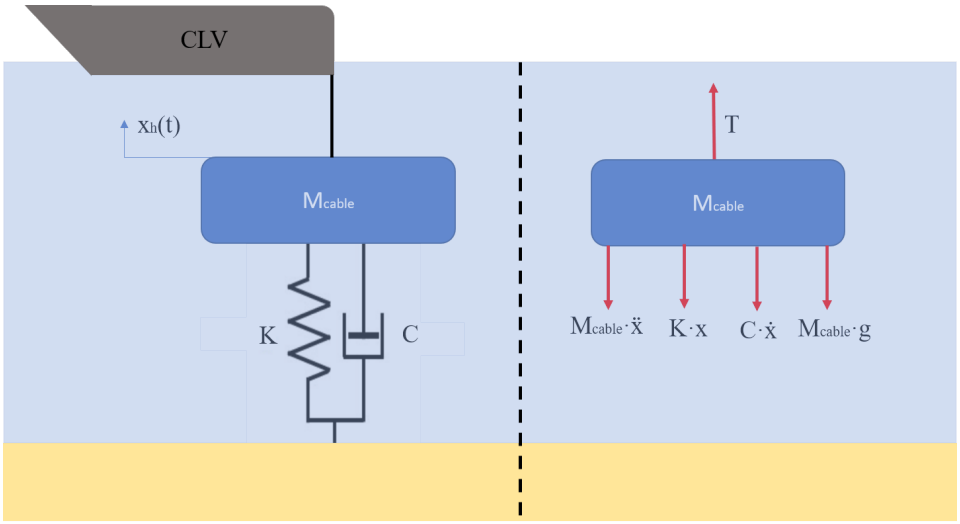

Figure 2.16: Left: Simplified 1-DOF cable tension model. Right: FBD of simplified tension model.

3

Dynamic cable lay model

The dynamic cable lay model is built in Orcaflex. Orcaflex is a 3D non-linear time-domain finite element software for dynamic analysis of marine structures. Orcaflex is selected for the excecution of this thesis due to its high reputation in the offshore industry, aswell as the in house expertise regarding the sofware package at Van Oord. First, the set-up of the normal lay model is described in section 3.1. Second, the base case considered in this thesis is presented in section 3.2. The calculation procedure used by Orcaflex is outlined in section 3.3 and section 3.4 for the static and dynamic calculation, respectively. Finally, the non-linearities involved with the modelling of the normal lay installation are discussed in section 3.5

3.1. Model set-up

An overview of the model is given in Figure 3.1. The model is build out of three main components: the cable, the CLV and an elastic shape element representing the chute of the CLV. Additionally, the seabed and seawater are found in the model. The model, including identification of the different components, is given in Figure 3.1. The cable is modelled as a line by the use of line segments in Orcaflex. The cable modelling is discussed in more detail in subsection 3.1.1. The characteristics of the elastic shape element are found in subsection 3.1.3. The modelling of the CLV, the Nexus, is elaborated on in subsection 3.1.2. The soil model is described in subsection 3.2.3 and the friction model in subsection 3.1.5.

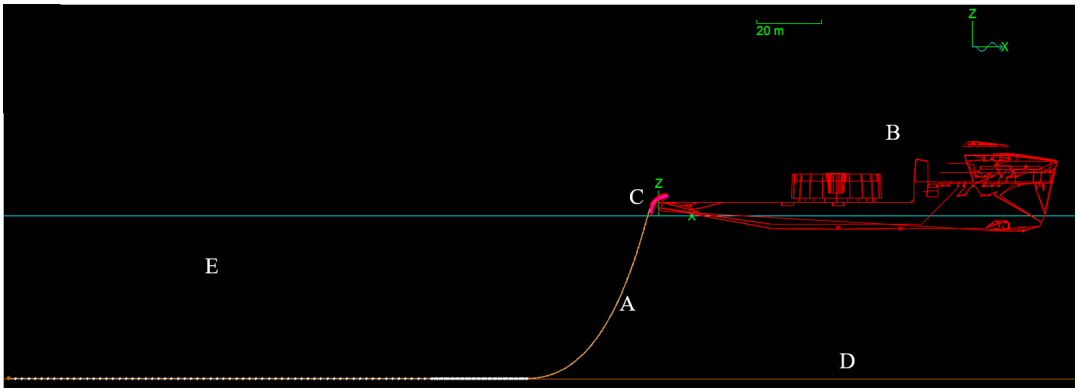

Figure 3.1: Overview of the normal cable lay model in Orcalfex. A) Cable B) CLV C) Chute D) Seabed E) Seawater

3.1.1. Cable

Orcaflex uses a lumped mass model to represent the cable structure. In this type of model the masses are lumped together and connected by springs. A detailed overview of the lumped mass model is given in Figure 3.2. The nodes represent the lumped masses of the cable, while the segments are the springs connecting the lumped masses. The nodes carry the properties of the cable, like weight, buoyancy and drag and inertial forces. All axial and torsional properties are contained in the springs. The bending stiffness of the cable is modelled by a rotational spring damper system between the axial direction of the node $\mathbf{n}_z$ and the axial direction of the segment $\mathbf{s}_z$. Similarly, the axial stiffness is modelled by a displacement spring damper system along the longitudinal of the line segment. One end of the cable is connected to the vessel at the top of the chute. The second end of the cable is anchored to the seabed. The axial anchoring is required to limit the size of the model, as the axial friction must act over a long distance in order to keep the cable in place. In this construction it is important to keep an eye on the shear forces at the second end of the cable. These should stay low in order to give a realistic representation of the normal lay operation in the model and thus govern the location of the anchoring position.

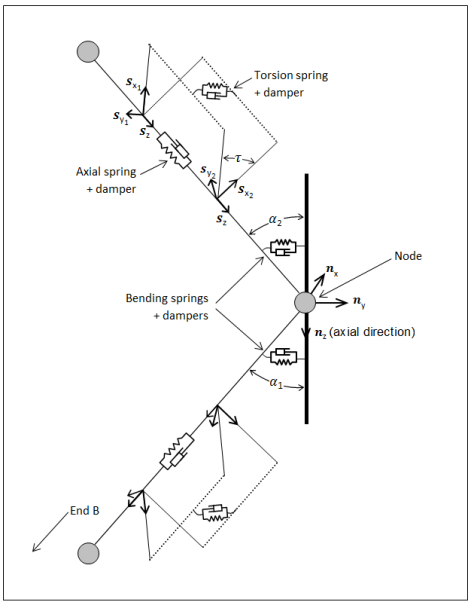

Figure 3.2: Detailed overview of lumped mass method for cable modelling.

3.1.2. Vessel

The Nexus is modelled using a vessel object in Orcaflex. The movements of the vessel are described by the use of displacement RAOs, which were already discussed in subsection 2.5.4. The origin of these RAOs is described with respect to the local reference frame of the vessel, which is a right handed axis system at the vessel origin. The wave heading definitions with respect to the vessel orientation in Orcaflex, together with the local reference frame of the vessel, are depicted in Figure 3.3.

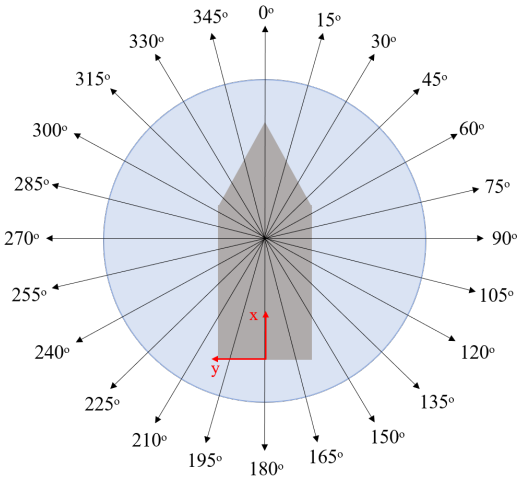

Figure 3.3: Wave headings and local vessel reference frame.

3.1.3. Chute

The chute is modelled by means of an elastic shape element in Orcaflex. An elastic shape element represents a physical barrier for lines. Upon contact between the chute and the cable, a normal force

and frictional force are generated. This type of object allows for penetration by lines, which means the cable penetration into the chute results from the axial stiffness of the chute. The frictional force is defined by the friction model as described subsection 3.1.5. Therefore the elastic shape element is used to properly model cable-chute interaction in the normal lay model.

3.1.4. Soil modelling

The seabed is modelled by the elastic seabed model. The modelling of the soil can be divided into three sub compartments, namely the behaviour of the soil in the normal and axial and transverse direction. The contact normal to the soil is modelled using distributed elastic springs and distributed dampers. The interaction force depends on the spring stiffness and indentation depth. For each element having one or two nodes making contact with the seafloor the corresponding spring stiffness and damping is added to the stiffness matrix and damping matrix of the element accordingly.

The axial and transverse reaction of the soil is modelled by the friction model in Orcaflex. The model is described in subsection 3.1.5. In real life the soil-cable interaction is much more complicated, as it includes effects like soil displacement and accumulation due to the movement of the cable.

3.1.5. Friction model

A modified Coulomb friction model is used to define the frictional forces in the model. The reaction forces are modelled by a spring stiffness in combination with a friction coefficient. The overall effect is graphically illustrated by Figure 3.4. The frictional force acts as a distributed spring with constant stiffness, the shear stiffness, until the maximum friction force is exceeded and the element starts to slide, without further force increase. The maximum friction force is given by $f_{\text{friction,max}} = \mu R$, where μ is the friction coefficient and R the normal reaction force acting on the element. The corresponding D_{crit} can be found as function of the shear stiffness k_s and the contact area a_s by Equation 3.1

$$D_{crit} = \frac{\mu R}{k_s a_s} \tag{3.1}$$

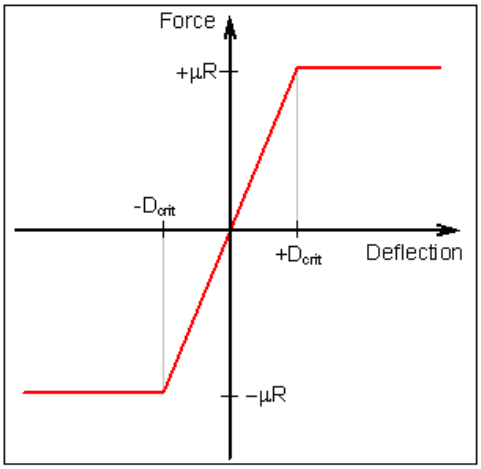

Figure 3.4: Wave headings and local vessel reference frame.

3.2. Model description

The analysis performed in this study are conducted using a base case. Lateron, in the sensitivity analysis some input parameters of the model are changed to investigate their influence on the results. The changed parameters are provided in the sensitivity analysis itself. The input parameters to the model are discussed in the following sections.

3.2.1. Cable type

The cable used in the base cable is an export cable with linear bending stiffness. A summary of the cable properties is provided in Table 3.1. The drag coefficient of the cable is modelled as a Reynolds dependent drag coefficient for a rough cylinder. Its dependency on the Reynolds number is displayed in Figure 3.5. The large drop in the magnitude of the drag coefficient occurs upon the

change from laminar to turbulent flow Triton [1988]. This is a conservative approach as the drop seen in the drag coefficient is much larger for smooth surface cylinders.

Table 3.1: Properties of export cable in base case model.

Mass	100 [kg/m]
Diameter	0.267 [m]
Bending stiffness	90 [kN·m^2]
Axial stiffness	525·10^6 [kN]
Torsional stiffness	185 [kN·m]
T_{max}	225 [kN]
MBR_{min}	4.10 [m]

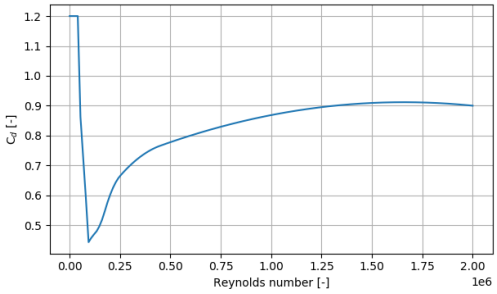

Figure 3.5: Dependency of C_D on Reynolds number for rough cylinder.

3.2.2. Wave parameters

Both regular and irregular wave simulations are executed for the base case. For the irregular wave simulations the JONSWAP spectrum is used as input spectrum. The peak enhancement factor of the JONSWAP spectrum is displayed in Figure 3.6, following the DNVGL-RP-C205 [2010] guidelines. The base case deals with unidirectional waves with a wave heading of 180deg.

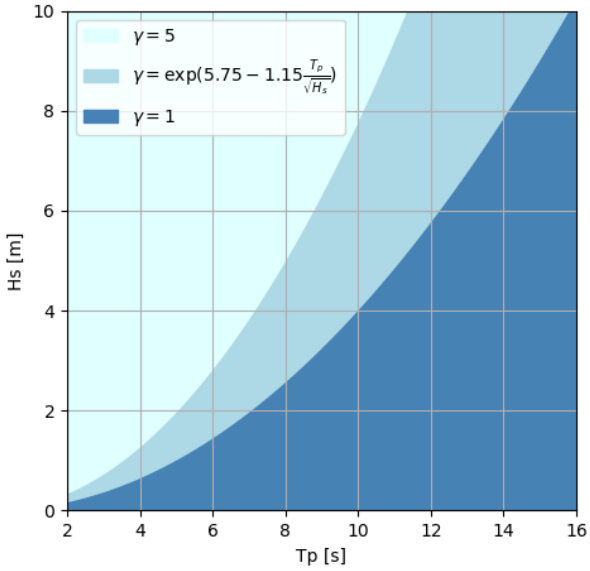

Figure 3.6: Peak shape factor for different T_p and H_s combinations.

3.2.3. Soil description

The soil properties used in the base case definition are summarized in Table 3.2. The soil properties are based on typical soil properties found in API RP 17B [2002]. Damping is not included for the soil in the base case model.

Table 3.2: The properties of the soil in the base case model.

Normal stiffness	**Shear stiffness**	**Normal friction**	**Axial friction**
100 [kN/m/m^2]	100 [kN/m/m^2]	0.6 [-]	0.6 [-]

3.3. Static calculation

The static configuration corresponds to the configuration where the internal loads in the structure are in equilibrium with the external loads applied to the system. This configuration is determined by use of the static analysis procedure. The static analysis comprises of two steps. First the line statics are determined while all other object are fixed. This is done by the static catenary analysis and the static finite element analysis. The static catenary analysis is based on the principles as discussed in subsection 2.5.2. It is used as a supplement to the finite element analysis, as it is less time consuming. It provides an initial estimate for the configuration of the cable for the static finite element analysis.

In the first step the line statics are determined, while all other objects are fixed. In the last step of the statics, all DOF are released and Orcaflex uses Newton-Raphson iteration to find the statics of the whole system. In this iteration method, the incremental displacement is determined based on the stiffness of the system in the previous configuration. Iteration is continued until the convergence criteria are met or until the predefined number of iteration steps is reached.

3.3.1. Static configuration

The static configuration of the base case model is determined by means of the static calculation. An important parameter to obtain static convergence is the mesh size of the cable. Therefore a mesh size sensitivity analysis is performed during the static calculation. The goal is to obtain proper convergence and smooth results along the catenary of the cable. The analysis is based on the variation of the curvature in the static analysis. This parameter has large fluctuations along the length of the cable due to it's configuration and is therefore a good indicator.

The static analysis is performed for four different mesh sizes, ranging from 0.25m and 2m. The mesh sizes considered are: 0.25m, 0.5m, 1.0m and 2.0m. Due to the catenary shape of the cable during installation, there are three sections where the variation of the curvature is the highest: near the connection to the CLV, in the overbend and near the TDP. In these areas the mesh size is most critical, therefore the analysis is focused on these area's.

The curvature near the connection to the CLV, in the overbend and around the TDP are presented in Figure 3.7, Figure 3.8 and Figure 3.9, respectively. The two largest mesh sizes, 1m and 2m, show quite some deviations in all of the inspected areas of the catenary. The most critical area seems to be the area around the top of the catenary. As a rule of thumb, often a cable mesh size of 2-3 times the diameter of the cable is used. Given this, the fact that the curvature in the sagbend area is of most interest and the fact that decreasing mesh size increases computational time, a mesh size of 0.5m is selected. For the first element of cable Orcaflex uses a reduced mesh size by itself, making that the selection of a mesh size of 0.5m will not compromise the accuracy in the results of the top tension of the cable.

The tension and lay angle in the static configuration can be altered by changing the length of the cable in the model, as the connection points remain fixed. For the base model the static configuration parameters are found in Table 3.3. The parameters are chosen such that they comply with both the allowable departure angles of the Nexus and the typical TDP tensions for a typical normal lay configuration (T_{TDP} =±3-10 [kN]).

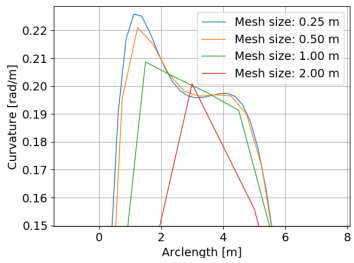

Figure 3.7: Mesh size sensitivity near the connection to the CLV.

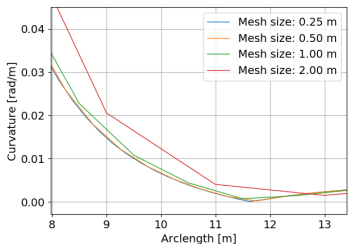

Figure 3.8: Mesh size sensitivity in the sagbend area.

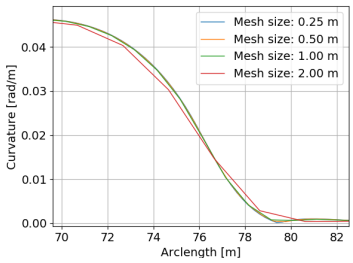

Figure 3.9: Mesh size sensitivity near the TDP of the cable.

Table 3.3: Parameters characterising the static configuration of the base case model.

TDP tension [kN]	**Top tension [kN]**	**Lay angle [deg]**
7.37	35.5	16.6

3.4. Dynamic calculation

In this thesis the dynamic calculations are carried out in time domain in order to fully account for the non-linear behaviour of the system. The time domain simulations start with a ramp up phase, in which the vessel motions are slowly increased to the full magnitude. This is done in order to reduce transient responses, which eventually reduces the required simulation time.

In the dynamic analysis the equation of motion given in Equation 3.2 is solved for each time step. Here M is the inertia load on the system, C the damping load in the system, K the stiffness load and F the external load on the system. These loads are dependent on p, the position, v, the velocity, and a, the acceleration, of the system, which in their turn are dependent on time. The system geometry is updated for each time step making sure the full non-linear behaviour of the system is taken into account. Either an implicit or explicit integration scheme can be used by Orcaflex to perform the numerical integration.

$$M(p,a) + C(p,v) + K(p) = F(p,v,t) \tag{3.2}$$

Explicit time integration uses the current state of the system to calculate the state of the system at the end of the time step. This means the acceleration at the beginning of the time step is determined by the dynamic equilibrium equation. The velocity and position at the end of the time step follow from integration of the acceleration and velocity, respectively. Explicit time integration requires a small time step in order to produce stable results.

In an implicit scheme the dynamic equilibrium equations are solved at the end of the time step. Implicit integration is an iterative process as p, v and a are unknown at the end of the time step. This iterative nature causes the computation time of a single time step to be longer for implicit integration than explicit integration. However the method is much more stable, and therefore longer time steps are allowed. This feature often makes the implicit time integration scheme faster, making this the method of choice in this thesis.

3.5. Non-linearities in cable lay model

As mentioned above the system is solved in the time domain in order to be able to fully account for the non-linear behaviour of the system. Below, the non-linearities contained in the model are discussed to give insight in the non-linear behaviour of the model

3.5.1. Geometric non-linearity

A geometrically non-linear system characterizes itself by a change in the geometric stiffness of the system due to a change in the geometry. This is the case when the position of the components becomes significantly different than the initial state. In a system subject to rotation this already becomes important for small angular rotations, because the linear approach assumes $\sin(\theta) = \theta$ and $\cos(\theta) = 1$. Therefore, geometrical non-linearity is for cables already important in small deformation analysis [Peksen, 2018] [NTNU, cited August 2020].

In Orcaflex the geometry of the cable is updated for every time step. The stiffness matrix is updated accordingly, taking full account of the geometric non-linearities. Two causes of the geometrical non-linearity in the cable system are rotations and tension stiffening. Tension stiffening refers to the phenomen where an axial load in the cable contributes to the stiffness of the cable in the transverse direction. This requires an update of the geometrical stiffness matrix of the system.

3.5.2. Non-linear boundary condition

In the dynamic analysis of the cable model as described above, the position of the TDP changes in time. Figure 3.10 shows an example of this variation. In the figure the highlighted elements show the variation of the TDP along the arc length of the cable. Within this range the cable sometimes is in contact with the seabed, and sometimes not. This movement of the TDP introduces a non-linearity into the system. For the nodes contained in the highlighted part of the cable, the inclusion of the soil contact forces in the equation of dynamic equilibrium depends on whether the node is in contact with the soil at its instantaneous position. The movement of the TDP is accompanied with the introduction of impulse loads in the system. This type of non-linear behaviour is classified as a contact of boundary non-linearity. In addition it is possible to model the hysteretic behaviour of the soil, however in the soil model described in subsection 3.2.3 this is not included.

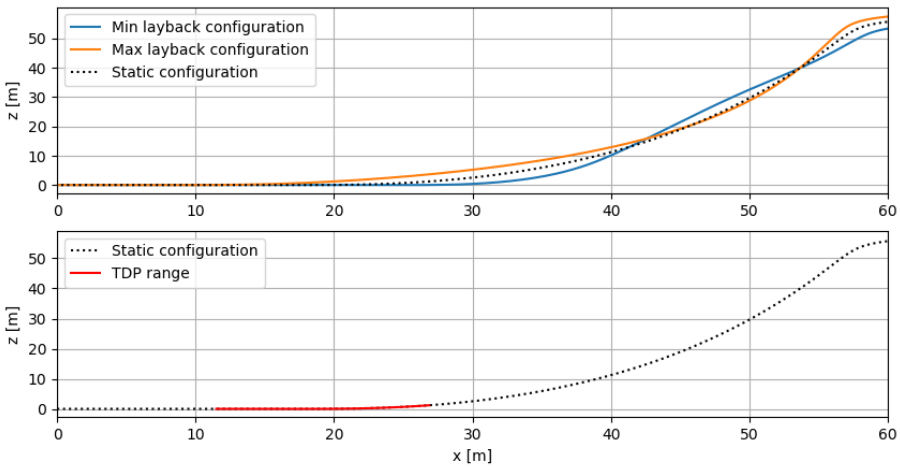

Figure 3.10: The configuration of the cable corresponding to minimum and maximum layback together with the corresponding TDP range displayed in the static configuration of the cable, based on a Hs=2.5m, Tp=8s seastate.

3.5.3. Drag non-linearity

The principle of a drag force on slender structures when the structure moves through water was already discussed in Figure 2.5.3. From Equation 2.19, it is concluded that the drag force on the cable is proportional to the relative velocity of the cable squared, as given in Equation 3.3. Therefore, the drag force introduces a non-linearity into the model.

$$F_D \propto (u_n - \dot{r})|u_n - \dot{r}| \tag{3.3}$$

4

Vessel motion limit criteria assessment

In this chapter the vessel motion limit criteria assessment is performed. The aim of this assessment is to identify the strengths and weaknesses of the use of vessel motion limit criteria in normal lay analysis. First, the location of the maximum cable response is studied in section 4.1. Second, the contribution of the vessel motions to the full cable dynamics is identified in section 4.2. The most suitable vessel motion for application of vessel motion limit criteria is identified in section 4.3. Finally, the use of vessel limit criteria is compared to the current practice, wave limit criteria, in section 4.4.

4.1. Location of cable response

This study comprises the maximum tension response and maximum curvature response of the cable to vessel motions and direct cable loads. The location of this cable response is important when studying the results, therefore the first step is identification of the location of the maximum cable response of different inputs. This location is investigated on the basis of regular wave simulations.

The maximum tension in the cable is always found in the first node of the cable, which corresponds to the top of the cable, where the cable is connected to the CLV in the Orcaflex model. The location of the maximum curvature response of the cable is found to be dependent on both wave period and wave height. Figure 4.1 gives the spreading of the location of maximum curvature for a variety of wave periods and for a specific wave height. The general observation is that the spreading of the location of the curvature increases as the wave height increases.

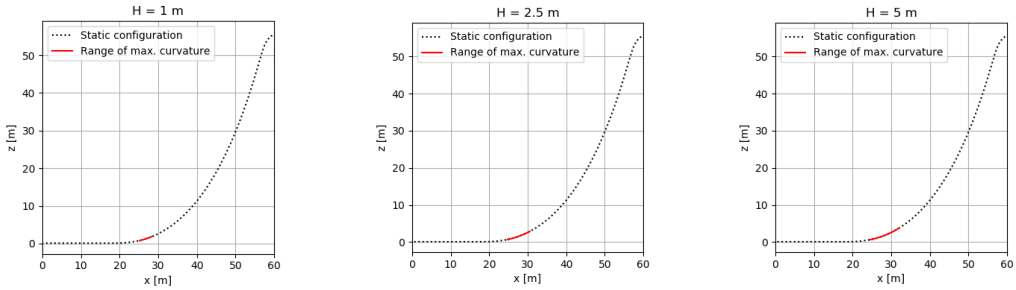

Figure 4.1: The variation of the location of maximum curvature for wave periods between 3 to 25 seconds.

Figure 4.2 provides a more detailed view on the spreading of the location of the maximum curvature.

In light of the results in Figure 4.2, the configuration of the cable during the occurrence of the maximum curvature in the cable is studied. The results are presented in Appendix A.1. Both the effect of the wave period and the effect of the wave height on the location of the maximum curvature are examined. It is found that the shape of the cable at the moment the maximum curvature occurs, is changing with both the wave period and the wave height to which the system is subjected. For short period waves, the configuration is similar to the catenary shape of the cable, resulting in a graduate curvature change in the sagbend of the cable. Therefore the location of the maximum curvature is prone to large changes, as the whole area is subject to significant curvatures and a small change in the configuration can lead to a large change in the location of the maximum curvature.

For longer period waves, the shape of the cable gives a more straight profile up to the sagbend, where the curvature along the arc length changes rapidly. For periods ranging from 10-25s, the location of the point of maximum curvature is approximately constant relative to the TDP for each specific wave height. However, the shape of the cable along the catenary is slightly less straight for longer wave periods, causing it to take up slightly more cable which explains the graduate increase in the arc length location. Increasing the wave height in this same area also results in a more straight cable configuration, making the area near the TDP to be located at smaller arc lengths and explaining the distinction in the location of maximum curvature for varying wave height. Concluding, the general behaviour of the cable changes with wave height and wave period, where larger wave heights and longer wave periods result in a more straight cable configuration compared to the more catenary like shape for shorter periods and wave heights at the moment of maximum curvature.

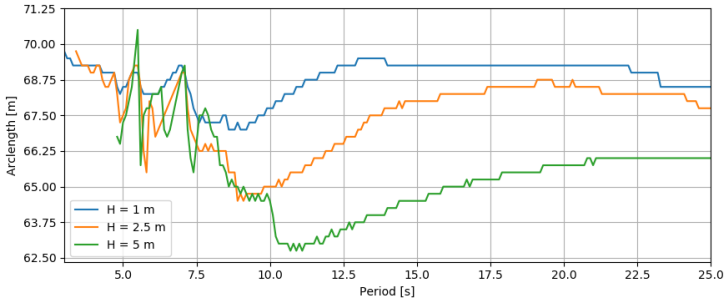

Figure 4.2: The variation of the location of maximum curvature for varying regular wave input.

As final step in the analysis of the location of the maximum curvature, snapshots of the cable movement are generated. The snapshots are created for T_{wave} = 5.5s and T_{wave} = 12.5s and they show the cable configuration at $\frac{1}{2}$ and $\frac{1}{4}$ wave period before and at $\frac{1}{2}$ and $\frac{1}{4}$ wave period after the occurrence of the maximum curvature. This way the full cycle of the cable movement is depicted. The results are presented in Figure 4.3 and Figure 4.4, for T_{wave} = 5.5s and T_{wave} = 12.5s, respectively. For T_{wave} = 5.5s the configuration shows small fluctuations around the catenary configuration, while for T_{wave} = 12.5s the shape of the cable changes significantly during a wave cycle. In the cable response cycle to a longer period wave, T_{wave} = 12.5s, the straight maximum curvature configuration results from a reduced layback distance in combination with the mid-section of the cable having a delay in response to the new configuration, which is caused by the inertia and drag force resisting the movement of the cable through the water. The TDP moves forward due to the weight of the cable itself. In the bottom graph of Figure 4.4, which displays the behaviour of the cable after the occurrence of the maximum curvature, the delay in the response of the mid-section is clearly visible between the cable configuration of $\frac{1}{4}T_{wave}$ and $\frac{1}{2}$ T_{wave} after the moment of maximum curvature.

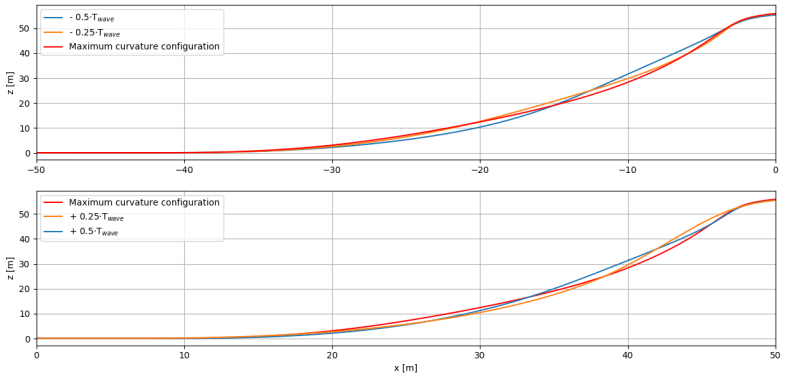

Figure 4.3: Variation of the cable shape at $\frac{1}{4}$ T$_{wave}$ and $\frac{1}{2}$ T$_{wave}$ before and $\frac{1}{4}$ T$_{wave}$ and $\frac{1}{2}$ T$_{wave}$ after the occurrence of the maximum curvature for a regular wave of T = 5.5s and H = 5.0m.

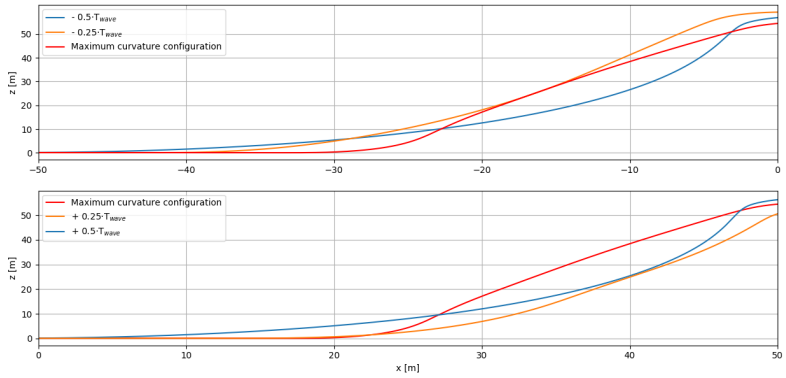

Figure 4.4: Variation of the cable shape at $\frac{1}{4}$ T$_{wave}$ and $\frac{1}{2}$ T$_{wave}$ before and $\frac{1}{4}$ T$_{wave}$ and $\frac{1}{2}$ T$_{wave}$ after the occurrence of the maximum curvature for a regular wave of T = 12.5s and H = 5.0m.

4.2. Contributions to cable dynamics

To assess the potential use of vessel motion limit criteria for normal lay analysis the individual contribution of the vessel motions and direct cable loads to the cable dynamics is studied. The cable dynamics in the two types of simulations described below are compared to the cable dynamics resulting from normal regular wave simulations.

Vessel motion based simulations: Only the vessel motions resulting from the regular wave input are included. The wave kinematics, and therefore direct cable loads, are discarded.

Direct cable loads based simulations: The movement of the vessel to the regular wave input is disregarded. Hence the wave kinematics are the only dynamic input considered in these simulations.

The differences in the maximum curvature and maximum tension response in the cable in the two types of simulations described above, and in normal regular wave simulations, are presented in Figure 4.5 and Figure 4.6, respectively. The presented results are for a wave height of five meters and for varying wave periods. An important side note on these plots is that due to the non-linear nature of the system, it is unknown whether the effects of direct cable loading and vessel motions cooperate or counteract each other in the regular wave simulations. A clear example of this behaviour is seen for a wave period of seven seconds, where the maximum curvature due to direct cable loads only, is higher than the maximum curvature resulting from both direct cable loads and vessel motions.

The aim of this analysis is to identify the effects which govern the cable dynamics. Ideally, the handling limits of the cable are described by the parameter which most effects the cable dynamics. Lack of this relationship can result in the limit criteria being fulfilled, while other parameters that effect the cable dynamics are changed in such a way that a handling limit is exceeded.

From inspection of both Figure 4.5 and Figure 4.6, it is found that for both the maximum curvature and the maximum tension in the cable the vessel motions are governing for longer wave periods, starting from eight seconds for both the maximum curvature and the maximum tension response. This is favourable for the application of vessel motion limit criteria. However, for short period regular wave input the dynamics of the cable are to a large extent governed by the direct cable loads. This is a direct result from the fact that the CLV hardly reacts to short period waves. Although short period waves with a waveheight of five meter are not likely to occur in a real sea states, this effects still persists for lower wave height simulations. This might jeopardise the use of vessel limit criteria especially in areas with sea states characterised by short peak periods. However, these types of sea states, characterised by short wave periods and low wave heights, are not likely to result in exceedance of the cable handling limits, which is beneficial for the use of vessel limit criteria.

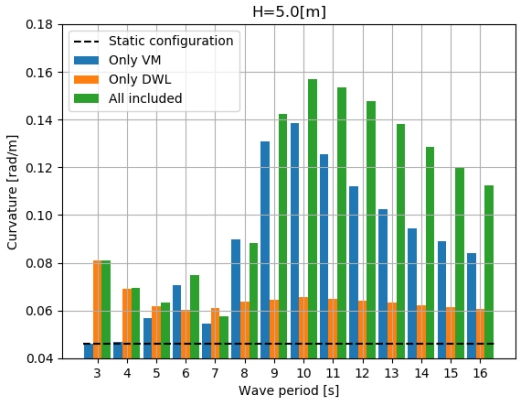

Figure 4.5: The maximum curvature in the cable during regular wave simulations with a) only vessel motions b) only wave kinematics and c) the full dynamic response.

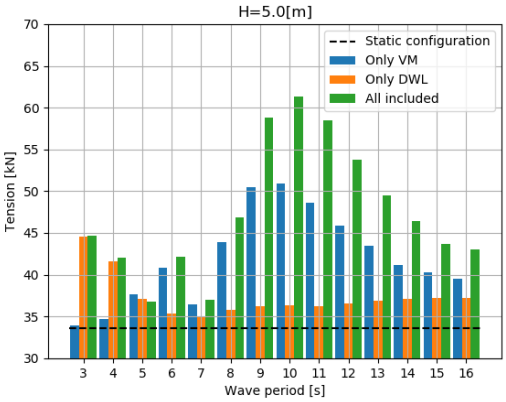

Figure 4.6: The maximum tension in the cable during regular wave simulations with a) only vessel motions b) only wave kinematics and c) the full dynamic response.

4.3. Vessel motion selection

The aim of this section is to identify the vessel motion governing the tension and curvature response of the cable. Later on, this knowledge is used for definition of the relation between the vessel movements at the chute of the CLV and the cable responses. In order to provide insight in the governing vessel motion, the Time Lagged Cross Correlations (TLCC) between the cable response and vessel motions at the chute of the CLV are determined based on a set of irregular wave simulations. The TLCC, detoned by the symbol $\rho^k_{i,j}$, is defined in Equation 4.1 [Dean, R. and Dunsmuir, W., 2016]. It is a function of the time lagged covariance $\gamma^k_{i,j}$ of the two signals and the standard deviation of each signal. The time lagged covariance can by found using Equation 4.2, where k presents the time step for which the TLCC is calculated. The TLCC is valued between minus one and one (-1$\leq \gamma_{i,j} \leq$ 1). The absolute value of the correlation gives an indication of the extent to which the signals are linearly related, and the sign is an indication of the nature of the signal, a negative or positive relation.

$$\rho^k_{i,j} = \frac{\gamma_{i,j}}{\sqrt{\sigma_i^2 \sigma_j^2}} \tag{4.1}$$

$$\gamma^k_{i,j} = \frac{1}{N} \sum_{t=1}^{N} \left[\left(x_i^t - \bar{x}_i \right) \left(x_j^{t+k} - \bar{x}_j \right) \right] \tag{4.2}$$

4.3.1. Curvature

The TLCC's between the motion of the chute and the curvature response of the cable element which experiences the maximum curvature during the full simulation, is presented in Figure 4.7 to Figure 4.12. The abbreviations used in the figures are documented in Table A.1 in Appendix A.2. The correlations are determined for a significant wave height of H_s=2.5m and for a peak period range of 6.0s$\leq T_p \leq$16.0s. In order to select the most suitable vessel motion, a set of selection criteria is established. An outline of the selection procedure is given below.

1. The maximum absolute correlation for each simulation is compared to the maximum correlation found between the cable response and the wave elevation. All vessel motions performing worse than the wave elevation are discarded. The correlation between the cable response and

wave elevation is set as lower boundary in order to select a parameter which performs better than the current parameter used to define limits in dynamic cable analysis.

2. It is checked if causality is possible between the vessel motion and cable response. This criterion requires the maximum absolute correlation to appear when the vessel motion is leading. In case the maximum absolute vessel motion is present for a leading curvature signal, a dependency deficiency is detected, as this correlation has no physical meaning.

3. In this step the vessel motions which are unfeasible based on theoretical dynamic behaviour of a cable are rejected. This is the case when the sign of the correlation is not in correspondence with the theoretically expected behaviour, see subsection 2.5.5.

4. In the last step of the selection, the remaining vessel motions are rated based on the absolute value of their correlation with the cable response.

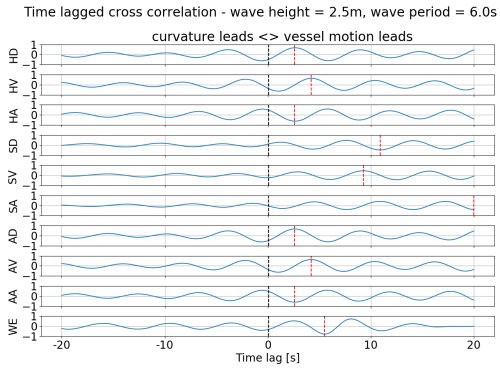

Figure 4.7: The TLCC of the curvature response of the cable for all vessel motions and the wave elevation, calculated for T_p = 6.0s H_s=2.5m.

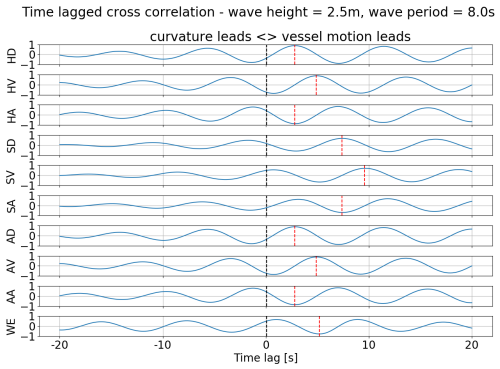

Figure 4.8: The TLCC of the curvature response of the cable for all vessel motions and the wave elevation, calculated for T_p = 8.0s H_s=2.5m.

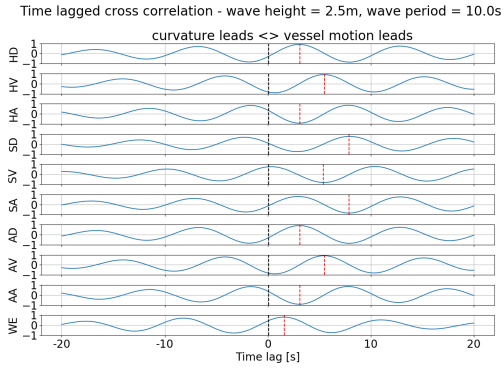

Figure 4.9: The TLCC of the curvature response of the cable for all vessel motions and the wave elevation, calculated for T_p = 10.0s H_s=2.5m.

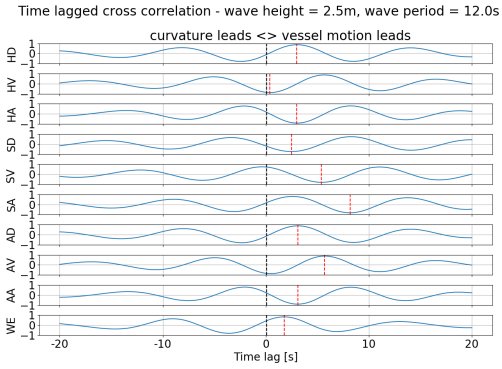

Figure 4.10: The TLCC of the curvature response of the cable for all vessel motions and the wave elevation, calculated for T_p = 12.0s H_s=2.5m.

The details of the analysis are presented in Appendix A.2. Heave acceleration and axial acceleration are identified as most suitable parameters for application of vessel limit criteria for the normal lay configuration considered in this assessment. For the application of vessel motion limit criteria, ideally a vessel motion with a as much as possible linear relationship to the cable response is selected, as this implies that an increase in the magnitude of the vessel motion is indeed related to an increase in the cable response. Thus, a vessel motion with a as high as possible TLCC is preferred.

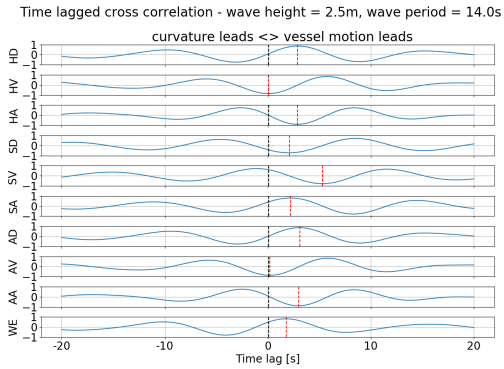

Figure 4.11: The TLCC of the curvature response of the cable for all vessel motions and the wave elevation, calculated for T_p = 14.0s H_s=2.5m.

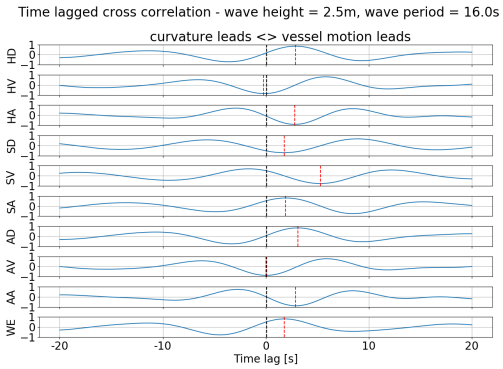

Figure 4.12: The TLCC of the curvature response of the cable for all vessel motions and the wave elevation, calculated for T_p = 16.0s H_s=2.5m.

Both of these vessel motions complied with the selection criteria mentioned above and overall have the highest absolute TLCC. The heave acceleration and axial acceleration were selected based on the negative TLCC value. The time lag between the heave acceleration time history and the maximum curvature response of the cable is between 2.5-3.5 seconds.

4.3.2. Tension

For the maximum tension response of the cable the same approach is followed as for the curvature response of the cable. The corresponding plots are presented in Appendix A.2. The results show similar behaviour as for the curvature response, only now the TLCC is positive. Therefore here also the heave acceleration and axial acceleration are identified as most suitable vessel motions for the application of vessel motion limit criteria.

4.4. Linear regression analysis

The last step of the vessel motion limit criteria assessment is to apply linear regression between, on one hand the peaks in the vessel motion and the peaks in the wave elevation time history, and on the other hand the corresponding peaks in the cable response. This can help to assess the applicability of vessel motion limit criteria compared to sea state limit criteria, as well as give preliminary insight in the possibilities to reduce the computational time involved with dynamic cable lay analysis. The analysis is applied to a sea state of H_s = 2.5m and T_p = 9.5s, as sea states in this range were identified as suitable for vessel limit criteria in section 4.2.

First an outline of the approach is given. The peaks and throughs, with at least an amplitude of 50% of the maximum elevation, in the vessel heave acceleration response are identified. As seen in section 4.3, a time lag of 2.5-3.5 seconds exists between the heave acceleration and both the tension and curvature response of the cable. Therefore, the maximum cable response in the 4 seconds after the occurrence of the peak/through in the heave acceleration is selected. The peaks in the heave acceleration time history are related to the occurrence of maximum tension in the cable, while the throughs are related with the maximum curvature response. The selected points are plotted in a scatter diagram, to which linear regression is applied. The 95% prediction bands are identified as well. These regions enclose 95% of the data and are an indication of the amount of spreading of the data around the linear regression. This same procedure is carried out for the wave elevation at the RAO origin of the vessel. However, the exact relation between the wave elevation and cable response with respect to the time lag is not studied and is partly related to the combined pitch and

heave response of the vessel. Based on observation of the most positive and most negative TLCC of the wave elevation in Figure 4.7 to Figure 4.12, the search domain is extended to 8 seconds and both the peaks and the throughs are studied in relation to the maximum tension and the maximum curvature in the cable.

The results for the maximum curvature response are given in Figure 4.13 and Figure 4.14. The curvature in relation to the wave elevation peaks is added in Appendix A.3. In the same manner, the results for the maximum tension response are given in Figure 4.15 and Figure 4.16 for the heave acceleration and wave elevation peaks, respectively. The results of the maximum tension with respect to the wave elevation throughs is added in Figure A.10 in Appendix A.3.

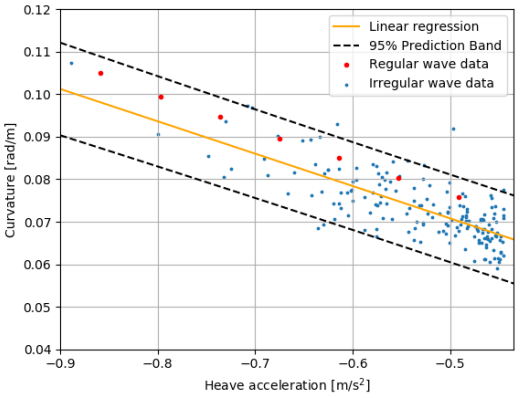

Figure 4.13: Linear regression, including 95% predictions bands, between the maximum curvature and heave acceleration throughs for T_p=9.5s and H_s =2.5m.

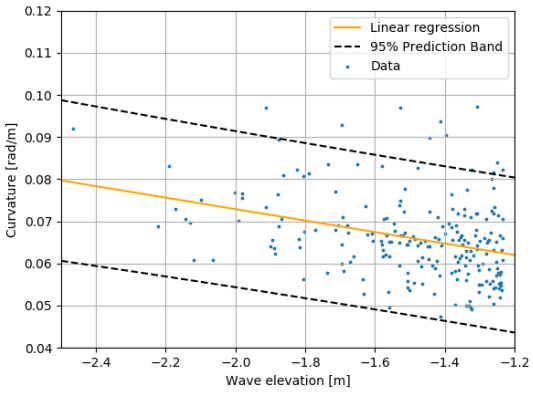

Figure 4.14: Linear regression, including 95% predictions bands, between the maximum curvature and wave elevation throughs for T_p=9.5s and H_s =2.5m.

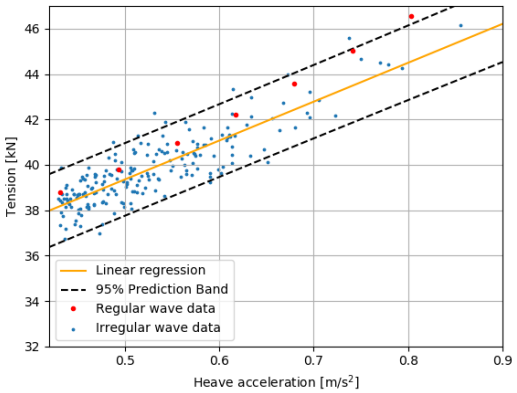

Figure 4.15: Linear regression, including 95% predictions bands, between the maximum tension and heave acceleration peaks for T_p=9.5s and H_s =2.5m.

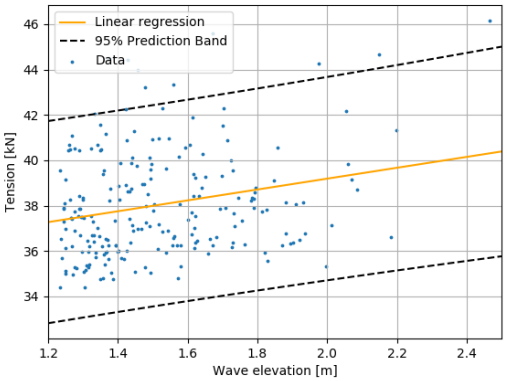

Figure 4.16: Linear regression, including 95% predictions bands, between the maximum tension and wave elevation peaks for T_p=9.5s and H_s =2.5m.

For the application of vessel motion limit criteria, two aspects are of importance. First of all the slope of the linear regression line, as this identifies whether an increase in the limit parameter is also related to an increase in the cable response. Another important aspect is the width of the 95% prediction bands, which signifies the spreading of the observations around this trend. Higher spreading results in a less suitable limit parameter. The slopes and accompanied band widths are given in Table 4.1. These support the observations which can already be identified based on the plots. The slopes associated with vessel motion limit criteria show higher values compared to the linear

Table 4.1: Slopes and 95% prediction band widths of the linear regression.

Correlation	Slope	95% prediction band width
Curvature - HA	-0.076 $[\frac{rad \cdot s^2}{m^2}]$	0.010 [rad/m]
Curvature - WE (through)	-0.0136 $[\frac{rad}{m^2}]$	0.013 [rad/m]
Curvature - WE (peak)	0.0143 $[\frac{rad}{m^2}]$	0.018 [rad/m]
Tension - HA	17.15 $[\frac{kN \cdot s^2}{m}]$	1.62 [kN]
Tension - WE (peak)	0.8 $[\frac{kN}{m}]$	4.48 [kN]
Tension - WE (through)	-3.4 $[\frac{kN}{m}]$	4.11 [kN]

trend resulting from the wave elevation, for both the maximum curvature and the maximum tension response. Taking into account the fact that the magnitude range of the heave acceleration excitation is approximately 2-3 times smaller than the wave elevation range for this sea state, the relative steepness of the slope of the heave acceleration linear regression line is still higher. This means that an increase in the heave acceleration is stronger related to an increase in the cable response than the wave elevation, making heave acceleration a more suitable limit parameter. Furthermore, the bandwidth of the 95% prediction interval is significantly smaller for heave acceleration limit criteria compared to wave elevation limit criteria. This means higher certainty can be given to limits expressed in the heave acceleration compared to wave elevation, which eventually has a positive influence on the workability.

Finally, as a first step towards simplification of the dynamic cable lay analysis the trend observed based on regular wave analysis is added to the plots in Figure 4.13 and Figure 4.15. For the curvature response the regular wave results are all within 95% prediction band, but an over prediction with respect to the linear regression is present. For the tension response the regular wave results are providing an over prediction as well, but the results for higher regions of the heave acceleration fall outside the 95% predictions bands. This sets the the framework for a possible options towards simplification of the calculation of the cable responses, which will be continued in Chapter 7.

5

Reduced time domain simulations

In Chapter 7, the use of a transfer function to reduce the computational time of dynamic cable lay analysis is assessed. Another in industry emerging method is the reduced time domain method. In the reduced time domain method the cable simulation time is reduced and concentrated around a certain maximum in the wave or vessel parameters in the model. Here, the applicability of this method with respect to vessel motions is evaluated. Both the heave acceleration and velocity are examined. The velocity is added on top of the heave acceleration based the proposed approach found in industry. In this thesis the maximum tension in the cable and maximum curvature are the main focus, therefore the applicability of this method is evaluated with respect to these two parameters.

5.1. Reduced time domain method for vessel motions

First, a three hour time domain simulation of the vessel motions is created for a given sea state. The maximum and minimum vessel motion reponse are then selected and a full dynamic simulation, including the cable, is carried out from 125s before to 125s after the occurrence of the absolute minimum and maximum vessel motion in the three hour simulation. Both the minimum and the maximum is selected as different cable responses are governed by different inputs. Maximum tension is effected by upward movements of the vessel, whereas maximum curvature is governed by the downward movements. Therefore, both domains are included in the analysis and the final result is based on the results of both simulation domains combined.

If the cable handling limits are not exceeded during the reduced time domain analysis, the case is accepted and deemed workable. The simulation time is thus reduced from 10800s to 500s, which means a reduction of approximately 95%, as the computational time required for the calculation of the vessel motion is almost negligible compared to the full cable dynamics. A graphical representation of the selected simulation domain is given in Figure 5.1.

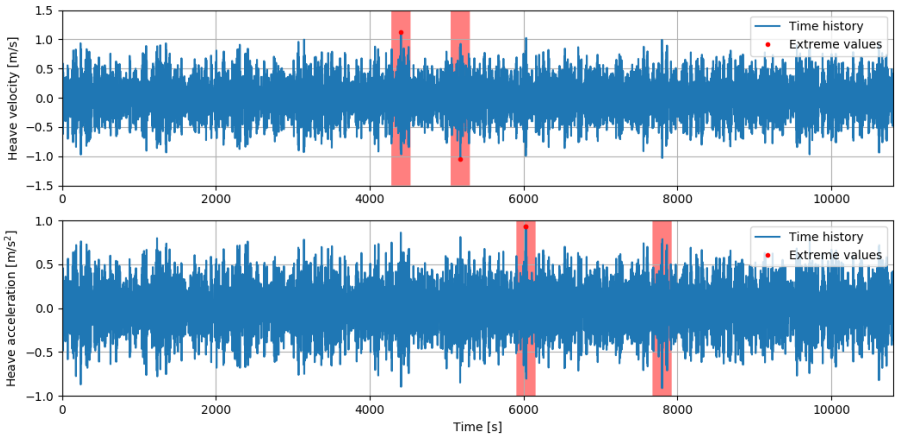

Figure 5.1: Graphical representation of the reduced time domain method. The red bars represent the selected time domain for full dynamic simulation, selected based on the vessel motion response.

5.2. Applicability of reduced time domain method

In this section, the applicability of the reduced time domain method applied to vessel motions is studied. The method is tested for three different cable installation configurations. An overview of the characteristics of these configurations is given in Table 5.1.

Table 5.1: Overview of the cable installation set-ups.

	Set-up 1	**Set-up 2**	**Set-up 3**
Cable	Export cable	Export cable	Array cable
Water depth	25m	50m	25m
Static departure angle	24.9 [deg]	16.7 [deg]	25.5 [deg]
Static TDP tension	7.00 [kN]	[7.37] kN	3.13 [kN]

For each cable set-up the reduced time domain method is tested for a set of sea states, which are representable for on site conditions during a normal lay operation. The full set of sea states is given in Table 5.2, where γ is determined following Figure 3.6. Each sea state is simulated for the full 360° of wave heading angles with a step size of 15°, following the conventions given in Figure 3.3. This brings the total of cases to 192 simulations per cable set-up. Based on this simulations set, the applicability of the reduced time domain method with respect to the maximum curvature and maximum tension is the cable is assessed.

Table 5.2: Overview of sea states for which the reduced time domain method is tested.

Seastate	1	2	3	4	5	6	7	8
$\mathbf{H_s}$ **[m]**	1.0	1.0	1.5	1.5	2.0	2.0	2.5	2.5
$\mathbf{T_p}$ **[s]**	4.5	5.5	5.5	6.5	6.5	7.5	7.5	8.5
γ **[-]**	1.78	1.0	1.80	1.0	1.59	1.0	1.34	1.0

5.2.1. Results

The results of the reduced time domain method applied for the heave velocity of the vessel are presented in Table 5.3. Equivalent results for the reduced time domain method applied for the heave acceleration are given in Table 5.4. In order to be able to compare the results between the different set-ups, the tension and curvature increase with respect to the maximum tension and maximum curvature in the static configuration is studied. This tension amplitude is defined by Equation 5.1 and the curvature amplitude is found by Equation 5.2.

$$\Delta T_{\text{top}} = T_{\text{top,max}} - T_{\text{top,static}} \tag{5.1}$$

$$\Delta \kappa_{\text{max}} = \kappa_{\text{max}} - \kappa_{\text{max,static}} \tag{5.2}$$

Table 5.3: The performance of the reduced time domain method, applied to the heave velocity of the vessel.

	Set-up 1		**Set-up 2**		**Set-up 3**	
	Curvature	Tension	Curvature	Tension	Curvature	Tension
Mean error	6.0 %	7.9 %	5.5%	3.4%	5.3 %	3.0 %
Error std	8.8 %	9.9 %	8.9%	7.0%	8.6 %	5.3 %
Success rate	84	68	105	102	102	101
Largest error	40.6 %	38.8 %	38.3%	40.1%	39.3 %	26.0 %

Table 5.4: The performance of the reduced time domain method, applied to the heave acceleration of the vessel.

	Set-up 1		**Set-up 2**		**Set-up 3**	
	Curvature	Tension	Curvature	Tension	Curvature	Tension
Mean error	5.8 %	5.3 %	6.2%	3.6%	4.9 %	3.2 %
Error std	8.3 %	8.9 %	9.0%	7.0%	8.0 %	5.4 %
Succes rate	83	97	78	99	101	94
Largest error	33.7 %	36.6 %	38.3%	35.9%	32.9 %	26 %

The mean error shows the mean under prediction in percentage of the maximum tension amplitude and maximum curvature amplitude over all 192 cases for each set-up. The corresponding standard deviation of the mean error is provided as well. The success rate gives the number of cases in which the maximum cable response in the cable was found using the reduced time domain method. The largest error is the largest error in the cable response amplitude over all 192 cases.

The general observation is that the reduced time domain method does not capture the maximum cable response found during a full three hour time domain simulation, as is desired. The best success rate found in this study is $105/192 \approx 55\%$, which is still relatively low. For the remaining 45% of the cases, there exists a risk of falsely accepted installation conditions. The average error lies between 3-10%, which could be solved by implementation of a safety factor in the reduced time domain method. However, the standard deviation of this error as well as the extreme errors found in this study are quite severe, making this approach less suitable. Based on the current results no conclusion can be drawn on whether the reduced time domain method can best be applied to the heave velocity or heave acceleration of the vessel. The performance is set-up specific and varies dependent on the performance parameters under investigation.

The results given in Table 5.3 and Table 5.4 give the errors with respect to the cable response amplitude. The most severe absolute errors are given here to get a better understanding of the true

magnitude of the under prediction. The largest absolute error in the curvature response is found for set-up 3, when the reduced time domain method is applied to the heave acceleration of the vessel. In this case the reduced time domain method reports a maximum curvature of 0.202 [rad/m], while the full time domain simulation reports a maximum curvature of 0.241, which corresponds to an error of 16.17%. Likewise, the largest error in the tension response is found for set-up 1, when the reduced time domain method is applied to the heave velocity of the vessel. For this specific case the maximum tension reported by the reduced time domain method is 35.71kN, against 39.75kN for the full time domain simulation.

Combining these observations, the reduced time domain method does not capture the absolute maximum as found during the required full three hour dynamic simulation time as specified in [DNVGL-RP-N103, 2017]. On top, the variation in the error is quite large making the required safety factor high, which is undesirable. Therefore, the reduced time domain method is not deemed applicable for normal cable lay analysis based on the results obtained in this study.

6

Spectral Analysis

In the spectral analysis, Airy's linear wave theory is used to generate the wave input for the simulations. Simulations for waves exceeding the breaking limit ,as described in subsection 2.5.3, are excluded from the analysis. This chapter focuses on acquiring a fundamental understanding of the behaviour of the cable during normal lay operations. Then the non-linearities of the system with respect to the frequency response of the cable are studied using Discrete Fourier Transform (DFT) analysis in section 6.1. In section 6.2 extra attention is given to the effect of the non-linear drag in the normal lay model. In the next section, section 6.3, the behaviour of the cable with respect to the input amplitude of the waves and the corresponding cable response amplitude is examined. Then, the contribution of higher order components in the cable response to the total response of the cable is studied in section 6.4. Finally, the governing loading regime in the normal lay model is identified in section 6.5, to support the understanding of the system behaviour.

6.1. Discrete Fourier Transform analysis

A DFT analysis is carried out to give insight in the non-linearities of the cable lay system with respect to the maximum tension and maximum curvature response. The analysis is carried out using regular wave simulations.

The DFT determines the frequency domain representation of a time domain signal, therefore it is an helpful tool to identify the frequency components contained in a time domain signal. The maximum frequency the DFT is able to capture is known as the Nyquist frequency and defined as $f_{\text{nyquist}} = 0.5 f_s$, where f_s is the sampling frequency of the time history. The minimum frequency is limited by the length of the signal and thus $f_{\text{min}} = \frac{1}{t_{\text{signal}}}$. The single sided DFT ranges from [f_{min},f_{nyquist}] and is calculated by Equation 6.1, where x_m represents the signal. The DFT is complex valued and thus encodes both the amplitude and the phase of the sinusoidal signal component. The amplitude and phase of the response are found by Equation 6.2 and Equation 6.3, respectively. The curvature time history of the node experiencing the maximum curvature during the full simulation time is used as input for the curvature DFT. The tension DFT is determined based on the tension time history in the first node of the cable model, which corresponds to the node of maximum tension as seen in section 4.1. In this section the focus is on the amplitude spectrum of the cable responses.

$$X_m = \frac{2}{n} \sum_{m=0}^{n-1} x_m \exp -2\pi i \frac{mk}{n} \tag{6.1}$$

$$|X(f)| = \sqrt{\left(\mathrm{Re}(X(f)\right)^2 + \left(\mathrm{Im}(X(f)\right)^2} \tag{6.2}$$

$$\phi(f) = \arctan\left(\frac{\mathrm{Im}(X(f)}{\mathrm{Re}(X(f)}\right) \tag{6.3}$$

6.1.1. Curvature

The curvature response spectrum was studied for a wide range of input waves with wave heights in the range of $1.0 \leq \mathrm{H}_{wave} \leq 2.5$ and periods in the range of $3.0 \leq \mathrm{T}_{wave} \leq 16.0$. The curvature response spectrum to a regular wave input of [T_{wave}=10s,H_{wave}=2.5m] is given in Figure 6.1.

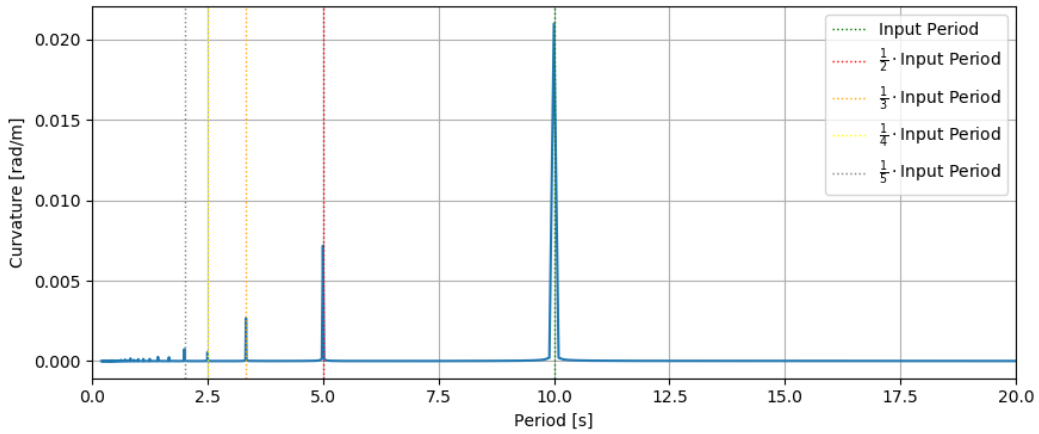

Figure 6.1: The amplitude spectrum of the maximum curvature response (arclength from vessel connection = 65m) for T_{wave}=10[s],H_{wave}=2.5[m].

The following observations are done based on the curvature DFT analysis:

1. Multiple period components are present in the period response of the curvature. This is an indication of the non-linearity in the system, as only a single input period was given.
2. The periods contained in the period response can be identified as a fraction of the input period, where the denominator is given by n=1,2,3,4,5.
3. For an input wave period with T>10s, the amplitude of the sinusoidal complex component of the DFT reduces as the period corresponding to the component reduces. For shorter input periods, the decreasing order is disturbed, most often by the $\frac{1}{3}$ component.

Observation 1 and observation 2 show the generation of sum frequencies in the cable response. This means multiple integers of the input frequency of the system are present in the response. This is a general characteristic of non-linear systems. Another often seen characteristic in non-linear systems is difference frequency generation. A difference frequency is a frequency with a magnitude equal to the difference between two other frequency components in the response. This difference can for example be between the input frequency and a frequency component introduced by a non-linearity in the system.

An example of such a non-linearity is the drag force in the Morison equation. In case this force is applied to a nonmoving structure, the frequency components contained in the signal can be identified by the Fourier series of the drag force time history. The drag force on a rigid pile is of the form seen in Equation 6.4, where $\hat{u}$ is the amplitude of the wave particle velocity.

$$F_D \propto \hat{u}^2 \sin^2(\omega t) \cdot \text{sign}(\sin(\omega t)) \tag{6.4}$$

This type of signal is odd and contains a half-wave symmetry. Based on Fourier series theory, this means that the drag force will contain uneven integer multiples of the input frequency (f_1, f_3, f_5,...). The contribution at each frequency reduces as the frequency increases [Osgood, 2007].

However, the drag force implemented in the normal lay model is dependent on the movement of the cable itself. The resulting time history of the drag force is thus dependent on the velocity of the cable. As a result, the signal loses its half wave symmetry and odd nature and is influenced by the frequencies in the velocity response of the cable. Therefore, none of the coefficients in the Fourier series reduces to zero and all integer multiples of the input frequency are likely to, to some extent, be represented in the drag force time history. Furthermore, the effect of the seabed is tested based on an one degree of freedom mass spring system, where the spring is supplemented with a Heaviside step function component. The Heaviside function in this simplified model represents the different stiffness with regards to up and downward movement of the cable. This showed that this kind of non-linearity introduces a significant component at the second frequency component, equal to twice the input frequency to the system.

The presence of both sum frequency generation and difference frequency generation in non-linear systems makes it difficult to pinpoint the frequency components to specific non-linearities in the system. In order to further investigate the effect of the non-linear drag in the system, a drag linearisation is applied. The approach and results are outlined in section 6.2.

6.1.2. Tension

The DFT of the tension response is studied in a similar way as for the curvature response. The tension response spectrum to a regular wave input of [T_{wave}=10s,H_{wave}=2.5m] is presented in Figure 6.2. The observations are listed below the figure.

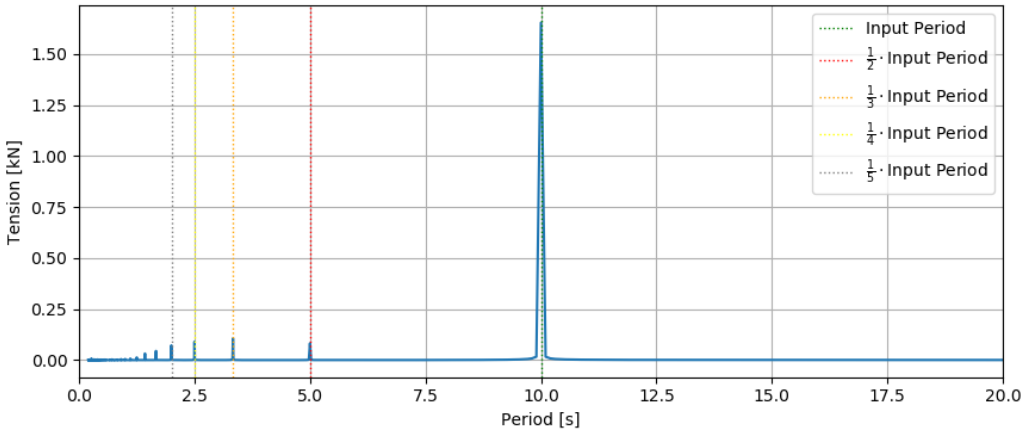

Figure 6.2: The amplitude spectrum of the top tension response for [T_{wave}=10s,H=2.5m].

1. In general, the tension response shows relatively smaller peaks for higher order components

in the response, compared to the curvature response.

2. The $\frac{1}{3}$ period element in the DFT of the maximum tension response in the cable is often higher than the $\frac{1}{2}$ period element.

Based on observation 1, it is concluded that the tension response of the cable is less affected by the non-linearities in the system then the curvature response of the cable. Furthermore, the high frequency components in the tension response of the cable are likely to be affected by the movement of the TDP of the cable. The cable making contact with the seabed introduces an impulse through the cable as a result of the instantaneous introduction of reaction forces with the seabed. In the DFT of the cable response this is represented by low frequency components in the DFT.

6.2. Drag linearisation

In this section the drag in the normal lay model, described in section 3.1, is linearised. The DFT of the original model is compared to the DFT of a normal lay simulation executed with the linearised drag model, to provide insight in the effect of the non-linear drag in the cable response.

6.2.1. Model set-up

Orcaflex does not allow for drag linearisation directly. Therefore the normal lay model is adjusted in order to allow drag linearisation in normal lay simulations.

The linearised drag model is created by the use of spar bouys. Spar buoys are cylindrical 6D buoys in Orcaflex, which allow for a linear damping force to be implemented on the spar buoy. These spar bouys are attached to cable in order to take over the drag force on the cable. The drag coefficient of the cable itself is set to zero and the linear damping force of the spar bouys is then used for the implementation of the drag linearisation. The inertia force is still taken into account by the actual cable in the model.

One spar buoy is attached to each cable node. This means the spar buoys have a length of 0.5m and are rigidly attached to the node by means of a constraint. Each spar buoy thus spans half of the cable element above the node, and half of the cable element below the node. The spar buoys have a diameter in the order of 10^{-12}m and the weight is set so that the spar buoy is neutrally buoyant. This small diameter, and consequently small weight, aim at reducing the effect of the spar buoy on the inertia forces in the model.

The last step is the implementation of the linearised drag force by means of the linear damping force of the spar buoys. The linear damping force of the spar buoys is defined by Equation 6.5, where UDF is the Orcaflex User Defined Function, which in this application represents the damping force value.

$$f_D = -UDFv_{rel} \tag{6.5}$$

Now, the UDF is set to the linearised form of the drag force as defined in Equation 6.6

$$UDF = \frac{1}{2}\rho_w C_D \Delta l K_L \tag{6.6}$$

Here K_L is the drag linearisation coefficient. The full procedure to obtain the value of this coefficient is explained in Appendix B.2. The drag linearisation coefficient is dependent of the relative velocity of the cable node to which the spar buoy is attached. Therefore, the drag linearisation coefficient

has a different value for each of the spar buoys attached to the cable. Furthermore, the calculation of the drag linearisation is an iterative process, as the relative velocity of the cable is dependent of the magnitude of the drag force itself. A flowchart of the procedure followed for the execution of linear drag simulations is shown in Figure 6.3.

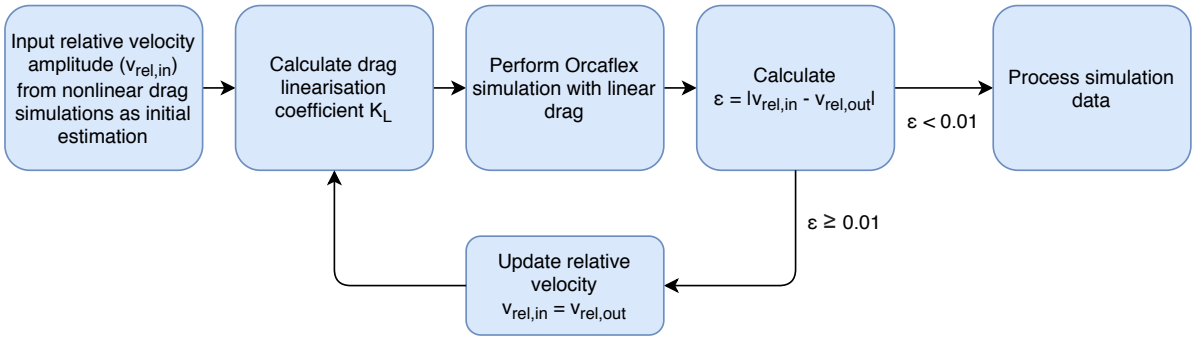

Figure 6.3: Flowchart of the iterative process for the excecution of linear drag simulations in Orcaflex.

6.2.2. Model verification

After building the model, the first step is the verification of the new normal lay model.

Static

The static results of the original normal lay model and the new spar buoy model are presented in Table 6.1. Both the top tension and the maximum curvature along the catenary of the cable are equal and the curvature occurs at the same node. In addition, the layback is checked and found to be equal for both models. Therefore, the spar buoy model is a good representation of the original normal lay model in the static state and considered statically verified.

Table 6.1: Static validation of the drag linearisation model in Orcaflex.

Model	Top tension	Maximum curvature
Original cable model	35.54 [kN]	0.04626 [rad/m] (node 139)
Spar buoy model	35.54 [kN] (±0.00%)	0.04626 [rad/m] (node 139) (±0.00%)

Dynamic

The next step is the dynamic verification of the drag linearisation model. In the original model, a Reynolds number dependent drag coefficient was used. As a spar buoy does not allow for a Reynolds dependent drag coefficient, additional simulations of the original model with a constant drag coefficient of C_D = 1.2 are executed. These results are compared to the results obtained from the spar buoy model, where the drag coefficient of the spar buoys is set equal to C_D = 1.2. The drag area of the spar buoy is modified so that it corresponds to the drag area of a single cable element. The comparison between the results of these simulations is provided in Figure 6.4 and Figure 6.5.

The curvature and tension response of the cable shows a similar shape and magnitude. The error in the maximum magnitude of the curvature response is -0.1% and the error in the maximum magnitude of the tension response is +0.2 %. The slight variation might be the result of the really small weight of the spar buoys on the cable. The curvature is then decreased by the slightly higher inertia force in the spar buoy model based on the diameter of the spar buoys, while the extra weight causes the magnitude of the tension variation to slightly increase.

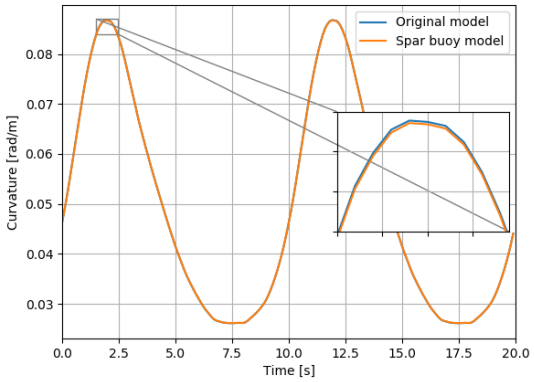

Figure 6.4: Comparison between the maximum curvature response of the original and the spar buoy model.

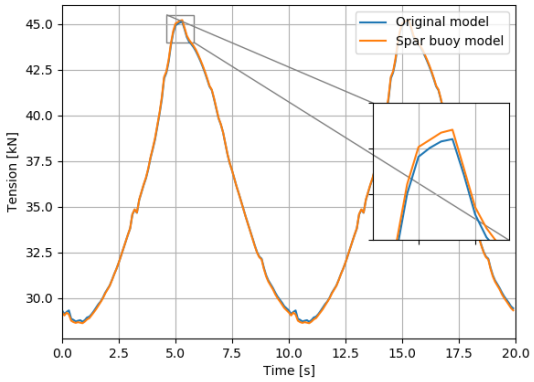

Figure 6.5: Comparison between the maximum tension response of the original and the spar buoy model.

6.2.3. Results

A short sample of the time history of the tension response of the cable, for a simulation with quadratic drag and a simulation with linear drag, is presented in Figure 6.6. Similarly, a short sample of these time histories of the curvature response of the cable are given in Figure 6.7. The plots clearly show that the maximum tension response of the cable and the maximum curvature response of the cable are reduced due to the drag linearisation in the normal lay model.

The DFT of the tension of the cable for quadratic drag and linear drag is presented in Figure 6.8. Note that the DFT for quadratic drag is not exactly the same as the one presented in Figure 6.2, as now the drag coefficient is kept constant in order to comply with the spar buoy model. The plot shows that the first order component is increased, the second order component is decreased and the third order component is increased again, as linear drag is implemented. Based on theory, particularly a reduction of the third component would be expected. This because the linear drag force will mainly represent itself at the input frequency, while the quadratic drag also has a significant component at the third sum frequency. Thus, the dynamic complexity of the system is such that no direct conclusion can be drawn based on the results of drag linearisation. Furthermore, the quadratic drag DFT contains more higher frequency components. This might result from the fact that the quadratic drag term includes more higher frequency components in combination with the generation of sum

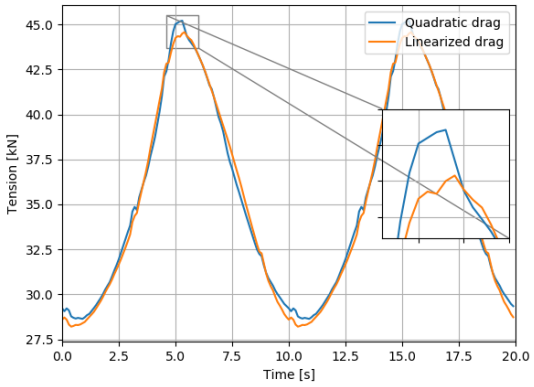

Figure 6.6: Comparison between the time history of the tension response for a linear and a quadratic drag regular wave simulation with T_{wave}=10s and H_{wave}=2.5m.

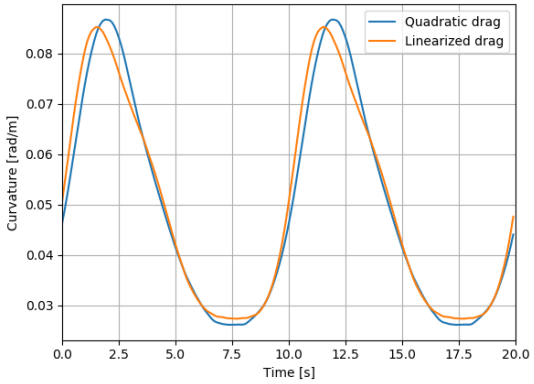

Figure 6.7: Comparison between the time history of the curvature response for a linear and a quadratic drag regular wave simulation with T_{wave}=10s and H_{wave}=2.5m.

frequencies with these frequency components. By inspection of Figure 6.10, which shows the linear and quadratic drag profile for a non-moving structure, the linear drag clearly shows a single frequency component, while the quadratic shows also significant influence of the third frequency component. The principle of sum frequency generation with linear drag is shown in Equation 6.7. This same principle in combination for the third order component of the quadratic drag in shown Equation 6.8. This can cause the shift towards higher frequency components for quadratic drag compared to the linear drag model.

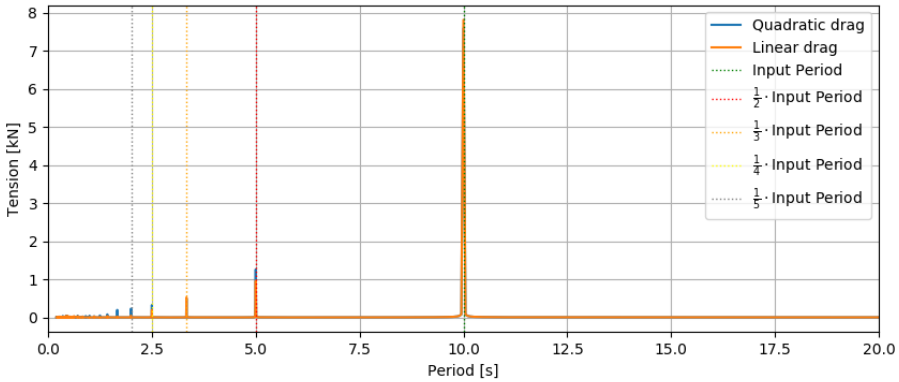

Figure 6.8: The DFT of the maximum tension response of the cable for [T_{wave}=10s,H_{wave}=2.5m] based on simulation with linear and quadratic drag.

$$\text{Linear drag} = \begin{cases} f_1 + f_2 = f_3 \\ f_1 + f_3 = f_4 \end{cases} \tag{6.7}$$

$$\text{Quadratic drag} = \begin{cases} f_3 + f_2 = f_5 \\ f_3 + f_3 = f_6 \end{cases} \tag{6.8}$$

The DFT of the curvature response of the cable for both quadratic and linear drag is presented in Figure 6.9. The first and second component of the DFT are reduced due to the implementation of drag linearisation. The reduction of the first component might be the result of the overall reduction

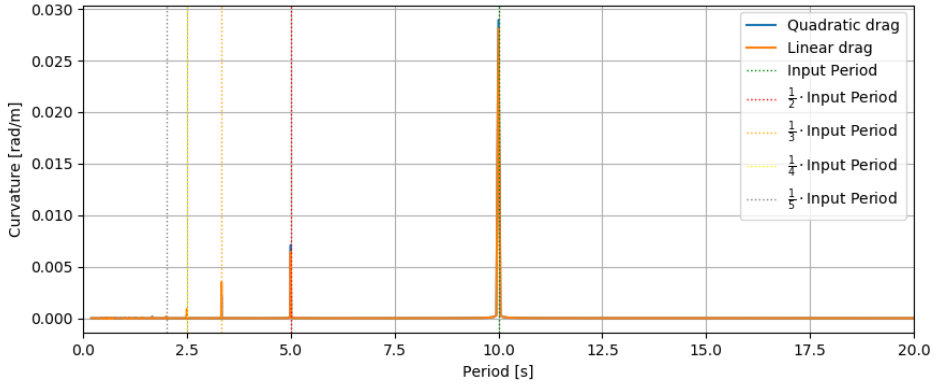

Figure 6.9: The DFT of the maximum curvature response of the cable for [T_{wave}=10s,H_{wave}=2.5m] based on simulation with linear and quadratic drag.

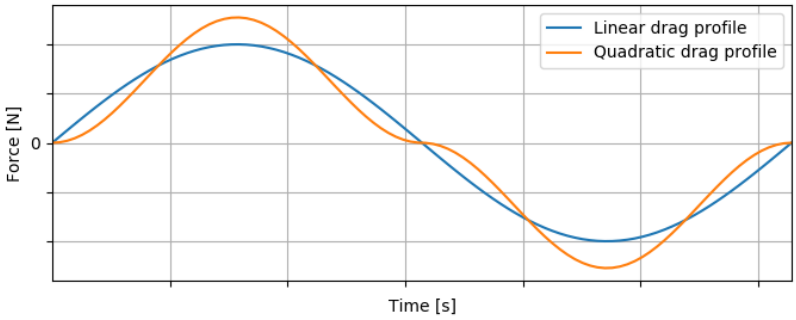

Figure 6.10: Profiles of the quadratic and linear drag in time.

of the magnitude of the signal. With respect to the higher order component, the observation is that the higher order components increase due to the linear drag definition. This might imply that the higher order components of the curvature response are dominated by difference frequency generation instead of sum frequency generation, following the same reasoning as for the tension response of the cable.

As stated above, both the maximum tension and the maximum curvature response of the cable were decreased as a results of the implementation of linear drag into the normal lay model. A possible explanation for this behaviour is change in the shape of the drag profile as a function of time, upon the change from quadratic towards linear drag in the model. An example of the shape of both profiles is given in Figure 6.10. Later on, in section 6.3, it is discussed that the relative velocity in the sagbend of the cable is dominated by the movement of the cable itself, therefore $v_{rel} \approx 0$ around the extreme curvature instance of the cable. It is seen that in the extremes of the cable curvature response ($v_{rel} \approx 0$), the linear drag force contains slightly more impulse than the quadratic drag force. Hence, in the extremes of the cable movement, the movement of the cable itself is slightly less counteracted by the quadratic drag force than by the linear drag force. As a result, the cable in the quadratic drag mode is 'overshooting' a little more, resulting in a higher extreme curvature.

6.3. Spectral amplitude of the cable response

It is clear that the period of the input to the cable lay system affects the response. In the previous section the effect of the non-linearities of the system on the frequencies contained in the cable

response were discussed. In this section the relation between the amplitude of the input and the amplitude of the output of the system is studied. The peak in the DFT of the cable response at the input period is scaled by the wave height, see Equation 6.9. The result provides insight in the non-linear behaviour of the cable with respect to the input amplitude. Only the first order component of the response is chosen instead of the total magnitude of the response in light of the application of the first order component in a cable response transfer function, see Chapter 7. In this section the system is considered positively non-linear if a doubled input amplitude results in a more than doubled cable response. Likewise, the system is considered negatively non-linear if a doubled input amplitude results in a less than doubled cable response.

$$X_{\text{scaled}} = \frac{X_{\text{response}}\,|_{T=T_{\text{input}}}}{H_{\text{input}}} \tag{6.9}$$

6.3.1. Curvature

The maximum curvature response of the cable for unit vessel wave height based on the first order DFT component of the response is given in Figure 6.11.

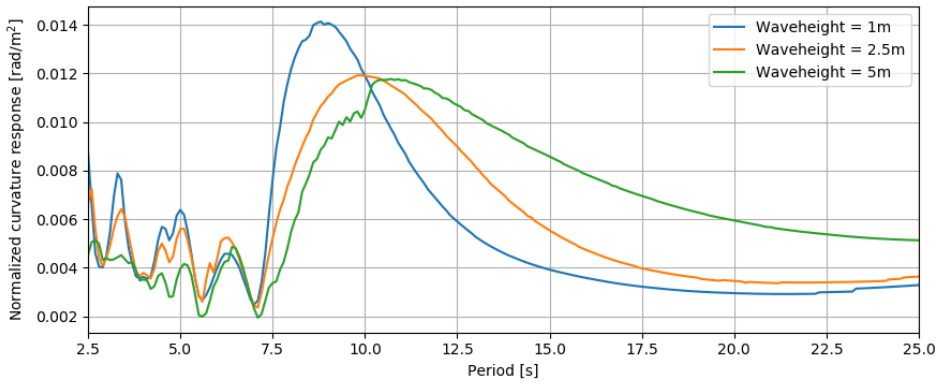

Figure 6.11: The maximum curvature response of the cable for unit wave height determined based on regular wave input of H=1.0m,H=2.5m,H=4.0m and H=5.0m.

Based on Figure 6.11 the following observations are made:

1. The system shows non-linearities with respect to the input wave amplitude, as the lines show variation with respect to eachother. Due to the linear properties of the use of RAO's for vessel motion calculation it can be concluded that the cable curvature response is non-linear with respect to the amplitude of the vessel motions.
2. For T_{wave}>10s, the system is positively non-linear.
3. For T_{wave}<10, the system is in most cases negatively non-linear.

To get a better understanding of the behaviour of the cable as discussed above, the drag and inertia forces on the cable are studied.

The inertia force consist of two components, the hydrodynamic mass force, which is dependent on the relative acceleration of the cable, and the Froude-Krylov force, which is independent of the movement of the cable itself. The drag on the cable is dependent on the relative velocity of the cable. The sea, cable and total acceleration in the horizontal direction is studied for three different

sea states, with peak periods varying between T_{wave}= 6.0s, T_{wave}= 10.0s and T_{wave}= 16.0s. The results for T_{wave}=10s are given in Figure 6.12. The results for T_{wave}=6s and T_{wave}=16s are given in Appendix B.1. In addition, the sea, cable and total velocity in the horizontal direction are studied for the three sea states specified above. The results for T_{wave}=10s are given in Figure 6.13. Noticeable is that for both the relative acceleration and the relative velocity the movements of the cable itself have a significant effect on the total relative acceleration and total relative velocity of the cable. The acceleration and velocity of the cable itself is most significant in the sagbend area of the cable, where mostly the maximum curvature response is experienced.

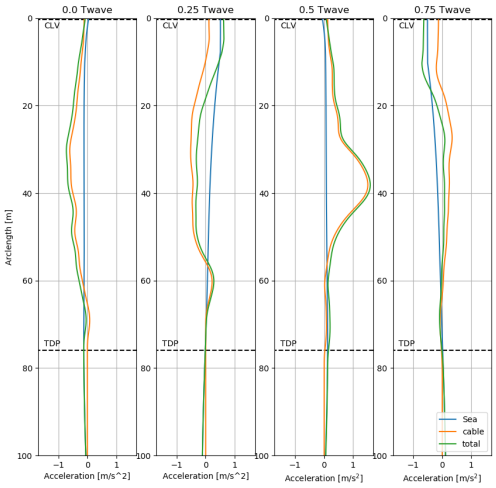

Figure 6.12: The acceleration of the sea, cable and total acceleration for T_{wave}=10s and H = 2.5s along the full catenary of the cable at four instances during the regular wave period.

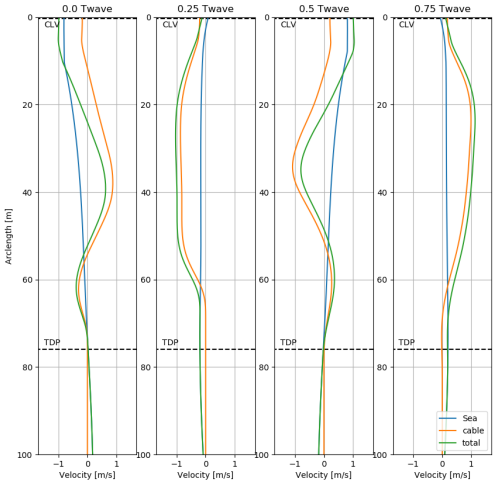

Figure 6.13: The velocity of the sea, cable and total velocity for T_{wave}=10s and H = 2.5s along the full catenary of the cable at four instances during the regular wave period.

The movement of the cable can be approximated by a sinusoidal function, as given in Equation 6.10. Consequential, the velocity and acceleration of that same point on the cable can be found by Equation 6.11 Equation 6.12, respectively. This implies that for higher frequencies an increase in the amplitude of the movement of the cable results in a larger increase of the inertia force and drag force compared to the same amplitude increase for lower frequencies. The part of the inertia force resulting from the cable acceleration itself will be counteracting that same movement. Likewise, the part of the drag force resulting from the cable velocity counteracts the cable movement as well. Therefore, for higher frequencies the positive non-linear cable geometry, meaning higher scaled cable responses for higher inputs, is diminished by the effect of the inertia and drag force resulting from the cable movement itself.

$$x = A \cdot \sin(\omega t) \tag{6.10}$$

$$v = -\omega A \cdot \cos(\omega t) \tag{6.11}$$

$$a = -\omega^2 A \cdot \sin(\omega t) \tag{6.12}$$

6.3.2. Tension

The maximum top tension response of the cable for unit wave height is presented in Figure 6.14. The observations made based on Figure 6.14 are stated below.

1. The graph shows multiple scaled tension results per input period depending on input wave height. This signifies that the system has a non-linear relationship between the input wave height and tension response of the cable.

2. For T>7s, the tension response is positive non-linear with respect to the input amplitude.

3. For T<7s, it is quite unpredictable whether the system is positively or negatively non-linear with respect to the input amplitude for the top tension. The results vary for the input period within this range.

4. The tension response shows approximately linear behaviour between 6.25≤T≤7.25s with respect to the input amplitude to the system.

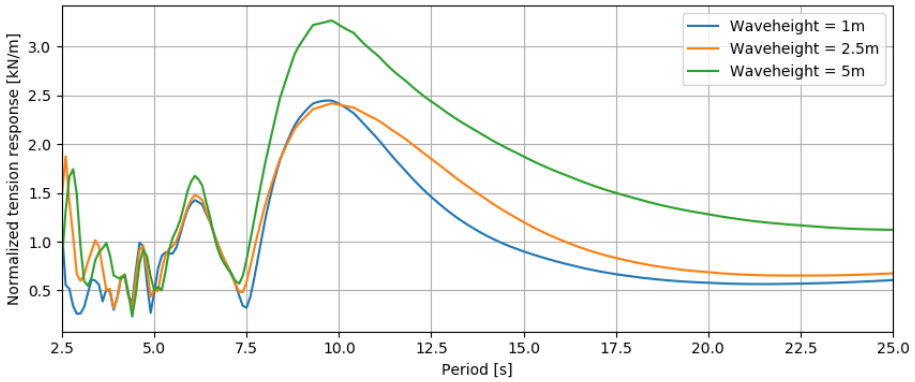

Figure 6.14: The maximum top tension response of the cable for unit wave height determined based on regular wave input of H=1.0m,H=2.5m,H=4.0m and H=5.0m.

6.4. Contribution of higher order effects to total cable response

The contribution of the higher order components of the DFT to the total response of the cable are studied in this section. In order to determine the contribution of the higher order components detected by the DFT of the cable response, the maximum cable response amplitude with respect to the static configuration to a regular wave with a specific period and wave height is compared to the corresponding first order component of the amplitude DFT. The results for the maximum curvature response are presented in Figure 6.15 and the results for the maximum tension in the cable are given in Figure 6.16. Based on these plots it is concluded that the contribution of the higher order components the cable response is most significant between T_{wave}=8s and T_{wave}=12s. Furthermore a positive relationship between an increase in the wave height and the contribution of the higher order components in the cable response to the total response is detected for the curvature as well as the tension response of the cable. This information is relevant during the assessment of the performance of the first order regular wave transfer function in Chapter 7.

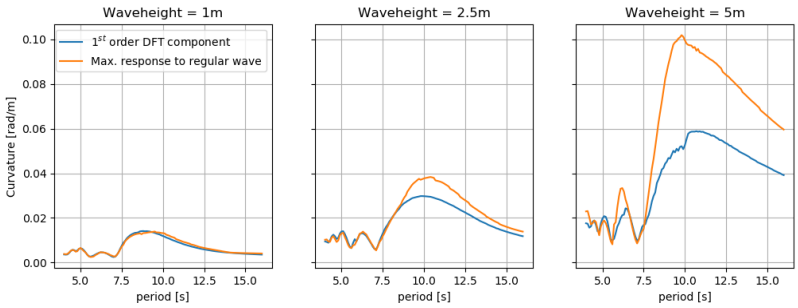

Figure 6.15: The amplitude of the first order component of the DFT of the maximum curvature response and the maximum curvature response amplitude with respect to the static configuration found from regular wave simulations for varying wave periods and wave heights.

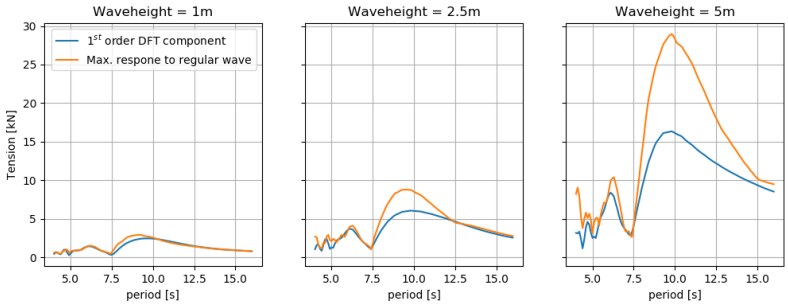

Figure 6.16: The amplitude of the first order component of the DFT of the maximum tension response and the maximum tension response amplitude with respect to the static configuration found from regular wave simulations for varying wave periods and wave heights.

6.5. Dominating loading regime

The Keulegan-Carpenter (KC) number is defined by Equation 6.13. Here u_{max} is the maximum wave particle velocity at the sea surface. T_{wave} is the wave period and D the diameter of the cable. The KC number provides an indication of the loading regime on the cable. The different loading regimes are defined below [Journée and Massie, 2001].

$$K_c = \frac{u_{max} T_{wave}}{D} \tag{6.13}$$

KC<3 The system is inertia dominated. In this region the potential flow theory is applicable (I).

3≤KC≤45 Both the contribution of the inertia and drag force are significant (I & D).

KC>45 The system is drag dominated. In this region the frictional forces on the cylinder dominate the force response (D).

To get an idea of the dominating loading regime in the normal lay simulations the KC number in the simulations is calculated for various regular wave inputs. The results are presented in Table 6.2. The results show that for higher periods the system tends to be drag dominated, while for lower periods the inertia force starts to contribute as well. Furthermore, the drag force has a larger effect at the top of the catenary, but since the drag force tends to reduce faster than the inertia force, the inertia force becomes more dominant in the lower parts of the catenary i.e. at the location of maximum curvature. This is due to the quadratic nature of the drag force.

Another point of interest is that quite some cases where both the inertia and drag force have a significant effect where detected. For the range of KC numbers 10-25 the Morison equation is limited in application because of a contradiction [Sarpkaya, 2010]. The definition of the inertia force is based on the potential flow theory, which in turn is based on the assumption of an inviscid flow, while the drag force in the Morison equation originates from frictional forces. In this region the effect of the randomness of the few vortices that form around the cylinder are effecting the accuracy of the Morison equation. This inaccuracy is mostly covered by the mitigating effects of the sea environment, like omidirectional wave spreading. In this study omnidirectional wave spreading is not implemented, possible resulting in some inaccurate load estimations of the Morison equation.

Table 6.2: Keulegan-Carpenter numbers for in normal lay simulations.

T_{wave} [s]	6	6	6	10	10	10	16	16	16
H_{wave} [m]	1.0	2.5	5.0	1.0	2.5	5.0	1.0	2.5	5.0
KC number [-]	12	29	58	12	30	60	17	38	75
Loading regime	I & D	I & D	D	I & D	I & D	D	I & D	I & D	D

7

Transfer function set-up & performance

In this chapter the use of a transfer function to calculate the maximum cable response is evaluated. The transfer function is based on the first order response of the cable to regular waves. The set-up of the transfer function is discussed in section 7.1. In addition, the calculation of the RAO of the vessel for the selected vessel motions found in section 4.3 is presented in subsection 7.1.1, as this is required for the application of the transfer function. Next, in section 7.2, the performance of the transfer function for approximating the maximum cable response is evaluated. The procedure followed to obtain the cable response based on the transfer function is outlined in subsection 7.2.1. In the same way, the procedure used to obtain the maximum response based on the statistics of Orcaflex simulations is described in subsection 7.2.2. Next, the results of the transfer function and the Orcaflex simulations are compared in subsection 7.2.3. Finally, the cable response spectrum calculated by the transfer function is compared to the cable response spectrum resulting from Orcaflex simulation to provide insight in the behaviour of the transfer function.

7.1. Transfer function set-up

The transfer function is established with the use of the DFT representation of the cable response to regular waves. This approach allows for the set up of the transfer function without requiring long expensive simulations, as regular wave simulations are significantly faster and once in steady state, repetitive. Taking only the first order component means all higher order effects are neglected. However, the total response to an irregular sea state generally does not contain all frequencies, while in the case of a transfer function a continuous range of frequency components is excited. The DFT response of the cable to regular waves was already discussed in section 6.3. The first order component comprises the peak of the DFT found at the frequency at which the system is excited, in this case corresponding to the wave period of the regular wave given as input to the simulation. The transfer function is then defined by Equation 7.1 and provided with respect to the heave acceleration of the CLV. This choice is based on the findings in section 4.3 and the definition of the RAO of the chosen vessel response in subsection 7.1.1.

$$RAO_{cable} = \frac{X_{response}\,|_{T=T_{input}}}{X_{HA}\,|_{T=T_{input}}} \tag{7.1}$$

Following this approach, the transfer function is defined in the range between 2.5-25 seconds. The lower boundary of this range is set by the lower bound for which the RAO's of the Nexus are defined.

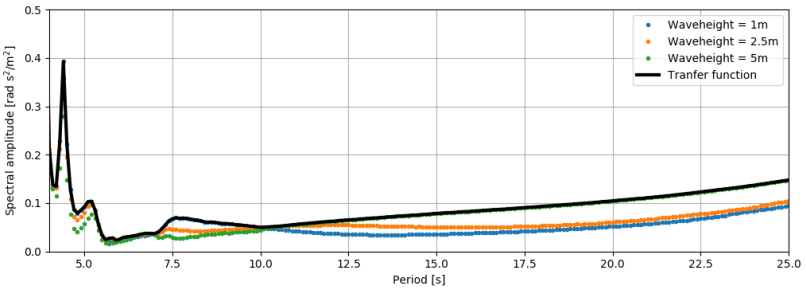

Figure 7.1: Transfer function for the maximum curvature response of the cable.

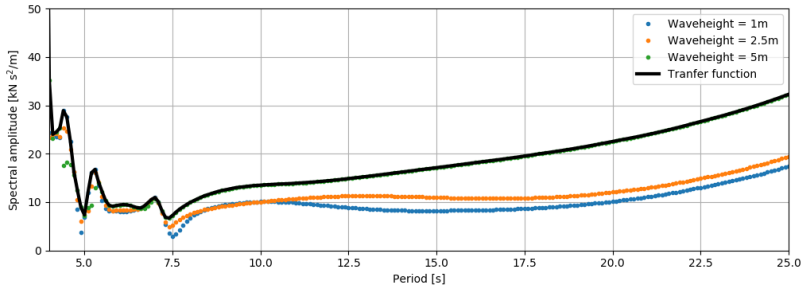

Figure 7.2: Transfer function for the maximum tension response of the cable.

The upper boundary on the other hand is based on the JONSWAP spectrum, which does not show significant values above this upper limit for sea states with a peak period up to at least 12 seconds, which is a reasonable upper boundary for the peak periods found at a specific site.

Due to the non-linear amplitude behaviour of the first order component, as discussed in section 6.3, a worst case scenario approach is used for the set-up of the transfer function. The Nexus is able to perform normal lay up to significant wave heights of 2.5m. Therefore, the maximum expected wave height is approximately five meter, see subsection 2.5.3. Regular wave simulations with H=1.0m, H=2.5m and H=5.0m are performed and the worst case result is selected for the transfer function. This approach, together with the final transfer function, is presented in Figure 7.1 and Figure 7.2 for the curvature and the tension response, respectively. These plots only span the transfer function between 4-25 seconds, due to the high values below this range a full range plot reduces the detail of the plot. The full transfer function is provided in Appendix C.1.

7.1.1. RAO transformation

The displacement of the vessel is defined at the RAO origin. For the application of the transfer function, is required to have a transfer function for the selected vessel motion at the chute of the vessel. For the axial acceleration the RAO is dependent on the movement of the cable, namely the departure angle. This complicates the definition of the RAO for axial acceleration of the chute. However, the transformation of the displacement RAO's at the RAO origin into the RAO of the heave acceleration at the chute is quite straightforward. Therefore it was chosen to define the transfer function with respect to the heave acceleration of the vessel. First the displacement RAO is found by Equation 7.2. As the current case contains a wave heading of 180°, the yaw component does not have to be included, as its contribution is approximately zero. Based on the assumption that the movement of the chute of the vessel can be represented by a sinusoidal function, the acceleration RAO at the chute is defined by Equation 7.3.

$$RAO_{z-chute} = RAO_z + RAO_\theta \bar{x} + RAO_\theta \bar{z} + RAO_\phi \bar{y} \tag{7.2}$$

$$\ddot{z}_{chute} = -\omega^2 RAO_{z-chute} \tag{7.3}$$

7.2. Transfer function performance

The next step is to test the performance of the transfer function in estimating the maximum cable response expected during a certain duration of cable simulation.

7.2.1. Transfer function approach

A flowchart of the steps to estimate the maximum cable response with the use of the transfer function is given in Figure 7.3. Each one of the steps is clarified below.

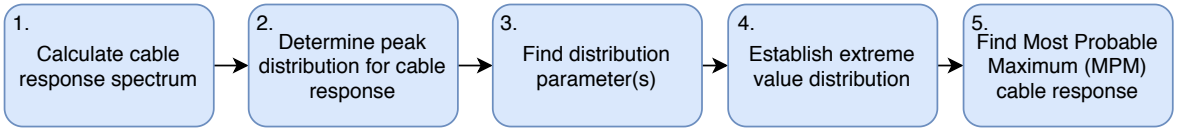

Figure 7.3: Flowchart of the procedure to estimate the maximum cable response with the use of the transfer function.

1. The cable response spectrum is calculated by Equation 7.4. Here $S_\zeta(f)$ is the wave spectrum of the considered sea state and $RAO_{\ddot{z}}$ the response amplitude operator for the heave acceleration of the Nexus.

$$S_{\text{cable}}(f) = S_\zeta(f)|RAO_{\ddot{z}}|^2|RAO_{\text{cable}}|^2 \tag{7.4}$$

2. In this step the distribution of the peaks in the cable response (CR) is selected. The time history of the cable response found by the transfer function approach is built up out of two components, the static cable response and a dynamic component, which is defined by the transfer function, see Equation 7.5.

$$CR = CR_{\text{static}} + CR_{\text{dynamic}} \tag{7.5}$$

First the procedure to obtain the time history of the dynamic component of the cable response is outlined. The time history representation of the dynamic part of the cable response, based on the transfer function, is defined in Equation 7.6.

$$CR_{\text{dynamic}} = Ae^{i\theta} = \sum_{j=1}^{n} A_j e^{i\phi_j} \tag{7.6}$$

The amplitude of the cable response A_j is found from the cable response spectrum by Equation 7.7 and the phases ϕ_j are uniform distributed between [-π,π].

$$A_j = \sqrt{2 \cdot S_{\text{cable}} \cdot (f) \cdot \Delta f} \tag{7.7}$$

The amplitude of the total cable response A is Rayleigh distributed if **a)** the phases ϕ are uniform distributed between [-π,π] and **b)** the amplitudes A_j are random and statistically independent [Beckmann, 1962]. Assumption **a** is fully fulfilled by the definition of the time history

response of the cable. Assumption **b** is assumed to be correct as the error involved is acceptable, similarly to the way the wave height resulting from a wide JONSWAP spectrum is assumed fit a Rayleigh distribution [Holthuijsen, 2015].

3. The scale parameter of the Rayleigh distribution can be found from the cable response spectrum by Equation 7.8.

$$\sigma^2 = m_0 = \int_0^\infty \cdot S_{\text{cable}}(f) \cdot df \tag{7.8}$$

The first order moment of the cable response spectrum gives the variance of the time history response, which also corresponds to the scale parameter of the Rayleigh distribution, see Appendix C.2. The probability that any peak in the cable response is below a certain value x is given by the Cumulative Distribution Function (CDF), from now on defined as Q. The CDF of the Rayleigh distribution is found in Equation 7.9 and is fully defined by the scale parameter σ^2.

$$Q = p(CR \leq x) = 1 - \exp\left(\frac{-x^2}{2\sigma^2}\right) \tag{7.9}$$

4. The distribution of a single peak of the cable response is extended to the extreme value distribution over a period of three hours. This extreme value distribution is calculated by Equation 7.10, where the number of peaks contained in a three hour time representation, N_{peaks}, is estimated based on the mean zero up-crossing period of the signal.

$$Q_{3h} = [Q]^{N_{\text{peaks}}} \tag{7.10}$$

The zero up-crossing period of the signal is calculated by Equation 7.11. m_0 and m_2 are the zeroth and second moment of the cable response spectrum, respectively. The nth order moment of the cable response spectrum can be found by Equation 7.12.

$$\bar{T} = \sqrt{\frac{m_0}{m_2}} \tag{7.11}$$

$$m_n = \int_0^\infty f^n \cdot S_{\text{cable}}(f) \cdot df \tag{7.12}$$

A graphical representation of the transformation of the single peak distribution towards the extreme value distribution over a period of three hours is depicted in Figure 7.4. The figure clearly shows the asymptotically behaviour of the extreme value distribution with respect to increasing the number of peaks contained in the time frame.

5. The MPM cable response during a three hour time history of the cable response is identified. For the Rayleigh distribution this corresponds to the 37$^{\text{th}}$ percentile of the extreme value distribution found in step 4. The MPM is chosen based on the DNVGL standards as defined in [DNVGL-RP-N103, 2017].

The approach outlined above is used to estimate the MPM curvature response in the cable and MPM tension response in the cable during a three hour time domain representation of the cable response for a specific sea state. Later on, the results are compared to the Orcaflex simulations.

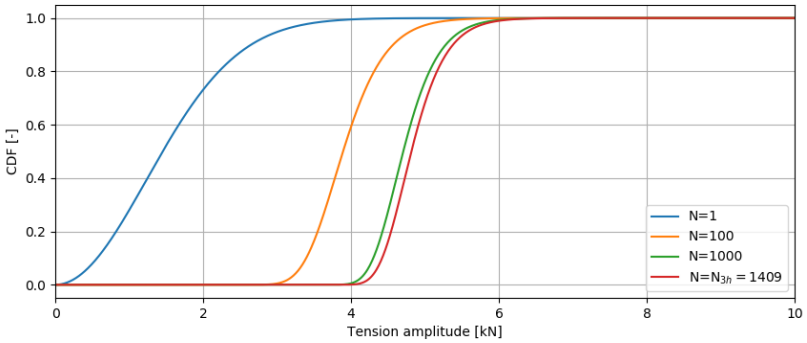

Figure 7.4: The extreme value distribution of the fluctuating component of the maximum tension response for sea state [H_s=2.5m,T_p=8.5s]. Intermediate stages are shown to demonstrate asymptotic behavior of extreme value distribution for increasing N.

7.2.2. Orcaflex simulation approach

In this section the estimation of the MPM cable response based on Orcaflex simulations is explained. A flowchart of the approach is given in Figure 7.5. The steps are explained below.

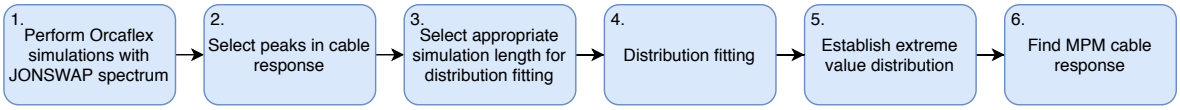

Figure 7.5: Flowchart of the procedure to estimate the maximum cable response based on Orcaflex simulations.

1. The maximum cable response time history is generated by a Orcaflex simulation for a specific sea state.

2. The peaks in the cable response are selected. The aim is to select one peak between two successive zero up-crossings. The peak selection in an arbitrary sample of the maximum tension response in the cable is shown in Figure 7.6.

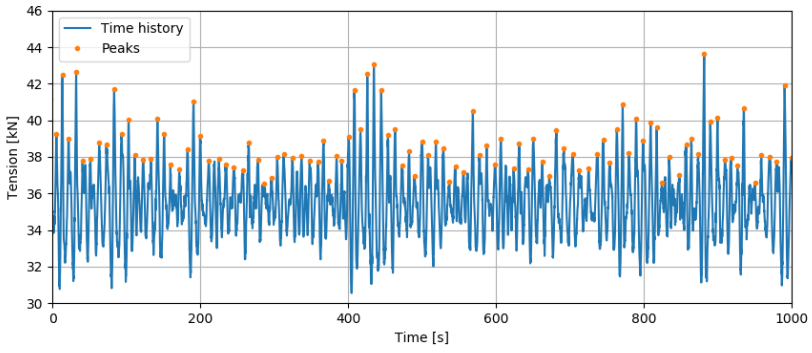

Figure 7.6: Peak selection in the maximum tension response in the cable for sea state [H_s=2.5m,T_p=8.5s].

3. The next step is to select an appropriate simulation length for the fitting of a probability distribution to the data set. The required simulation length is selected based on the convergence of the properties of the data set. The properties considered here are the mean, standard deviation, skewness and kurtosis. Once these properties have converged, additional simulation

time will not significantly improve the accuracy in the distribution fitting. An example of the development of the properties of the peak data set of the maximum tension response is given in Figure 7.7. The figure shows that the kurtosis converges much slower than the other properties given in the plot. This is due the fact that the kurtosis is a function of the fourth central moment of the data set, meaning it is highly influenced by the extreme values in the data set. Hence, explaining the slow convergence rate of this property.

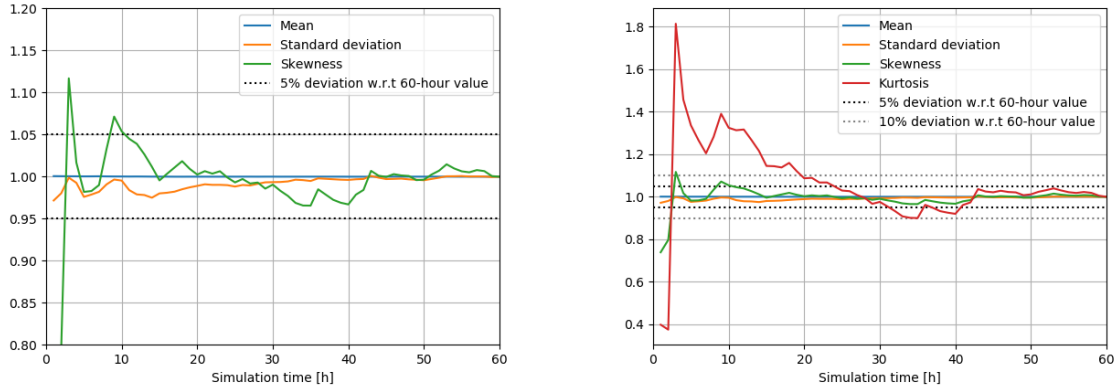

a) Mean, standard deviation and skewness.

b) Mean, standard deviation, skewness and kurtosis.

Figure 7.7: The development of the properties of the data set containing the peaks in the maximum tension response time history for sea state [H_s=2.5m,T_p=8.5s].

4. Now the data set is ready, the actual distribution fitting is executed. The data set is fitted to a list of 12 potential distribution functions. An example of the distribution fitting is given in Figure 7.8. The number of distributions presented in this plot is reduced for clarity.

   For each fit the Kolmogorov-Smirnov (KS) Goodness-of-Fit test is applied, where the hypotheses read:

$$H_0\text{: } \textit{The data is drawn from distribution 'x'.}$$
$$H_1\text{: } \textit{The data is not drawn from distribution 'x'.}$$

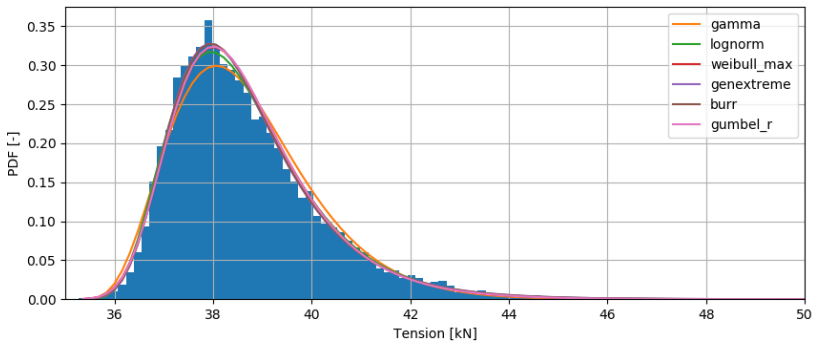

Figure 7.8: Distribution fitting of the maximum tension response for sea state [H_s=2.5m,T_p=8.5s] to the gamma distribution, the log-normal distribution, the weibull distribution, the generalized extreme value distribution, the Burr distribution and the Gumbel distribution.

The KS test returns a p-value. High p-values indicate a good fit. An alpha-level of 5% is selected. This means if the p-value is below 0.05, meaning there is less than 5% chance the data is selected from the specified distribution, the distribution is rejected.

In addition, the Least-Squares Error (LSE) between the fitted distribution and the normalized histogram of the actual data set is calculated to give more insight in the Goodness-of-Fit. The least-squared error between the data set and fitted distribution is calculated by Equation 7.13, where y_i represents the height of the bin of the normalized histogram of the dataset and $f(x_i)$ the values of the PDF of the fitted distribution at the midpoint of the histogram bin.

$$LSE = \sum_{i=1}^{n} \Big(y_i - f(x_i) \Big)^2 \tag{7.13}$$

From the distributions which are not rejected based on the KS-test, the one with the lowest least-squared error between the actual data-set and probability distribution is selected.

The final result of this step is a distribution describing the probability that a given peak in the cable response is below a certain value x, see Equation 7.14

$$Q = p(CR \leq x) \tag{7.14}$$

5. Step 5 is equal to step 4 in the approach for the transfer function. The extreme value distribution for a thee hour simulation is determined using Equation 7.10.

6. In order to comply with the approach followed for the transfer function, in this step the 37^{th} percentile of the extreme value distribution in step 5 is selected. Note that this is not the MPM in case another distribution than the Rayleigh distribution was selected.

7.2.3. Results comparison

The performance of the transfer function is tested using the approaches outlined above. Eight sea states are selected and the results are compared. These eight sea states represent a likely range of sea states at an installation site. The sea states are given in Table 7.1

Table 7.1: Overview of sea states for which the reduced time domain method is tested.

Seastate	1	2	3	4	5	6	7	8
$\mathbf{H_s}$ **[m]**	1.0	1.0	1.5	1.5	2.0	2.0	2.5	2.5
$\mathbf{T_p}$ **[s]**	4.5	5.5	5.5	6.5	6.5	7.5	7.5	8.5
γ **[-]**	1.78	1.0	1.80	1.0	1.59	1.0	1.34	1.0

For the Orcaflex simulation results, the distribution that overall fits the data best is selected. For the maximum tension response of the cable the generalized extreme value distribution is selected. For the maximum curvature response the beta distribution is selected. Some additional fitting analysis by means of P-P plots are executed for the distribution fitting of both the maximum tension and the the maximum curvature distribution fitting, because none of the fitted distributions was accepted following the KS-test for all the considered sea states. In P-P plots the empirical CDF of the data set is plotted against the CDF of the fitted distribution. The P-P plot is thus an indication of the deviation of the fitted distribution with respect to the actual data. An example of the P-P plot is given in Figure 7.9. The more the blue dots are concentrated around the red indicator line, the better the fit.

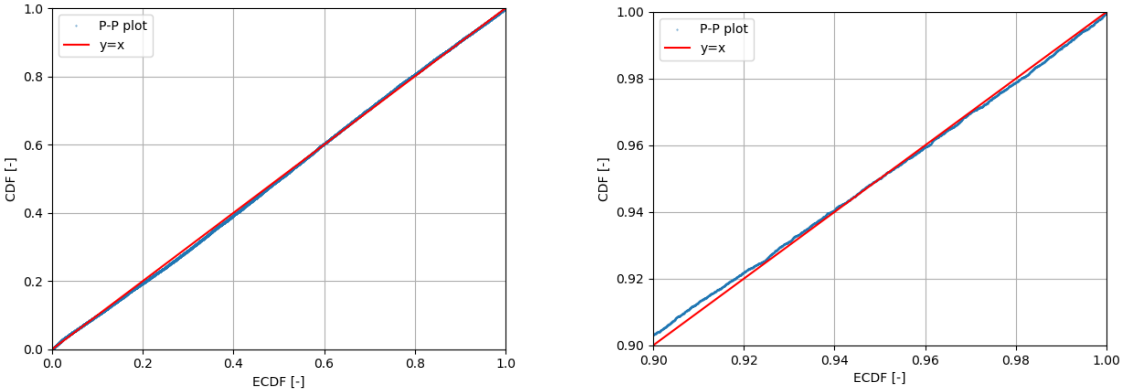

a) Full P-P plot

b) Zoom-in on P-P plot

Figure 7.9: P-P plot between the curvature response of the cable and the beta distribution for sea state 2.

Main focus in these plots is on the 90th percentile an up, as these will dominate the shape of the extreme value distribution. In addition, the errors introduced by the distribution fit with respect to the actual data are calculated for the sea states which were not accepted based on the KS-test. The errors at the single peak distribution function are calculated for the 95th and the 99th percentile, while the error in the extreme value distribution for N=1000 is calculated for the 37th percentile. For the tension response distribution fit all of the errors mentioned above are below 0.4% and for the curvature response distribution fit all errors stay below 0.6%. Based on these numbers, the extreme value distribution is used for the tension response of the cable and the beta distribution is applied for the maximum curvature response of the cable. A complete overview of the distribution selection is presented in Appendix C.3.

The comparison between the transfer function results and the Orcaflex simulation results is presented in Table 7.2 and in Table 7.3 for the maximum tension and the maximum curvature response in the cable, respectively. The error provided in these tables represents the error introduced by the use of the transfer function compared to the actual Orcaflex simulation distribution fit results. The negative value of this error indicates that the transfer function underestimates the most probable cable response, leading to the conclusion that the cable response can not be approximated by the first order response of the cable towards regular waves. In addition, the maximum cable response in an arbitrary three hour Orcaflex simulation is presented. This, in order to allow for comparison with the value based on the Orcaflex distribution fit of the cable response. The results show that indeed, due to the randomness involved with seed selection, in some cases the cable response is underestimated by analysing only a three hour simulation analysis.

The data in Table 7.2 and Table 7.3 shows that the estimation of the transfer function becomes worse for higher sea states. Likely, this results from the fact that higher order components start to have a larger effect on the cable response for these sea states, see section 6.4. The underestimation in the maximum curvature by the transfer function is larger than the underestimation found in the maximum tension prediction of the transfer function. This is most probably related to the fact that the curvature response (section 6.1) of the cable shows more higher order components in the cable response, which were neglected upon creation of the transfer function.

Table 7.2: Comparison between the maximum tension in the cable calculated based on the transfer function approach and the maximum tension in the cable determined based on Orcaflex simulations.

Sea state	**1**	**2**	**3**	**4**	**5**	**6**	**7**	**8**
Transfer function T_{max} [kN]	36.88	36.88	37.53	37.73	38.34	39.18	40.02	41.16
Orcaflex: distribution fit T_{max} [kN]	37.18	37.23	38.20	3869	39.87	41.40	43.47	46.91
Error T_{max} [%]	-0.8	-0.9	-1.7	-2.5	-3.5	-5.4	-7.9	-12.3
Maximum tension response 3h Orcaflex simulation [kN]	37.38	37.32	38.35	38.93	40.68	41.74	43.23	45.84

Table 7.3: Comparison between the maximum curvature in the cable calculated based on the transfer function approach and the maximum curvature in the cable determined based on Orcaflex simulations.

Sea state	**1**	**2**	**3**	**4**	**5**	**6**	**7**	**8**
Transfer function κ_{max} [rad/m]	0.0499	0.0497	0.0512	0.0520	0.0536	0.0559	0.0583	0.0605
Orcaflex: distribution fit κ_{max} [rad/m]	0.0567	0.0561	0.0589	0.0630	0.0662	0.0693	0.0754	0.0891
Error κ_{max} [%]	-12	-11.1	-13	-17.5	-19	-19.4	-22.7	-32.2
Maximum curvature response 3h Orcaflex simulation [rad/m]	0.0564	0.0560	0.0597	0.0626	0.0645	0.0704	0.0731	0.0874

7.2.4. Response spectrum comparison

In order to provide more insight in the behaviour of the transfer function approach, and to get a better understanding of the cause of the under prediction, the cable response spectrum resulting from the transfer function approach is compared to the cable response spectrum resulting from a three hour Orcaflex simulation for an arbitrary sea state. In Figure 7.10, the comparison is shown for the tension response of the cable. The peak at the peak frequency of the sea state, f_p, in the tension response is only slightly underestimated by the transfer function. However, the higher frequencies in the response, including the second peak which is located at approximately $1.5f_p$, are not predicted correctly and under estimated by the transfer function. This is because the transfer function completely leaves out these higher order effects in the cable response. The response at $1.5f_p$ is now only based on the response of the CLV at this frequency, which will be small because the CLV hardly responds to higher frequencies and the sea state given as input to the calculation rapidly reduces as the respective frequency is further away from the peak frequency.

Based on the size of the underestimation found in subsection 7.2.3 and the accompanied comparison between the cable response spectra of the tension, suspicions with regards to the assumption that the transfer function cable response follows a Rayleigh distribution are raised. Taking into account that the transfer function only represents the dynamic part of the tension response, the under prediction seems to be quite large in light of the amount of variation between the Orcaflex and transfer function approach cable response spectra. Furthermore it is found that for sea states with lower peak periods, the under prediction in the main peak in the tension response of the cable increases.

The same comparison for the curvature response is presented in Figure 7.11. The shape of the response is similar to the response spectrum of the tension. However, for the curvature response not only the peak at approximately f=$1.5f_p$ is mispredicted by the transfer function, also the main peak in the curvature response, located at the peak frequency of the wave spectrum, is underestimated.

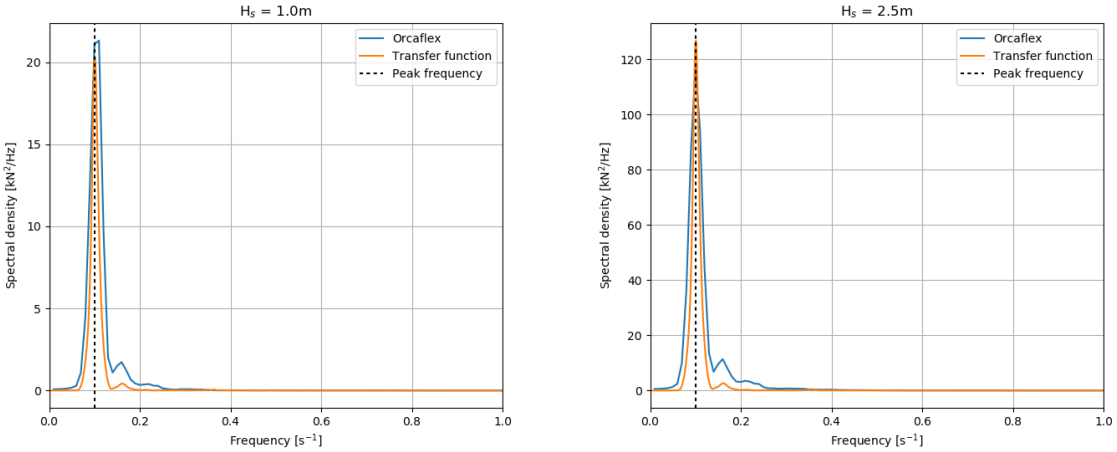

Figure 7.10: The response spectrum of the curvature response of the cable based on the transfer function approach and resulting from a three hour Orcaflex simulation for T_p = 5.0s

This results from the high dynamic complexity of the curvature response of the cable, demonstrated in the spectral analysis in Chapter 6. This leads to the large under prediction of the transfer function for the maximum curvature response.

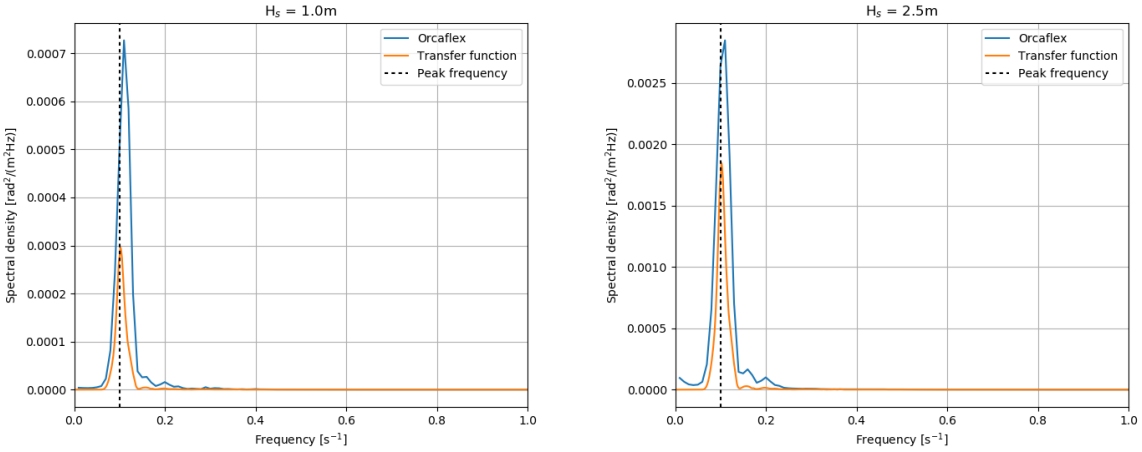

Figure 7.11: The response spectrum of the curvature response of the cable based on the transfer function approach and resulting from a three hour Orcaflex simulation for T_p = 10.0s

8

Sensitivity Analysis

In this chapter a sensitivity analysis is performed. First, the sensitivity of the DFT analysis is evaluated. In this analysis the different frequency components in the cable response were studied. In the sensitivity analysis the effect of a change in the bending stiffness and axial stiffness of the cable is studied. These cable properties are more complex to estimate than properties like for example mass or diameter. Therefore it sometimes occurs that the estimated values for these properties change along the course of a project on the basis of e.g recently performed tests. The procedure and results are discussed in section 8.1.

Second, the effect of a change in the normal cable lay configuration on the selection of the governing vessel motion for the use of vessel limit criteria is studied. For the practicality of the use of vessel limit criteria it is desirable that the selected vessel motion is not strongly affected by deviations in the normal lay configuration. This analysis is described in section 8.2.

8.1. DFT analysis

The DFT response of the cable is determined as described in section 6.1. In this study the bending stiffness and the axial stiffness are both reduced by 10 and 50%, respectively. All other properties of the normal lay configuration are kept unchanged.

8.1.1. Bending stiffness

The results for the reduction of the bending stiffness on the curvature of the cable are presented in Figure 8.1. The same plot for the tension response of the cable is given in Appendix D.1. As expected, the reduction of the bending stiffness causes an increase in the maximum curvature in the cable. The total increase of the maximum curvature with respect to the static curvature is +3.7% and +27.0%, for a reduction of respectively 10% and 50% of the bending stiffness. Based on the plot in Figure 8.1, the reduction of the bending stiffness most significantly increases the contribution of higher components in the signal. This results from the amplified movements of the cable, which highlight the non-linear geometry, as the bending stiffness itself is linear.

Although the effect of the reduction of the bending stiffness on the tension response is small, it still results in a small increase of the tension response. Here also the third component of the DFT of the tension response in the cable is affected the most.

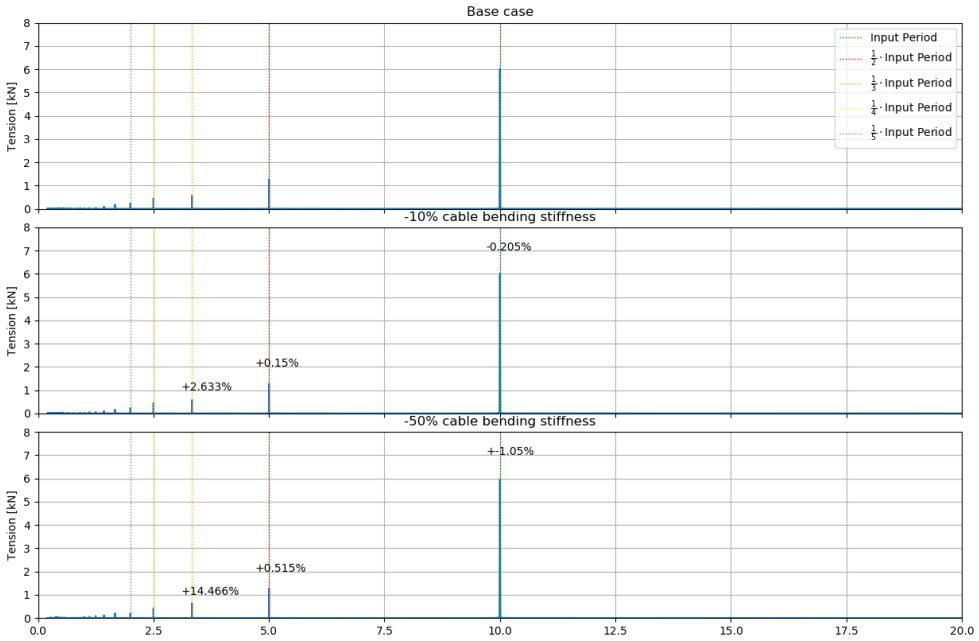

Figure 8.1: Plot depicting the sensitivity of the DFT of the curvature response of the cable towards a reduction in the bending stiffness of the cable.

8.1.2. Axial stiffness

The system is quite insensitive to a change in the axial stiffness of the cable. The total amplitude of the curvature response of the cable is reduced by only 0.07% and the tension response is increased by 0.16%, for a 50% reduction of the axial stiffness. The results for both the tension and curvature in the cable are presented in Appendix D.1. Some shifts occurs in the contributions of the different components to the total response. The curvature response for a 50% decrease in the axial stiffness, shows that the higher contributions increase, while the total response and first order component decrease. This is favorable in case the axial stiffness changes along the course of a project, as most likely the original analysis can still be assumed to be useful.

8.2. Vessel motion selection

In section 4.3, the governing vessel motion for the application of vessel motion limit criteria was studied for the normal lay configuration described in section 3.1. In this section the same analysis is performed for two different normal lay configurations. In the first case the export cable is changed to an array cable. This type of cable is located in-field of an offshore wind farm, which means they they transport lower amounts of electrical energy than an export cable. Consequently these types of cables are generally lighter and have a lower axial, bending and torsional stiffness compared to export cables. In the second case the water depth is decreased to 25m, with respect to 50m in the base case.

In Table 8.1 an overview of the normal lay configurations is presented. The properties of the array cable mentioned in Table 8.1 are given in Table 8.2. For comparison purposes, the properties of the export cable, which were already presented in Table 3.1, are also added to this table.

Table 8.1: Overview of the normal lay configurations in the sensitivity analysis

Configuration	Case 1	Case 2	Case 3
Specialty	-	Water depth	Cable type
Cable type	Export cable	Array cable	Export cable
Water depth [m]	50	50	25
Static top tension [kN]	35.5	24.50	9.32
Static departure angle [°]	16.6	24.78	24.25
Static TDP tension [kN]	7.37	6.99	3.13

Table 8.2: The cable properties of the subsea cables in the sensitivity analysis.

Cable type	Export cable	Array cable
Mass [kg/m]	100	29
Diameter [m]	0.267	0.136
Bending stiffness [kN·m^2]	90.0	11.1
Axial stiffness [kN]	525,000	385,000
Torsional stiffness [kN·m]	185.0	6.2
T_{max} [kN]	225.0	155.9
MBR_{min} [m]	4.10	2.22

The results of the vessel motion selection analysis for Case 2 and Case 3 are discussed in subsection 8.2.1 and subsection 8.2.2, respectively. The full details of each analysis are documented in Appendix D.2.

8.2.1. Case 2

Case 2 comprises a normal lay configuration with an array cable. The approach for the vessel motion selection described in section 4.3 is used. By inspection of the tension response of the cable in relation to the correlation with the vessel motions at the chute of the vessel, the heave acceleration and axial acceleration are selected. This is in agreement with the results obtained from case 1.

For the curvature response, none of the vessel motions shows higher correlations than the wave elevation. From all inspected vessel motions, the heave acceleration still shows the best results, which is in correspondence with the findings for case 1.

8.2.2. Case 3

Case 3 comprises the reduction of the water depth. Studying the tension response of the cable by the same approach as for the base case, the heave velocity and axial velocity of the CLV are selected instead of the heave acceleration and the axial acceleration. Although the heave acceleration and axial acceleration are not rejected based on either a dependency deficiency or performance below the sea state limit criteria, the absolute magnitude of the cross correlation of the heave velocity and axial velocity outperformed those of the heave acceleration and the axial acceleration. The shift is most likely the result of the shorter cable length caused by the reduction of the water depth. Therefore, the system is less dominated by the inertia of the cable itself and other effects, like drag, start to dominate.

In the analysis with respect to the curvature response of the cable, none of the inspected vessel mo-

tions performed overall better than the wave elevation. In this case this means that the average correlation between the cable response and the wave elevation is higher than the correlation between the cable response and any of the vessel motions. The correlation between the wave elevation and curvature response slightly decreased with respect to case 1, but the correlations between the curvature response and the vessel motions show quite a significant decrease. A possible explanation is the fact that in shallower water a larger fraction of the catenary is affected by wave forces.

The overall reduction of the magnitude of the correlations can be attributed to the reduction of the water depth, which in general moves the system towards less linear behaviour. The top excitation by the CLV is relatively larger compared to the total length of the system, highlighting the non-linear geometry of the system and in addition, a larger fraction of the cable is affected by the non-linear drag term.

8.2.3. Sensitivity of vessel motion selection

Overall, the sensitivity of the vessel motion selection for vessel limit criteria showed that the selected vessel motion for application of vessel motion limit criteria is subject to change upon variation in the normal lay configuration. Furthermore, for both inspected normal lay configurations the wave elevation showed higher correlations with respect to the curvature response of the cable than any of the inspected vessel motions.

Both observations reduce the attractiveness of the implementation of vessel motion limit criteria. First of all, it is undesirable that the used limit parameter shifts upon a change in the cable lay configuration. Furthermore, the curvature seems to cause problems for the implementation of vessel motion limit criteria, as the correlation between the curvature response of the cable and the vessel motions in general reduced quickly with the reduction of the water depth.

9

Conclusion & Recommendations

In this chapter the conclusions of this thesis report are documented and recommendations for future research are made.

9.1. Conclusion

The direct cable loads on the cable govern the cable dynamics for short period waves during normal lay operations with the lay configuration considered in this study. Starting from waves with a wave period of 8 seconds, the vessel motions take over and govern both the curvature and tension response of the cable. The latter is favorable for the application of vessel limit criteria, as it is desirable that installation limits are expressed in terms of the parameter which affects the cable dynamics the most. Short period waves are not likely to occur in combination with large wave heights, and in combination with low wave heights they are not likely to exceed the handling limits of the cable. Therefore, the independence of the cable dynamics on the vessel motions for short period waves is not preventing the use of vessel motion limit criteria for normal lay operations.

In order to apply vessel motion limit criteria, a vessel motion must be selected. This selection is based on the TLCC's between the cable response and the vessel motions at the chute of the CLV. Ideally, a limit parameter with an as much as possible linear relationship with respect to the cable response is selected, as this implies that an increase in the limit parameter is indeed related to an increase in the cable response. Based on the assessment, it was found that both heave acceleration and axial acceleration are most suitable for application of vessel motion limit criteria for the base case considered in this thesis.

Next, the use of vessel motion limit criteria was assessed with the use of a linear regression analysis on data of the heave acceleration of the chute of the CLV and the peaks in the cable response. It was found that higher certainty can be given to limits expressed in the heave acceleration of the vessel compared to the wave elevation, which eventually positively affects the workablility of the operation. This conclusion is based on the bandwidth of the 95% prediction bands and the relative steepness of the slopes of the linear regression lines between, on one hand, the cable response and heave acceleration of the CLV chute, and on the other hand, the cable response and the wave elevation. However, it should be kept in mind that the use of vessel motion limit criteria does come with the inability to express limits for short period sea states, especially at installation sites where sea states with short periods and relatively high significant wave heights occur. This is caused by the small response of the vessel to short period waves.

Furthermore, the principle of RTDM, namely that the maximum cable response occurs around the extremes in the vessel motions of the chute, was not found applicable for normal lay analysis. The method was not able to capture the maximum cable response when applied to either heave velocity or heave acceleration of the CLV.

In the sensitivity analysis, the sensitivity of the vessel motion selection towards a change in the normal lay configuration was investigated. For the tension response, a shift in the selected vessel motion was detected, from heave and axial acceleration towards heave and axial velocity, for the case which considered a reduction of the water depth. Furthermore, in both of the normal lay configurations studied in the sensitivity analysis, the wave elevation had a higher TLCC with respect to the curvature response than any of the vessel motions at the chute of the CLV. Both of these observations reduce the attractiveness of the implementation of vessel motion limit criteria. Therefore, the statement that vessel motion limit criteria are preferred over sea state limit criteria can not be generalised for all normal lay analysis.

To inspect the frequency response of the cable, a spectral analysis is performed. This showed that the curvature response of the cable contains more higher order components than the tension response of the cable. Additionally, the contribution of the higher order components of the response is most significant between T_{wave}=8s and T_{wave}=12s and increasing wave height results in general also in an increase of the contribution of higher order components in both the curvature and tension response. Most likely, this is because the dynamics of the curvature response of the cable are more affected by the non-linearties in the model compared to the tension response. Furthermore, drag linearisation was applied to the base case model. Drag linearisation results in a reduction of the maximum curvature response as well as the maximum tension response in the studied case. This is caused by a change in the profile of the drag force upon linearisation.

Finally, the use of a transfer function for estimation of the maximum cable response was evaluated. This transfer function is based on the first order response of the cable towards regular waves simulations. The approach is found unsuitable for estimation of both the maximum tension and maximum curvature response of the cable. The use of this method results in an underestimation of the extreme cable responses. This underestimation is found to be more severe for the curvature response than for the tension response of the cable and increases with an increase of the severity of the sea state.

9.2. Recommendations

Based on the work in this thesis, recommendations for future research are provided. With respect to the vessel motion limit criteria assessment a couple of suggestions are given. First of all, it is recommended to extend the number of cases to which the vessel motion limit criteria assessment is applied. Expansion of the number of wave headings and cable lay configurations is suggested. The area in which the vessel motions are dominating the cable dynamics should be investigated for each cable configuration, including the effect of a change in the wave heading. Next, the successive steps of the vessel motion limit criteria assessment, the vessel motion selection and linear regression analysis, must be applied to each new case. Furthermore, the effect of current is not considered throughout the case study conducted in this thesis and thus it is recommended to implement this in the extension of the vessel motion limit criteria assessment. This, in order to identify the full range for which vessel motion limit criteria are preferred over sea state limit criteria.

Another point of attention is the application of vessel motion limit criteria at short peak period sea states. Although it is expected that the inability of vessel motion limit criteria to express limits at less severe sea states is not directly preventing the use of vessel motion limit criteria, it is recommended

to further investigate the practical implications involved with this matter.

With regards to the transfer function approach, a couple of recommendations are made. First of all, the fact that the transfer function underestimates the cable response, leads to the recommendation to redefine the transfer function based on a conservation of energy approach. In this approach the total energy contained in the cable response towards a regular wave is transported to the input frequency of the system and the corresponding data point in the transfer function. This aims to reduce the underestimation of the transfer function, by taking into account all components of the response. Furthermore, the cable response spectrum comparison implicated that the assumptions, made during the set up of the distribution of the maximum cable response based on the transfer function, are not accurate. Therefore, is it recommended to test the performance of the transfer based on a time domain representation of the cable response calculated by the transfer function. This way, the dependency of the performance check on the assumption that the transfer function cable response follows the Rayleigh response is eliminated.

Last, a deeper research into the reliability of the current practice of a three hour time domain simulation for normal lay analysis is suggested. The difference between the results obtained from a three hour time domain simulation and the Orcaflex cable response distribution fit showed that this approach can result in falsely accepted cases in the cable installation analysis. The focus lies on mapping the size of the error introduced by this practice.

Bibliography

API RP 17B (2002). Recommended Practice for Flexible Pipe. *Api*, 44(THIRD EDITION,):71–90.

Beckmann, P. (1962). Statistical distribution of the amplitude and phase of a multiply scattered field. *Journal of Research of the National Bureau of Standards, Section D: Radio Propagation*, 66D (3):231. ISSN 1060-1783. doi: 10.6028/jres.066d.027.

Dean, R. and Dunsmuir, W. (2016). Dangers and uses of cross-correlation in analyzing time series in perception, performance, movement, and neuroscience: The importance of constructing transfer function autoregressive models. *Behavior Research Methods*, 48(2):783–802.

DNVGL-RP-0360 (2016). Subsea power cables in shallow water. (March). URL `www.dnvgl.com`.

DNVGL-RP-C205 (2010). Environmental Conditions and Environmental Loads. Technical Report October.

DNVGL-RP-N103 (2017). Modelling and analysis of marine operations. (July). URL `www.dnvgl.com`.

Dominic Reeve, A. C. and Fleming, C. (2004), *Coastal Engineering: Processes, theory and design practice*. Spon Press.

Faltinsen, O. (1990), *Sea Loads on Ships and Offshore Structures*. Cambridge Univeristy Press, Cambridge. ISBN 0521458706.

Hedges, T. S. (1995). Regions of validity of analytical wave theories. *Proceedings of the Institution of Civil Engineers: Water, Maritime and Energy*, 112(2):111–114. ISSN 17537819. doi: 10.1680/iwtme.1995.27656.

Holthuijsen, L. H. (2015), *Waves in Oceanic and Coastal Waters*. Cambridge University Press.

IWES, F. (2018). Windmonitor. `http://windmonitor.iee.fraunhofer.de/windmonitor_en/4_Offshore/2_technik/2_Kuestenentfernung_und_Wassertiefe/`.

Journée, J. and Massie, W. (2001), *Offshore Hydromechanics*. Delft University of Technology.

Knapp, R. H. (1979). Derivation of a new stiffness matrix for helically armoured cables considering tension and torsion. *International Journal for Numerical Methods in Engineering*, 14(4):515–529. ISSN 0029-5981. doi: 10.1002/nme.1620140405. URL `http://doi.wiley.com/10.1002/nme.1620140405`.

Koloshkin, E. and Saevik, S. (2016). *Torsion Buckling of Dynamic Flexible Risers*. PhD thesis, NTNU.

Kurt, J. P. (1984). Empirical factors in the prediction of helically armored cable axial stiffness. *Journal of Energy Resources Technology, Transactions of the ASME*, 106(4):521–526. ISSN 15288994. doi: 10.1115/1.3231117.

Loos, B. (2017). Operability limits based on vessel motions for submarine power cable installation. diploma thesis, TU Delft.

Marta, M., Mueller-Schuetze, S., Ottersberg, H., Isus, D., Johanning, L., and Thies, P. R. (2015). Development of dynamic submarine mv power cable design solutions for floating offshore renewable energy applications.

McConnon, D. J., Looby, T., Kearney, J., and O'Shaughnessy, J. (2017). Investigation of electrical defects arising from excessive sidewall force and excessive tensile strain on power cables. *2017 52nd International Universities Power Engineering Conference, UPEC 2017*, 2017-Janua:1–5. doi: 10.1109/UPEC.2017.8231910.

NTNU (2015). Drag forces in dynamic analysis. Lecture note of TMR4305 'Advanced Analysis of Marine Structures' NTNU.

NTNU (cited August 2020). Chapter 12 - nonlinear analysis. Memo of TMR4305 'Advanced Analysis of Marine Structures' NTNU.

Oord, V. (Oct 2015). Cable-laying vessel nexus. `https://www.vanoord.com/sites/default/files/leaflet_nexus_lr_1.pdf`.

Orcina (cited August 2020). Orcaflex documentation. `https://www.orcina.com/webhelp/OrcaFlex/Default.htm`.

Osgood, P. B. (2007). The fourier transform and its applications. Stanford University: Lecture Notes for EE 261.

Peksen, M. (2018), *Multiphysics Modeling*. Academic Press. ISBN 9780128118245.

Reda, A. M., Forbes, G. L., Al-Mahmoud, F., Howard, I. M., McKee, K. K., and Sultan, I. A. (2016). Compression limit state of hvac submarine cables. *Applied Ocean Research*, 56:12 – 34. ISSN 0141-1187. doi: https://doi.org/10.1016/j.apor.2016.01.002. URL `http://www.sciencedirect.com/science/article/pii/S0141118716000031`.

Sævik, S. Lecture notes in offshore pipeline technology (February 2017).

Sarpkaya, T. (2010), *Wave Forces on Offshore Structures*. Cambridge Univeristy Press. ISBN 9780521896252.

SER (2013). Energieakkoord voor duurzame groei. Technical report.

SINTEF Ocean (2019). RIFLEX 4.17.0 Theory Manual.

Tan, Z., Quiggin, P., and Sheldrake, T. (2009). Time domain simulation of the 3D bending hysteresis behavior of an unbonded flexible riser. *Journal of Offshore Mechanics and Arctic Engineering*, 131 (3):1–8. ISSN 08927219. doi: 10.1115/1.3058698.

Thies, P. R., Johanning, L., and Smith, G. H. Assessing mechanical loading regimes and fatigue life of marine power cables in marine energy applications. In *Proceedings of the Institution of Mechanical Engineers, Part O: Journal of Risk and Reliability*, volume 226, pages 18–32 (2 2012). doi: 10.1177/1748006X11413533.

Triton, D. (1988), *Physical Fluid Dynamics*. Clarendon Press. ISBN 978-94-009-9992-3.

Ultramarine (2011). Overview of seakeeping. `http://www.ultramarine.com/hdesk/runs/samples/sea_keep/doc.htm`.

Vaz, M., Estefan, S., and Brack, M. (1998). Experimental Determination of Axial, Torsional and Bending Stiffness of Umbilical Cables. *Proceedings of the International Conference on Offshore Mechanics and Arctic Engineering - OMAE*.

Worzyk, T. (2009), *Submarine Power Cables: Design, Installation, Repair, Environmental Aspects*. Springer. retrieved from: https://books.google.no/books?id=X8QfRT_SYDgC&pg=PA181&lpg=PA181&dq=subsea+power+cable+internal+structure&source=bl&ots=yTkdq476Jo&sig=ACfU3U1RBUn2FSO4dRrsQuUJvmO-M4t3fA&hl=nl&sa=X&ved=2ahUKEwjB9YijpdXlAhVL1qYKHWvkAH04ChDoATAIegQICRAB#v=onepage&q=subsea%20power%20cable%20internal%20structure&f=false.

A

Vessel motion limit criteria assessment

This appendix contains additional material of the vessel motion limit criteria assessment. In Appendix A.1 the plots concerning the cable configuration upon maximum curvature are documented. The data and plots used for the vessel motion selection procedure of the base case are given in Appendix A.2. Additional plots regarding the linear regression analysis are given in Appendix A.3.

A.1. Cable configuration upon maximum curvature response

Period effect

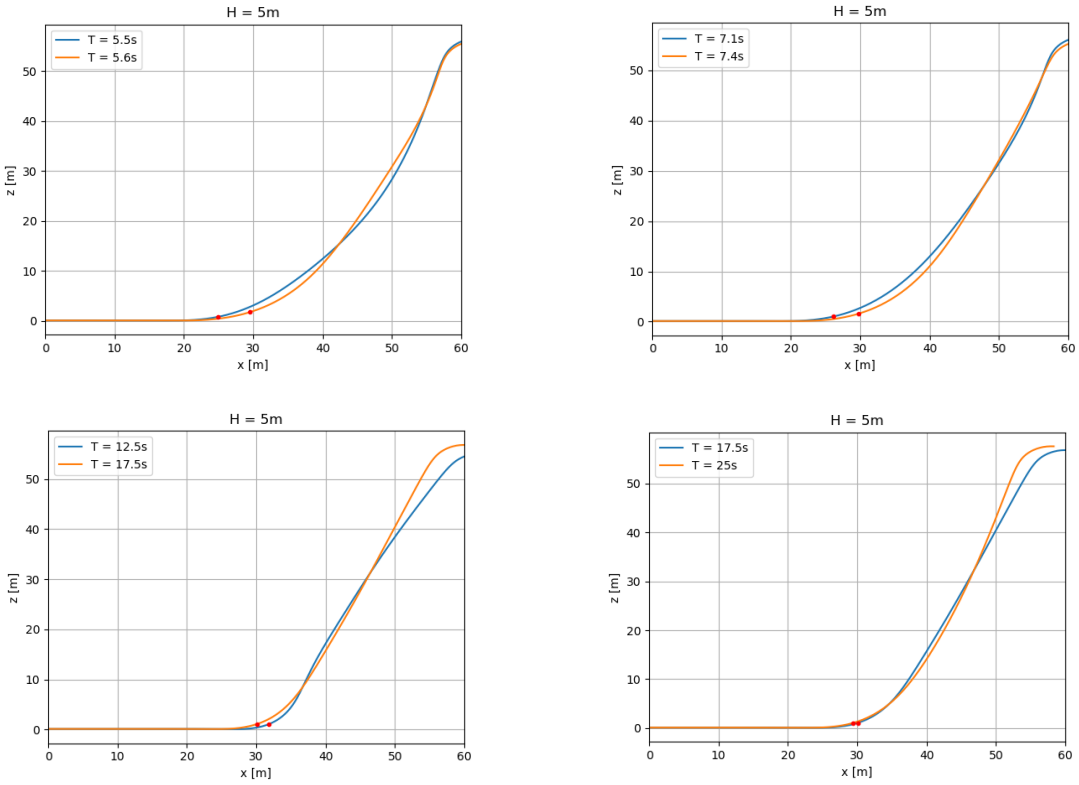

Figure A.1: Variation in cable shape upon maximum curvature for changing wave periods.

Wave height effect

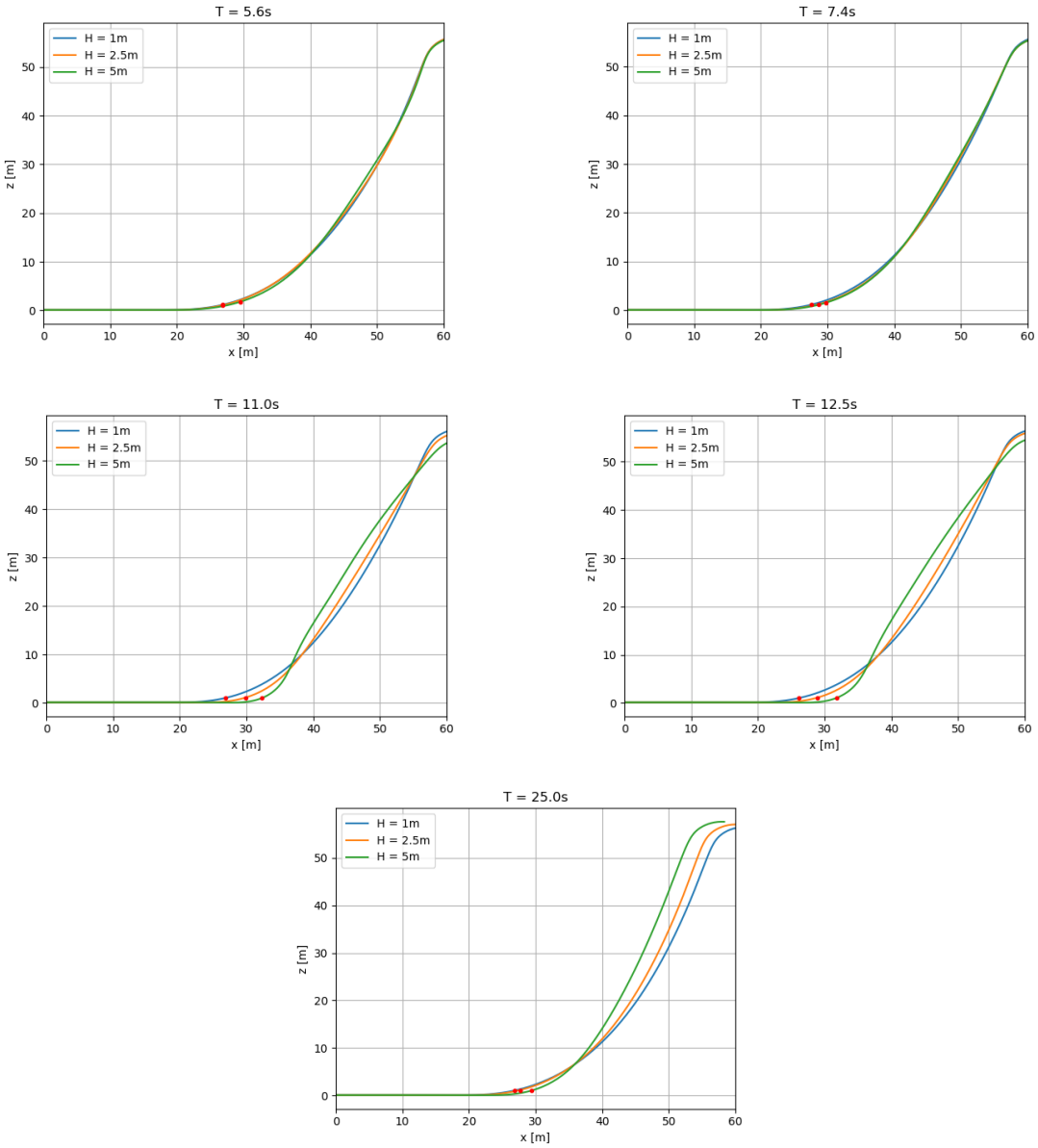

Figure A.2: Variation in cable shape upon maximum curvature for changing wave heights.

A.2. Vessel motion selection

The TLCC data of the vessel motion selection for the curvature response of the cable is provided in Table A.2. The TLCC plots of the tension response of the cable and accompanied data overview are presented in Figure A.3 to Figure A.8 and Table A.3, respectively.

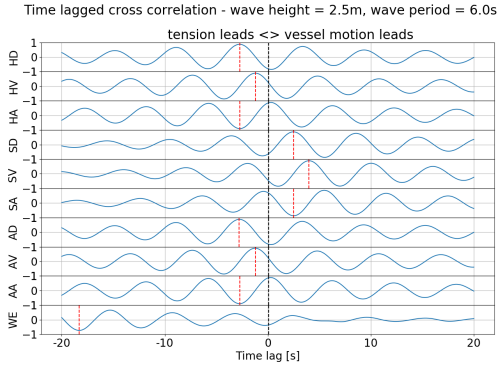

Figure A.3: The TLCC of the tension response of the cable for all vessel motions and the wave elevation, calculated for T_p = 6.0s H_s=2.5m.

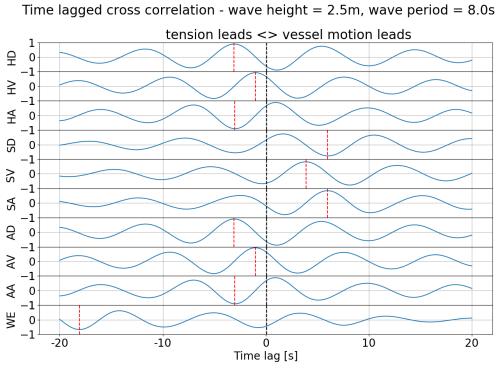

Figure A.4: The TLCC of the tension response of the cable for all vessel motions and the wave elevation, calculated for T_p = 8.0s H_s=2.5m.

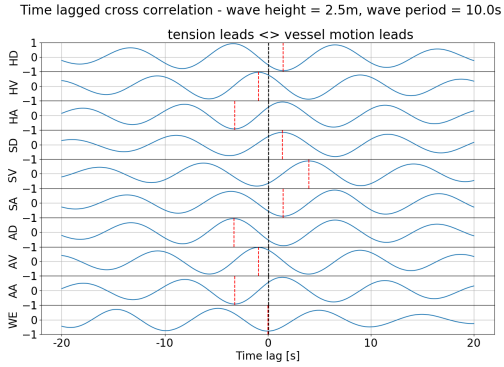

Figure A.5: The TLCC of the tension response of the cable for all vessel motions and the wave elevation, calculated for T_p = 10.0s H_s=2.5m.

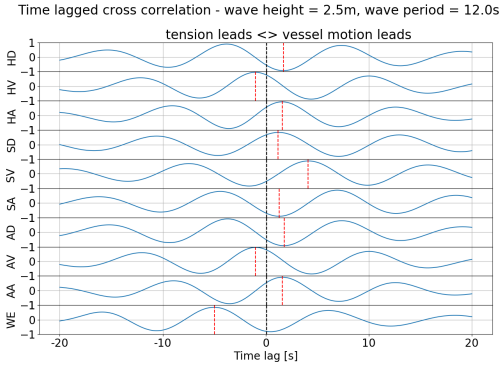

Figure A.6: The TLCC of the tension response of the cable for all vessel motions and the wave elevation, calculated for T_p = 12.0s H_s=2.5m.

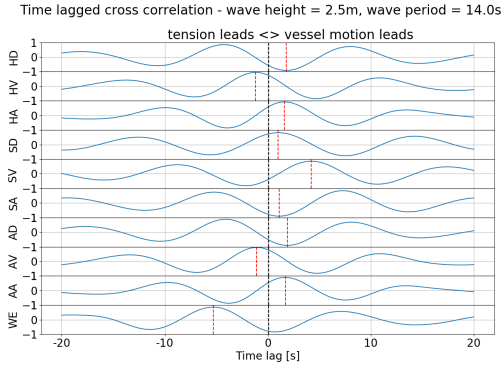

Figure A.7: The TLCC of the tension response of the cable for all vessel motions and the wave elevation, calculated for T_p = 14.0s H_s=2.5m.

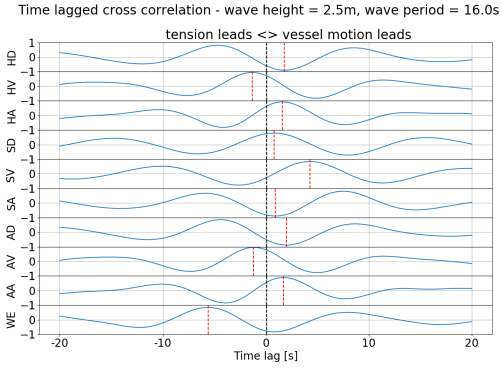

Figure A.8: The TLCC of the tension response of the cable for all vessel motions and the wave elevation, calculated for T_p = 16.0s H_s=2.5m.

Abbreviation	Description
HD	Heave displacement at the chute of the CLV
HV	Heave velocity at the chute of the CLV
HA	Heave acceleration at the chute of the CLV
SD	Surge displacement at the chute of the CLV
SV	Surge velocity at the chute of the CLV
SA	Surge acceleration at the chute of the CLV
AD	Axial displacement at the chute of the CLV
AV	Axial velocity at the chute of the CLV
AA	Axial acceleration at the chute of the CLV

Table A.1: Overview of abbreviations used in the TLCC plots.

Motion	Mean correlation	Maximum correlation	Minimum correlation
HD min	-0.762	-0.875	-0.622
HD max	0.839	0.901	0.673
HV min	-0.830	-0.898	-0.637
HV max	0.826	0.906	0.639
HA min	-0.854	-0.918	-0.619
HA max	0.754	0.860	0.591
SD min	-0.676	-0.748	-0.478
SD max	0.667	0.769	0.470
SV min	-0.713	-0.814	-0.441
SV max	0.678	0.780	0.451
SA min	-0.724	-0.855	-0.423
SA max	0.713	0.800	0.412
AD min	-0.777	-0.875	-0.615
AD max	0.837	0.907	0.664
AV min	-0.830	-0.893	-0.627
AV max	0.817	0.911	0.629
AA min	-0.844	-0.914	-0.608
AA max	0.757	0.851	0.581
WE min	-0.780	-0.798	-0.765
WE max	0.780	0.834	0.673

Table A.2: Overview of time lagged cross correlation results for curvature response of the cable for H_s=2.5m.

Motion	Mean correlation	Maximum correlation	Minimum correlation
HD min	-0.902	-0.931	-0.846
HD max	0.874	0.918	0.788
HV min	-0.857	-0.885	-0.820
HV max	0.939	0.956	0.898
HA min	-0.884	-0.923	-0.820
HA max	0.914	0.931	0.883
SD min	-0.792	-0.874	-0.715
SD max	0.815	0.875	0.732
SV min	-0.815	-0.851	-0.769
SV max	0.864	0.900	0.819
SA min	-0.881	-0.910	-0.801
SA max	0.854	0.885	0.790
AD min	-0.897	-0.927	-0.854
AD max	0.893	0.929	0.834
AV min	-0.838	-0.872	-0.771
AV max	0.943	0.958	0.943
AA min	-0.893	-0.926	-0.851
AA max	0.900	0.911	0.875
WE min	-0.780	-0.836	-0.673
WE max	0.769	0.865	0.598

Table A.3: Overview of time lagged cross correlation results for tension response of the cable for H_s=2.5m.

A.3. Linear regression plots

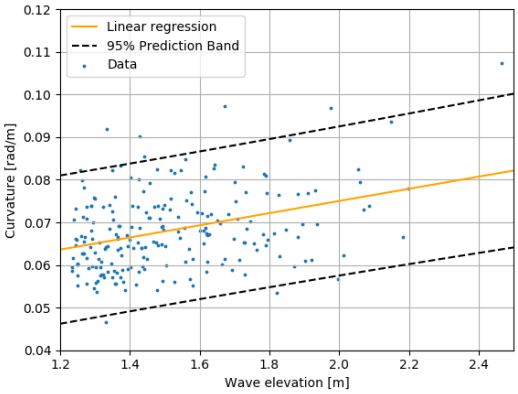

Figure A.9: Linear regression including 95% predictions bends between the maximum curvature and wave elevation peaks for T_p=9.5s and H_s =2.5m.

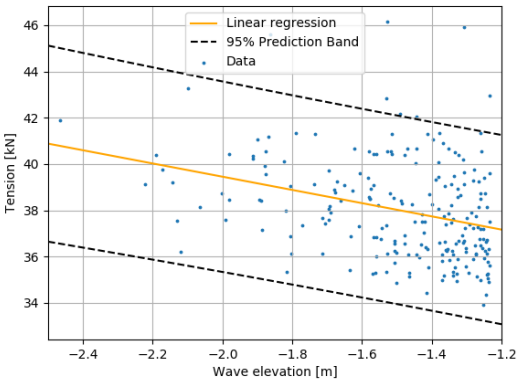

Figure A.10: Linear regression including 95% predictions bends between the maximum tension and wave elevation throughs for T_p=9.5s and H_s =2.5m.

B

Spectral analysis

This appendix contains complementary content to the spectral analysis in this thesis. In Appendix B.1, the velocity and acceleration profiles along the catenary of the cable for two additional wave periods are presented. Furthermore, the drag linearisation applied in the spectral analysis is worked out analytically in Appendix B.2.

B.1. Relative acceleration and velocity

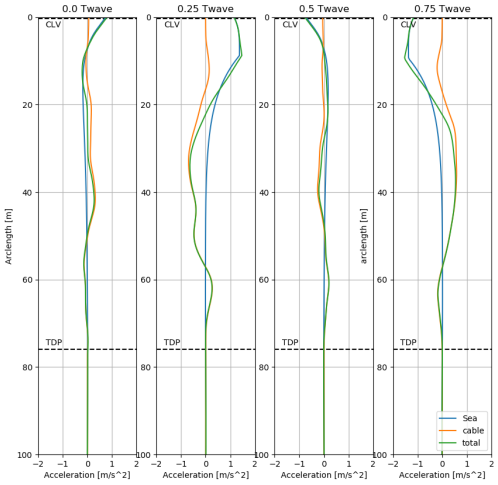

Figure B.1: The acceleration of the sea, cable and total acceleration for T=6s and H = 2.5s.

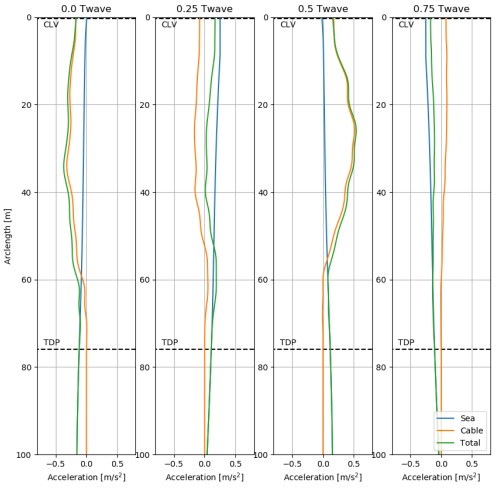

Figure B.2: The acceleration of the sea, cable and total acceleration for T=16s and H = 2.5s.

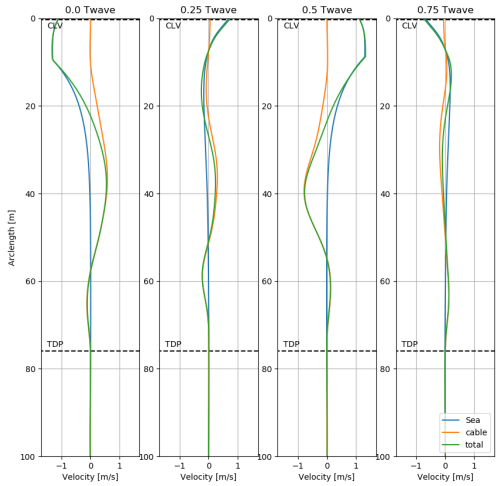

Figure B.3: The velocity of the sea, cable and total velocity for T=6s and H = 2.5s.

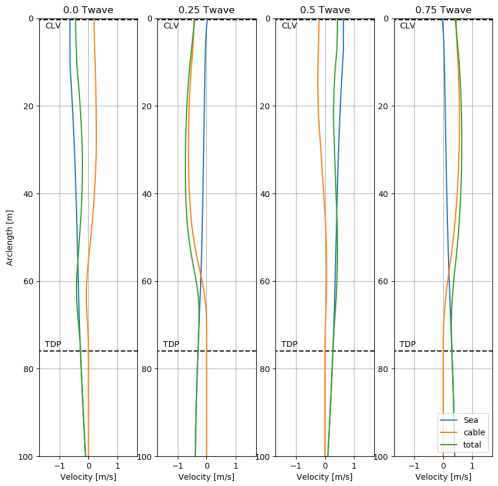

Figure B.4: The velocity of the sea, cable and total velocity for T=16s and H = 2.5s.

B.2. Drag linearisation

This appendix explains the linearisation of the drag force in the Morison equation and is based on [NTNU, 2015]. The drag force on the cable is given by Equation B.1. The linearised form of the drag force can be written by Equation B.2.

$$q_{NL} = \frac{1}{2} \cdot \rho \cdot C_D \cdot D \cdot \Delta l \cdot (u_w - \dot{r}) \cdot |u_w - \dot{r}| \tag{B.1}$$

$$q_L = \frac{1}{2} \cdot \rho \cdot C_D \cdot D \cdot \Delta l \cdot K_L \cdot (u_w - \dot{r}) \tag{B.2}$$

Here K_L is the drag linearisation coefficient and u_w the water particle velocity, which can be represented by a harmonic function, see Equation B.3

$$u_w = u_a \cos(\omega t) \tag{B.3}$$

The displacement of the cable can also be described by a harmonic function, however not necessarily with the same phase as the water particle velocity. Therefore, the displacement ,and consequently the velocity of the cable, can be represented as Equation B.4 and Equation B.5, respectively.

$$r(t) = r_1 cos(\omega t) + r_2 \cos(\omega t) \tag{B.4}$$

$$\dot{r}_t = -\omega r_1 \sin(\omega t) + \omega r_2 \cos(\omega t) \tag{B.5}$$

The total relative velocity can than be written as Equation B.6, where the amplitude A is given by Equation B.7. The phase is not considered as the drag force is a function of the relative velocity only.

$$u_r = A \cos(\omega t) \tag{B.6}$$

$$A = \sqrt{(u_a - \omega r_2)^2 + \omega^2 r_1^2} \tag{B.7}$$

Based on this new expression for the relative velocity of the cable, the non-linear and linear definition of the drag force can be written as Equation B.8 and Equation B.9, respectively. For simplicity, the notation in Equation B.10 will be used in the derivation from now on.

$$q_{NL} = \frac{1}{2} \cdot \rho \cdot C_D \cdot D \cdot \Delta l \cdot A^2 \cdot \cos(\omega t) | \cdot \cos(\omega t) | \tag{B.8}$$

$$q_L = \frac{1}{2} \cdot \rho \cdot C_D \cdot D \cdot \Delta l \cdot A \cdot \cos(\omega t) \tag{B.9}$$

$$C_D^* = \frac{1}{2} \cdot \rho \cdot C_D \cdot D \cdot \Delta l \tag{B.10}$$

Linearisation of the drag force will introduce an error. The error can be found by the difference between the linear drag force and the non-linear drag force. The squared error is given by Equation B.11.

$$e^2 = (q_L - q_{NL})^2 \tag{B.11}$$

The best possible linearisation is obtained for the linearisation coefficient for which the linearisation error over the full wave period is minimal. The squared error over the full wave period is defined by Equation B.12, and consequently the squared error is minimized by Equation B.13.

$$\bar{e}^2 = \int_0^T (q_L - q_{NL})^2 \tag{B.12}$$

$$\frac{d\bar{e}^2}{dK_L} = 0 \tag{B.13}$$

Implementation of Equation B.8 and Equation B.9 into Equation B.12 gives Equation B.14. Inserting the total error over a wave period into Equation B.13 given Equation B.15.

$$\bar{e}^2 = \int_0^T (q_L - q_{NL})^2 = \int_0^T {C_D^*}^2 \left[K_L A - A^2 |\cos(\omega t)|\right]^2 \cos^2(\omega t) dt \tag{B.14}$$

$$\frac{d\bar{e}^2}{dK_L} = \int_0^T 2{C_D^*}^2 A \left[K_L A - A^2 |\cos(\omega t)|\right] \cos^2(\omega t) dt = 0 \tag{B.15}$$

Further solving of Equation B.15 results in Equation B.17. By standard integration the optimal linearisation coefficient is found to be defined by Equation B.18.

$$\int_0^T K_L A \cos^2(\omega t) dt - \int_0^T A^2 \cos^2(\omega t) |\cos(\omega t)| dt = 0 \tag{B.16}$$

$$\int_0^T K_L A \cos^2(\omega t) dt - 4 \cdot \int_0^{\frac{T}{4}} A^2 \cos^3(\omega t) dt = 0 \tag{B.17}$$

$$K_L = \frac{8A}{3\pi} \tag{B.18}$$

C

Transfer function approach

This Appendix contains content supporting the transfer function approach described in Chapter 7. The extended version plots of the transfer function are displayed in Appendix C.1. The method used to obtain the distribution of the cable response, based on the cable response spectrum obtained on the basis the transfer function, is provided in Appendix C.2. Last, the distribution selection for the irregular wave Orcaflex simulations is documented in Appendix C.3.

C.1. Full transfer function

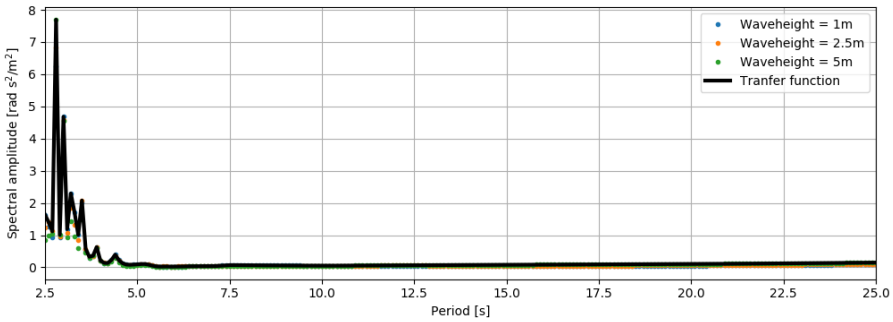

Figure C.1: Full transfer function for the maximum curvature response of the cable.

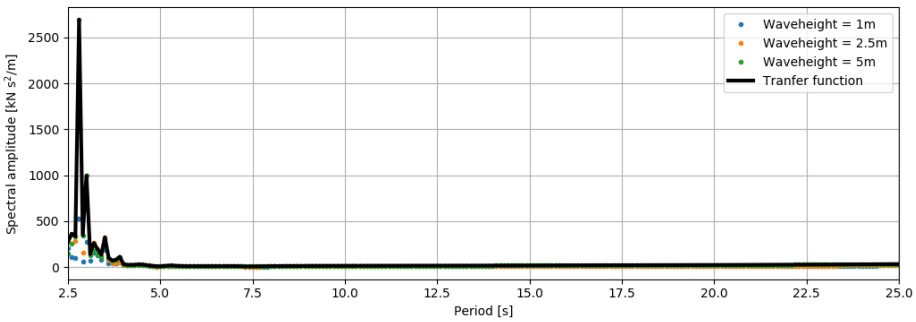

Figure C.2: Full transfer function for the maximum tension response of the cable.

C.2. Rayleigh distribution scale parameter

This Appendix describes the procedure and assumptions made to obtain the cable response distribution based on the cable response spectrum, which is obtained following the transfer function approach described in Chapter 7. The information in this note is based on [Holthuijsen, 2015].

Assumption a: The cable response spectrum is a narrow spectrum

Assumption b: The cable response is a stationary Gaussian process.

The average time interval between two successive up-crossings through level CR can be expressed in terms of the spectrum by Equation C.1.

$$\bar{T}_{CR} = \sqrt{\frac{m_0}{m_2}} \Big/ \exp -\frac{x^2}{2m_0} \tag{C.1}$$

Thr probability that any peak in the cable response spectrum is above a certain height x is given by Equation C.2

$$P(CR > x) = \frac{\text{number of peaks with (CR}_{peak} > \text{x) in duration D}}{\text{total number of peaks in duration D}} = \frac{D/\bar{T}_{CR}}{D/\bar{T}_0} \tag{C.2}$$

Using the definition of the average time interval between zero up-crossings the probability that a peak of the cable response exceeds a certain values x can be written as:

$$P(CR > x) = \frac{\bar{T}_0}{\bar{T}_{CR}} = \frac{\sqrt{\frac{m_0}{m_2}}}{\sqrt{\frac{m_0}{m_2}} \Big/ \exp -\frac{x^2}{2m_0}} = \exp -\frac{x^2}{2m_0} \tag{C.3}$$

Then the cumulative distribution function can be written as in Equation C.4.

$$P(CR < x) = 1 - P(CR > x) = 1 - \exp\big(-\frac{x^2}{2m_0}\big) \tag{C.4}$$

This corresponds to a Rayleigh distribution for which the scale parameter σ^2 is equal to the zeroth order moment of the cable response spectrum.

C.3. Distribution selection

In this note a full overview of the probability distribution selection for the maximum curvature and maximum tension response in the cable is provided.

C.3.1. Simulation length selection

The limits of convergence are set to 5% for the mean, standard deviation and skewness of the data set. Due to the high fluctuation in the kurtosis for some data sets and limited calculation resources, no absolute limit is set for the kurtosis of the data set, but the convergence of the kurtosis is checked by means of graph inspection. The simulation time is considered long enough when the mean, standard deviation and skewness stay within this limit for increased simulation time and the kurtosis has reached reasonable convergence.

The required simulation time for the tension response peaks in the maximum tension response signal is 30 hours. The peaks in the maximum curvature response of the cable shows slightly more variation in the properties of the data set. Following the same approach as for the tension, a required simulation length of 45 hours is selected for the distribution fitting of the peaks in the curvature response of the cable.

C.3.2. Tension distribution selection

The data set of the tension response peaks is fitted to 12 probability distributions. The results of the KS-test for the tension response are presented in Table C.1. In addition, the LSE between the distribution fit and the normalized histogram of the data set is given in Table C.2. The generalized extreme value distribution shows overall to be the best fit in both tables. The generalized extreme value distribution was not accepted for two sea states in this study. For those sea states a P-P plot is created, see Figure C.3 and Figure C.4 for sea state 1 and sea state 5, respectively. Finally, the error introduced by the distribution fit for the sea states for which the generalized distribution was not accepted based on the KS-test is evaluated in Table C.3.

Distribution	**Sea state 1**	**Sea state 2**	**Sea state 3**	**Sea state 4**	**Sea state 5**	**Sea state 6**	**Sea state 7**	**Sea state 8**	**Total ✓**
Beta	✗	✓	✗	✗	✗	✗	✗	✗	1
Burr	✗	✗	✗	✗	✗	✗	✓	✓	2
Chi	✗	✓	✗	✗	✗	✗	✗	✗	1
Frechet	✗	✗	✗	✗	✗	✗	✗	✗	0
Gamma	✗	✓	✗	✗	✗	✗	✗	✗	1
General extreme	✗	✓	✓	✓	✗	✓	✓	✓	6
Gumbel	✗	✗	✗	✗	✗	✗	✓	✗	1
Log normal	✓	✓	✗	✗	✗	✗	✗	✗	2
Normal	✗	✗	✗	✗	✗	✗	✗	✗	0
Pearson 3	✗	✓	✗	✗	✗	✗	✗	✗	1
Rayleigh	✗	✗	✗	✗	✗	✗	✗	✗	0
Weibull	✗	✓	✓	✓	✗	✗	✓	✗	4

Table C.1: KS-test results for the tension response of the cable.

Distribution	**Sea state 1**	**Sea state 2**	**Sea state 3**	**Sea state 4**	**Sea state 5**	**Sea state 6**	**Sea state 7**	**Sea state 8**	Total
Beta	0.2668	0.1761	0.1815	0.1166	7.7332	4.7795	2.7133	1.3936	17.3606
Burr	0.5412	0.3756	0.1846	0.0746	0.0480	0.0229	0.0086	0.0048	1.2603
Chi	0.2587	0.1757	0.1173	0.1197	0.0566	10.3211	0.0298	1.0317	12.1091
Frechet	3.3074	1.3453	0.9252	0.6635	0.2933	0.2093	0.1550	0.0833	6.9823
Gamma	0.2664	0.1757	0.1221	0.1197	0.0494	0.0332	0.0297	0.0176	0.8138
General extreme	0.1539	0.2083	0.0948	0.0769	0.0340	0.0205	0.0105	0.0043	0.6032
Gumbel	0.5350	0.3876	0.1669	0.1183	0.0886	0.0213	0.0083	0.0074	1.3334
Log normal	0.1572	0.2083	0.1050	0.1002	0.0404	0.0242	0.0161	0.0058	0.6572
Normal	1.8128	2.1464	0.7594	0.4651	0.2087	0.2111	0.1659	0.1245	5.8939
Pearson 3	0.2666	0.1756	0.1173	0.1197	0.0494	0.0333	0.0297	0.0176	0.8092
Rayleigh	19.8927	6.9042	5.7431	4.0346	1.8544	0.8535	0.4334	0.1291	39.8450
Weibull	0.1502	0.2052	0.0948	0.0769	0.0340	9.3749	0.0105	0.0074	10.2599

Table C.2: The LSE for the distribution fit of the tension response data set.

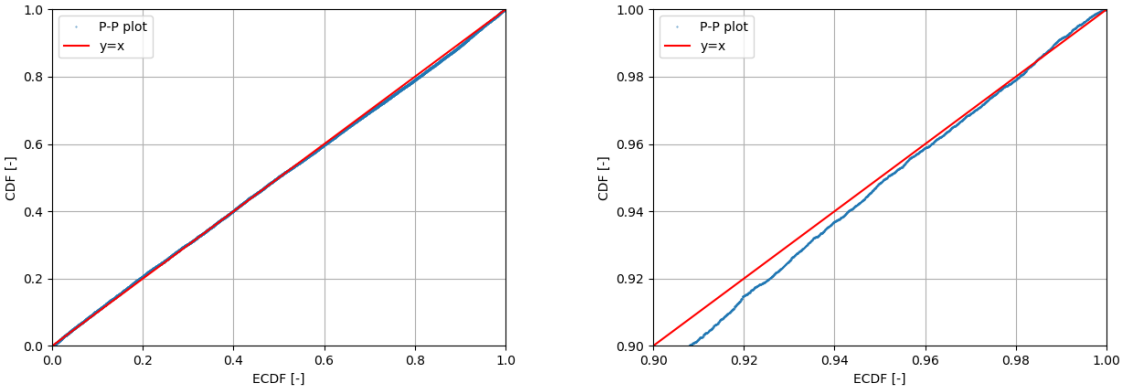

a) Full P-P plot

b) Zoom-in on P-P plot

Figure C.3: P-P plot of the tension response for sea state 1.

Error	**Sea state 1**	**Sea state 5**
N = 1 at 95%	-0.012	-0.010
N =1 at 99%	+ 0.050	+0.160
N = 1000 at 0.37%	+0.269	+0.372

Table C.3: Error in results between the ECDF of the actual data set and the results from distribution fit tot he generalized extreme value distribution.

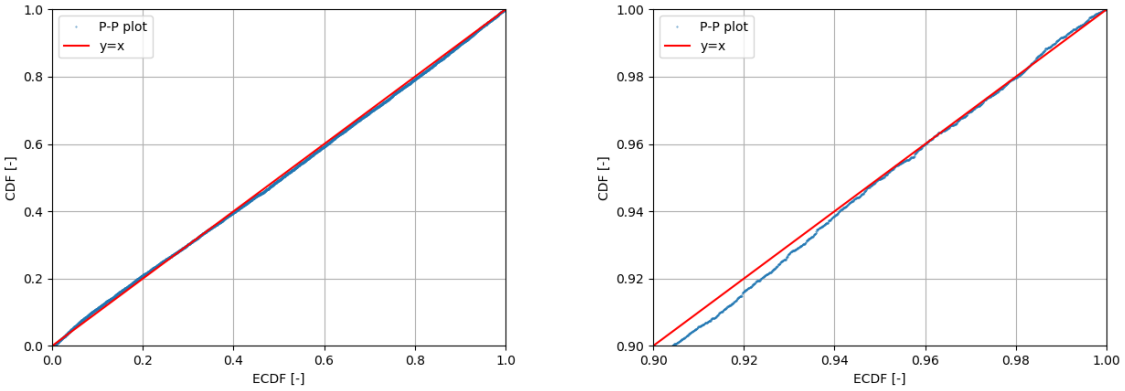

a) Full P-P plot

b) Zoom-in on P-P plot

Figure C.4: P-P plot pf the tension response for sea state 5.

C.3.3. Curvature distribution selection

The data set of the curvature response peaks is fitted to 13 probability distributions. The results of the KS-test for the curvature response are presented in Table C.4. In addition, the LSE between the distribution fit and the normalized histogram of the data set is given in Table C.5. The beta distribution shows overall to be the best fit in both tables. The beta distribution was not accepted for two sea states in this study. For those sea states a P-P plot is created, see Figure C.3 and Figure C.4 for sea state 1 and sea state 2, respectively. Finally, the error introduced by the distribution fit for the sea states for which the generalized distribution was not accepted based on the KS-test is evaluated in Table C.3.

Distribution	**Sea state 1**	**Sea state 2**	**Sea state 3**	**Sea state 4**	**Sea state 5**	**Sea state 6**	**Sea state 7**	**Sea state 8**	**Total ✓**
Beta	✗	✗	✓	✓	✓	✓	✓	✓	6
Betaprime	✗	✗	✗	✗	✗	✗	✗	✗	0
Burr	✗	✗	✗	✗	✗	✗	✗	✗	0
Chi	✗	✗	✗	✗	✗	✗	✗	✓	1
Frechet	✗	✗	✗	✗	✗	✓	✓	✗	2
Gamma	✗	✗	✗	✗	✗	✗	✗	✓	1
General extreme	✗	✗	✗	✓	✓	✗	✗	✓	3
Gumbel	✗	✗	✗	✗	✗	✗	✗	✗	0
Log normal	✗	✗	✗	✗	✗	✗	✓	✓	2
Normal	✗	✗	✗	✗	✗	✗	✓	✗	1
Pearson 3	✗	✗	✗	✗	✗	✗	✓	✓	2
Rayleigh	✗	✗	✗	✗	✗	✗	✗	✗	0
Weibull	✗	✗	✗	✗	✗	✗	✗	✗	0

Table C.4: KS-test results for the curvature response of the cable.

Distribution	**Sea state 1**	**Sea state 2**	**Sea state 3**	**Sea state 4**	**Sea state 5**	**Sea state 6**	**Sea state 7**	**Sea state 8**	Total
Beta	9641	6423	876	1216	702	660	279	126	19797
Betaprime	1240006	1400897	3793	408391	148955	63638	3479	44573	3269159
Burr	526668	798367	4507	176841	44270	65587	73550	512	1689790
Chi	1649865	7414	3307	1553	689	259856	127287	126	2049971
Frechet	38388	1835347	716072	561931	264019	638	111893	62302	3528288
Gamma	9746	7414	1789	1653	920	1046	241	126	22809
General extreme	14508	9060	3970	1284	445	1177	1243	156	31687
Gumbel	18117	17036	5069	8917	6627	7305	5556	375	68626
Log normal	13060	9555	3330	1836	959	1050	241	140	30031
Normal	56136	49910	27394	6121	1970	1025	238	2134	142794
Pearson 3	9743	7412	1789	1654	920	1046	241	126	22805
Rayleigh	185981	242068	9652	42410	61155	34592	25676	3391	601534
Weibull	1188836	1714814	4251	495356	259085	296743	118150	65689	4077235

Table C.5: The LSE for the distribution fit of the curvature response data set.

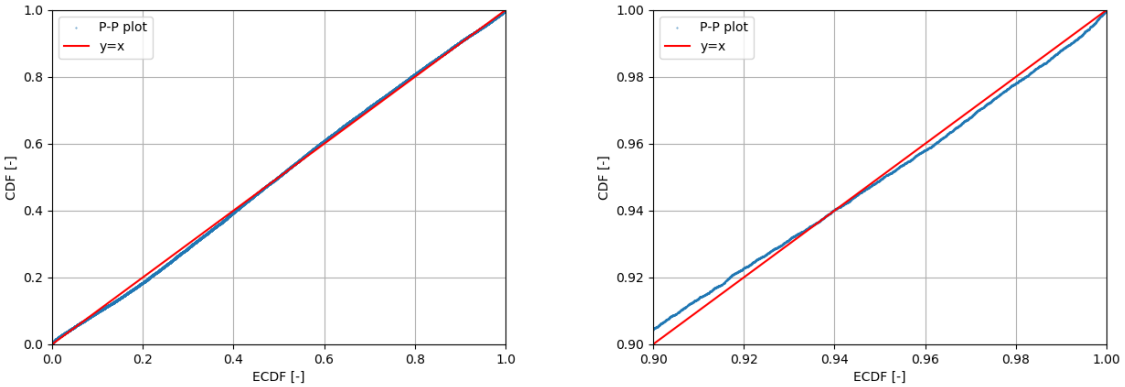

a) Full P-P plot **b)** Zoom-in on P-P plot

Figure C.5: P-P plot of the curvature response for sea state 1.

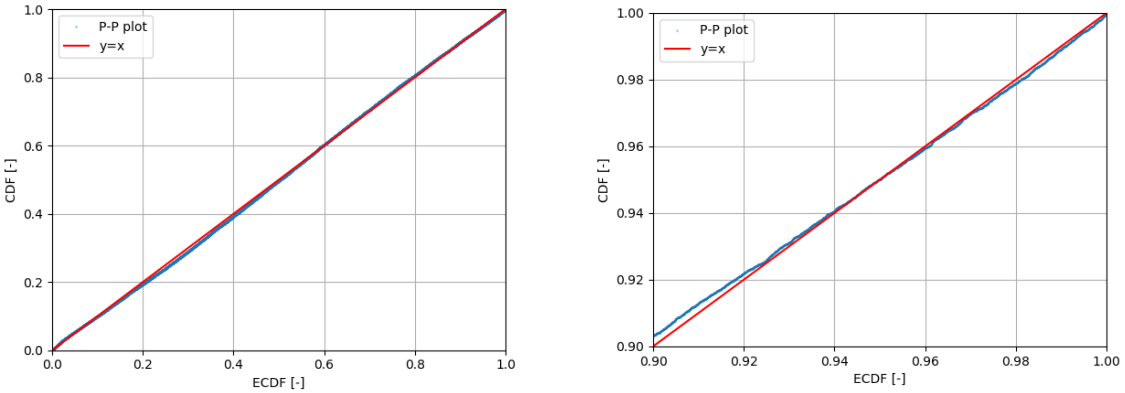

a) Full P-P plot **b)** Zoom-in on P-P plot

Figure C.6: P-P plot of the curvature response for sea state 2.

Error	**Sea state 1**	**Sea state 2**
N = 1 at 95%	-0.032	+0.003
N =1 at 99%	-0.285	-0.115
N = 1000 at 0.37%	-0.561	-0.571

Table C.6: Error in results between the ECDF of the actual data set and the results from distribution fit tot he generalized extreme value distribution.

D

Sensitivity analysis

This Appendix contains complementary data supporting the sensitivity analysis presented in Chapter 8. Additional plots of the sensitivity of the DFT analysis are provided in Appendix D.1. A complete overview of the TLCC data used in the sensitivity analysis of the vessel motion selection procedure is given in Appendix D.2.

D.1. Sensitivity plots of DFT analysis

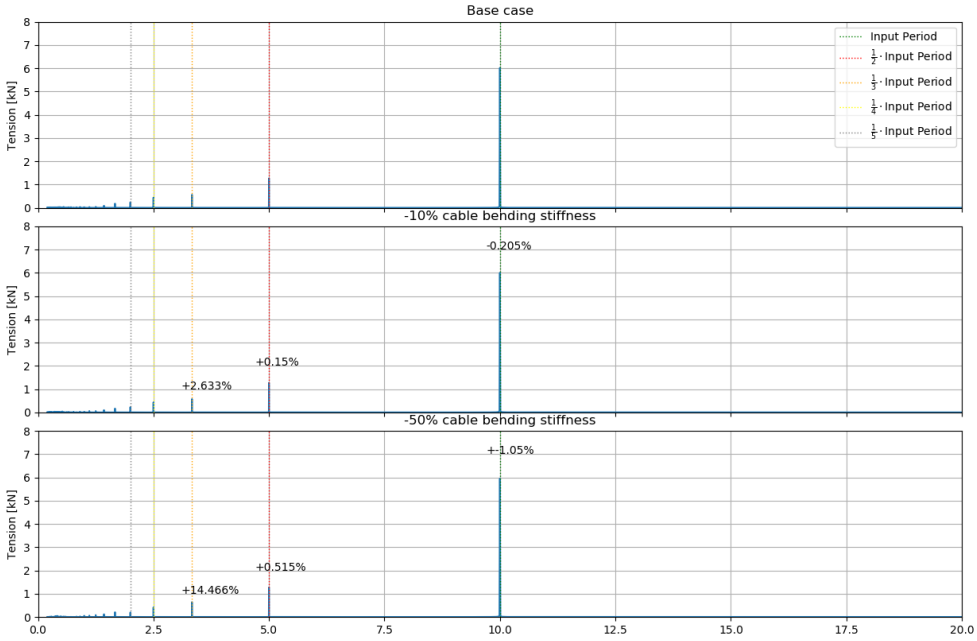

Figure D.1: Plot depicting the sensitivity of the DFT of the tension response of the cable towards a reduction in the bending stiffness of the cable.

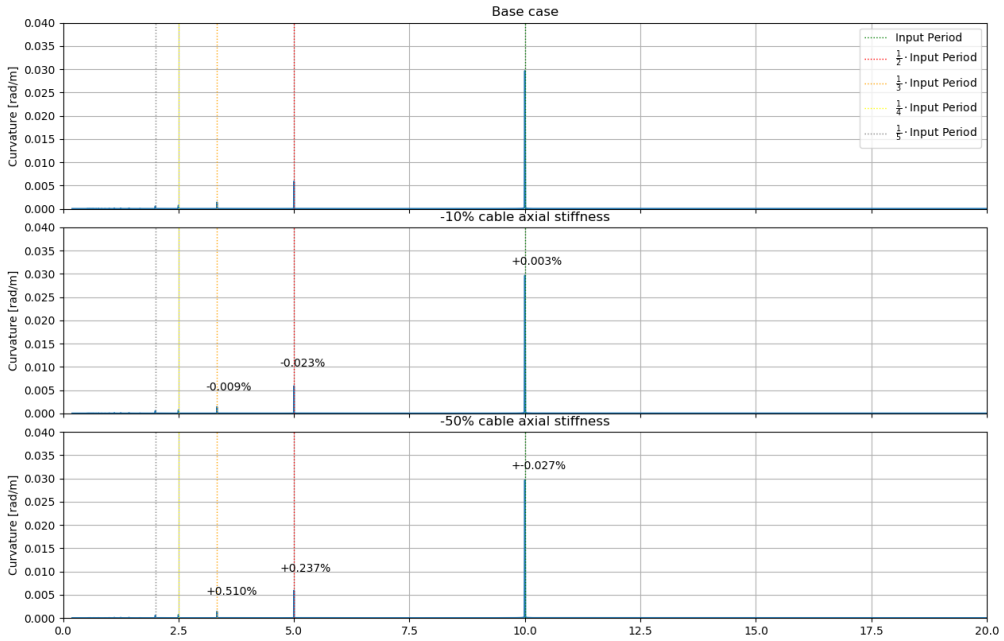

Figure D.2: Plot depicting the sensitivity of the DFT of the curvature response of the cable towards a reduction in the axial stiffness of the cable.

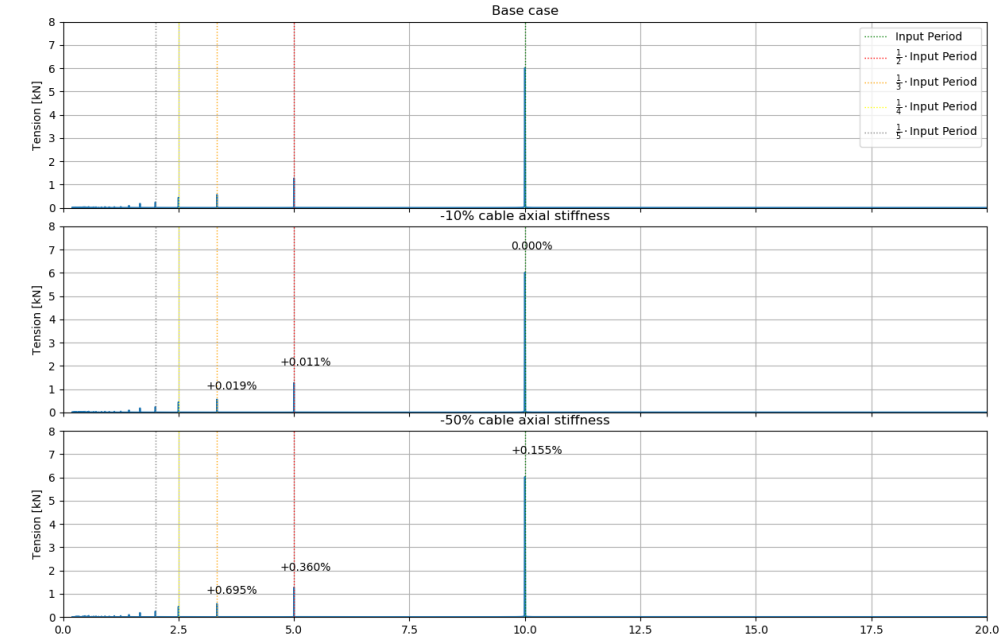

Figure D.3: Plot depicting the sensitivity of the DFT of the tension response of the cable towards a reduction in the axial stiffness of the cable.

D.2. Vessel motion selection sensitivity

Motion	Mean correlation	Maximum correlation	Minimum correlation
HD min	-0.689	-0.725	-0.664
HD max	0.764	0.850	0.642
HV min	-0.767	-0.802	-0.709
HV max	0.718	0.761	0.645
HA min	-0.742	-0.795	-0.623
HA max	0.694	0.760	0.598
SD min	-0.631	-0.786	-0.448
SD max	0.633	0.741	0.454
SV min	-0.685	-0.830	-0.491
SV max	0.632	0.715	0.489
SA min	-0.676	-0.763	-0.601
SA max	0.658	0.794	0.460
AD min	-0.733	-0.759	-0.692
AD max	0.757	0.807	0.649
AV min	-0.765	-0.796	-0.710
AV max	0.691	0.746	0.634
AA min	-0.717	-0.771	-0.615
AA max	0.708	0.762	0.641
WE min	-0.730	-0.863	-0.667
WE max	0.730	-0.863	-0.667

Table D.1: Overview of time lagged cross correlation results for curvature response of the cable for H_s=2.5m for case 2 in the sensitivity analysis.

Motion	Mean correlation	Maximum correlation	Minimum correlation
HD min	-0.902	-0.953	-0.803
HD max	0.856	0.885	0.807
HV min	-0.842	-0.889	-0.805
HV max	0.932	0.954	0.898
HA min	-0.864	-0.906	-0.768
HA max	0.885	0.913	0.803
SD min	-0.726	-0.774	-0.623
SD max	0.775	0.862	0.672
SV min	-0.758	-0.812	-0.622
SV max	0.816	0.904	0.720
SA min	-0.840	-0.929	-0.729
SA max	0.772	0.826	0.648
AD min	-0.885	-0.922	-0.803
AD max	0.894	0.908	0.868
AV min	-0.803	-0.888	-0.702
AV max	0.928	0.952	0.895
AA min	-0.868	-0.901	-0.799
AA max	0.846	0.908	0.786
WE min	-0.807	-0.887	-0.705
WE max	0.761	0.849	0.665

Table D.2: Overview of time lagged cross correlation results for the tension response of the cable for H_s=2.5m for case 2 in the sensitivity analysis.

Motion	Mean correlation	Maximum correlation	Minimum correlation
HD min	-0.611	-0.668	-0.492
HD max	0.692	0.796	0.513
HV min	-0.700	-0.752	-0.566
HV max	0.640	0.712	0.464
HA min	-0.700	-0.757	-0.576
HA max	0.628	0.702	0.549
SD min	-0.553	-0.744	-0.298
SD max	0.556	0.682	0.329
SV min	-0.602	-0.771	-0.351
SV max	0.569	0.680	0.395
SA min	-0.600	-0.704	-0.368
SA max	0.577	0.751	0.301
AD min	-0.654	-0.723	-0.507
AD max	0.680	0.748	0.521
AV min	-0.696	-0.747	-0.571
AV max	0.616	0.685	0.468
AA min	-0.675	-0.725	-0.574
AA max	0.645	0.705	0.549
WE min	-0.705	-0.850	-0.563
WE max	0.735	0.774	0.617

Table D.3: Overview of time lagged cross correlation results for the curvature response of the cable for H_s=2.5m for case 3 in the sensitivity analysis.

Motion	Mean correlation	Maximum correlation	Minimum correlation
HD min	-0.827	-0.890	-0.732
HD max	0.777	0.803	0.738
HV min	-0.766	-0.803	-0.672
HV max	0.862	0.908	0.769
HA min	-0.802	-0.839	-0.760
HA max	0.839	0.882	0.783
SD min	-0.642	-0.685	-0.539
SD max	0.686	0.792	0.547
SV min	-0.677	-0.765	-0.488
SV max	0.731	0.825	0.621
SA min	-0.756	-0.874	-0.601
SA max	0.701	0.753	0.601
AD min	-0.813	-0.862	-0.737
AD max	0.816	0.866	0.747
AV min	-0.733	-0.774	-0.674
AV max	0.860	0.907	0.763
AA min	-0.811	-0.840	-0.775
AA max	0.805	0.845	0.771
WE min	-0.747	-0.835	-0.616
WE max	0.715	0.812	0.622

Table D.4: Overview of time lagged cross correlation results for tension response of the cable for H_s=2.5m for case 3 in the sensitivity analysis.